

HOLE-TYPE AEROSPIKE COMPOUND NOZZLE THRUST VECTORIZING

A Thesis
presented to
the Faculty of California Polytechnic State University,
San Luis Obispo

In Partial Fulfillment
of the Requirement for the Degree
Master of Science in Mechanical Engineering

by
Stanley Ikuo Beebe
September 2009

©2009
Stanley Ikuo Beebe
ALL RIGHTS RESERVED

COMMITTEE MEMBERSHIP

TITLE: HOLE-TYPE AEROSPIKE COMPOUND
NOZZLE THRUST VECTORING

AUTHOR: STANLEY IKUO BEEBE

DATE SUBMITTED: SEPTEMBER 2009

COMMITTEE CHAIR: WILLIAM R. MURRAY, Ph. D.

COMMITTEE MEMBER: THOMAS W. CARPENTER, Ph. D.

COMMITTEE MEMBER: KIM A. SHOLLENBERGER, Ph. D.

ABSTRACT

Hole-Type Aerospike Compound Nozzle Thrust Vectoring

Stanley Ikuo Beebe

Compound aerospike nozzles were designed and tested as part of an ongoing experimental study to determine the feasibility of thrust vectoring an aerospike nozzle with the addition of a secondary port. Earlier phases of the study have indicated that a compound aerospike nozzle could provide sufficient thrust vectoring. The addition of a hole-type secondary port was found to provide effective thrust vectoring.

Experiments were carried out to determine the effects of secondary port size, secondary port inlet geometry and compound aerospike nozzle chamber pressure. Results show good predictability, axisymmetric flow, and emphasize the importance of a radius on secondary port inlet geometry.

Keywords: aerospike, thrust vectoring, compound nozzle.

ACKNOWLEDGMENTS

I would like to thank my mother and sister for their support during the many years of my enrollment at Cal Poly, and thanks Dad, wish you could have read this.

A special word of thank you to my thesis committee members William Murray, Thomas Carpenter and Kim Shollenberger. I appreciate the opportunity to be part of this project. I have learned much more than rocket science during the course of my study, thanks for your help and encouragement as friends and mentors.

Thanks to Ty and Trudie Safreno at Trust Automation for generous use of the facilities and resources.

This work was funded in part by grants from the NASA Dryden Flight Research Center STTR Grants: Phase II, Contract NND06AB82C, 06/06 – 08/08; Phase I, Contract NND05AA53C, 01/05 – 01/06.

Table of Contents

List of Tables.....	vii
List of Figures.....	viii
List of Figures.....	viii
Nomenclature.....	x
1. Introduction	1
Background.....	2
Research Objectives.....	2
2. Facilities and Equipment.....	3
Engines Lab	3
Rapid Prototype Manufacturing	4
Flow Visualization/Schlieren	4
Air Supply.....	5
Test Stand.....	6
Data Acquisition	6
Testing Procedure.....	7
3. Nozzle Design	10
Aerospike Design/Theory	10
Thrust Vectoring Design	11
4. Initial Testing	13
Initial Hole-Type Compound Aerospike Nozzle	13
Pressure Distribution on Nozzle Wall	15
6. Test Nozzles	19
7. Nozzle Performance.....	26
Chamber Pressure Variations.....	26
Turn Angle Prediction	27
8. Summary of Results.....	38
Flow Behavior and Inlet Radius Results.....	40
Metal Nozzles Results	42
Chamber Pressure and Turn Angle Results.....	44
Conclusions	48
Bibliography	49
Appendix A: Equations.....	51
Appendix B: Nozzle Geometry.....	52
Appendix C: Original Data	68

List of Tables

TABLE 1. ERROR IN TEST STAND MEASUREMENTS.....	3
TABLE 2. PRESSURE DISTRIBUTION ALONG NOZZLE WALL.....	17
TABLE 3. PHOTOS OF TEST NOZZLES.....	21
TABLE 4. PHOTOS OF METAL TEST AEROSPIKE NOZZLES.....	22
TABLE 5. CALCULATED AND MEASURED COMPOUND NOZZLE FORCES AND TURN ANGLES.....	37
TABLE 6. TABULATED SUMMARY OF RESULTS.	39

List of Figures

FIGURE 1. LAYOUT OF SUPPLY AIR SYSTEM SHOWING INDIVIDUAL COMPONENTS.	8
FIGURE 2. TEST STAND SHOWING BELLOWS, PLENUM, AND A TEST NOZZLE.....	9
FIGURE 3. LOAD CELLS AT BASE OF TEST PLATFORM.	9
FIGURE 4. DIAGRAM OF TERMS DESCRIBING COMPOUND AEROSPIKE NOZZLE GEOMETRY.	13
FIGURE 5. INITIAL HOLE-TYPE COMPOUND AEROSPIKE NOZZLE CONFIGURATION.	14
FIGURE 6. "NPR20 HOLE" SCHLIEREN PHOTOGRAPH AND CROSS-SECTION DRAWING..	14
FIGURE 7. PRESSURE TAP EQUIPPED NPR20 NOZZLE.	17
FIGURE 8. NOZZLE WALL STATIC PRESSURE VERSUS AXIAL POSITION PRESSURE TAP RESULTS.	18
FIGURE 9. SCHLIEREN PHOTOGRAPHS OF NON-COMPOUND AEROSPIKE NOZZLES.	22
FIGURE 10. SCHLIEREN PHOTOGRAPHS OF NPR6 COMPOUND NOZZLES.....	23
FIGURE 11. SCHLIEREN PHOTOGRAPHS OF NPR20 COMPOUND NOZZLES, NO INLET RADIUS.	23
FIGURE 12. SCHLIEREN PHOTOGRAPHS OF NPR50 COMPOUND AEROSPIKE NOZZLES.....	24
FIGURE 13. SCHLIEREN PHOTOGRAPHS OF NPR20 METAL AEROSPIKE NOZZLES.....	24
FIGURE 14. SCHLIEREN PHOTOGRAPHS OF NPR20 COMPOUND AEROSPIKE NOZZLES WITH SECONDARY PORT INLET RADII.	25
FIGURE 15. ABSOLUTE TURN ANGLE VERSUS NPR, RESULTS OF VARYING CHAMBER PRESSURE.	27
FIGURE 16. DIAGRAM OF COMPOUND AEROSPIKE NOZZLE FORCES.....	28
FIGURE 17. NPR6 HOLE 3 SECONDARY PORT MEASURED AND CALCULATED RADIAL VECTERING FORCE VERSUS NPR.....	29
FIGURE 18. NPR20 HOLE 3 SECONDARY PORT MEASURED AND CALCULATED RADIAL VECTERING FORCE VERSUS NPR.....	30
FIGURE 19. NPR20 HOLE 5 SECONDARY PORT MEASURED AND CALCULATED RADIAL VECTERING FORCE VERSUS NPR.....	30
FIGURE 20. NPR50 HOLE 3 SECONDARY PORT MEASURED AND CALCULATED RADIAL VECTERING FORCE VERSUS NPR.....	31
FIGURE 21. NPR6 HOLE 3 AEROSPIKE NOZZLE MEASURED AND CALCULATED AXIAL FORCE VERSUS NPR.	31
FIGURE 22. NPR20 HOLE 3 AEROSPIKE NOZZLE MEASURED AND CALCULATED AXIAL FORCE VERSUS NPR.	32
FIGURE 23. NPR20 HOLE 5 AEROSPIKE NOZZLE MEASURED AND CALCULATED AXIAL FORCE VERSUS NPR.	32
FIGURE 24. NPR50 HOLE 3 AEROSPIKE NOZZLE MEASURED AND CALCULATED AXIAL FORCE VERSUS NPR.	33
FIGURE 25. NPR6 HOLE 3 ABSOLUTE TURN ANGLE VERSUS NPR COMPARISON OF CALCULATED AND MEASURED RESULTS.	34
FIGURE 26. NPR20 HOLE 3 ABSOLUTE TURN ANGLE VERSUS NPR COMPARISON OF CALCULATED AND MEASURED RESULTS.	35
FIGURE 27. NPR20 HOLE 5 ABSOLUTE TURN ANGLE VERSUS NPR COMPARISON OF CALCULATED AND MEASURED RESULTS.	35
FIGURE 28. NPR50 HOLE 3 ABSOLUTE TURN ANGLE VERSUS NPR COMPARISON OF CALCULATED AND MEASURED RESULTS.	36
FIGURE 29. NPR20 HOLE 2 PRESSURE DISTRIBUTION AT INLET OF SECONDARY PORT.	41
FIGURE 30. SCHLIEREN PHOTOGRAPHS OF TWO NPR20 METAL NOZZLES.....	43
FIGURE 31. COMPARISON BETWEEN CALCULATED AND MEASURED TURN ANGLES FOR NPR6 NOZZLES ON A RUN-BY-RUN LEVEL.	46
FIGURE 32. COMPARISON BETWEEN CALCULATED AND MEASURED TURN ANGLES FOR NPR20 NOZZLES ON A RUN-BY-RUN LEVEL.....	46

FIGURE 33. COMPARISON BETWEEN CALCULATED AND MEASURED TURN ANGLES FOR NPR50 NOZZLES ON A RUN-BY-RUN LEVEL.....	47
FIGURE 34. NPR6 STRAIGHT DESIGN DRAWING.	53
FIGURE 35. NPR6 HOLE 2 DESIGN DRAWING.	54
FIGURE 36. NPR6 HOLE 3 DESIGN DRAWING.	55
FIGURE 37. NPR20 STRAIGHT DESIGN DRAWING.	56
FIGURE 38. NPR20 SLOT DESIGN DRAWING.....	57
FIGURE 39. NPR20 STRAIGHT HOLE DESIGN DRAWING.	58
FIGURE 40. NPR20 STRAIGHT PRESSURE TAP DESIGN DRAWING.....	59
FIGURE 41. NPR20 HOLE 2 DESIGN DRAWING.	60
FIGURE 42. NPR20 HOLE 3 DESIGN DRAWING.	61
FIGURE 43. NPR20 HOLE 5 DESIGN DRAWING.	62
FIGURE 44. NPR20 HOLE 6 DESIGN DRAWING.	63
FIGURE 45. NPR20 HOLE 7 DESIGN DRAWING.	64
FIGURE 46. NPR50 STRAIGHT DESIGN DRAWING.	65
FIGURE 47. NPR50 HOLE 2 DESIGN DRAWING.	66
FIGURE 48. NPR50 HOLE 3 DESIGN DRAWING.	67

Nomenclature

Right NPR	Nozzle Pressure Ratio measured on the right-hand plenum; the ratio between chamber pressure and ambient pressure.
F_x	Force measured in the radial “X” direction (lbf).
F_y	Force measured in the radial “Y” direction (lbf).
F_z	Force measured in the axial “Z” direction (lbf).
M_x	Moment measured about the “X” axis (in-lbf).
M_y	Moment measured about the “Y” axis (in-lbf).
M_z	Moment measured about the “Z” axis (in-lbf).
W_p	Measured mass flow rate of supply air (lbm/s).
W_i	Ideal (calculated) mass flow rate of supply air (lbm/s).
F_i	Ideal (calculated) nozzle force in the axial “Z” direction (lbf).
F_r	Measured resultant force of the nozzle (lbf).
δ_{pitch}	Angle of pitching force generated by the thrust vectoring (°).
δ_{yaw}	Angle of yawing force generated by the thrust vectoring (°).
δ_r	Overall resultant turn angle produced by the thrust vectoring (°).
δ_{calc}	Calculated resultant turn angle (°).
A_t	Throat area (in ²).
A_e	Exit area (in ²)
P_1	Chamber pressure (psi)
T_1	Chamber temperature (°F)
F_{calc}	Calculated force produced by the hole-type compound nozzle (lbf).
F_{vector}	Measured force produced by the hole-type compound nozzle (lbf).

1. Introduction

Inherent to the aerospike nozzle is high efficiency due to altitude compensation and throttling capability unique to the aerospike nozzle geometry. Very little research has been conducted regarding the thrust vectoring capability of the annular aerospike nozzle. The combination of high efficiency, throttling capability, and thrust vectoring is the ideal stepping stone to the future of commercial space access.

California Polytechnic State University, San Luis Obispo, has created a substantial research program to develop a thrust vectoring system for annular aerospike rocket nozzles. Preliminary testing has identified three potential methods for aerospike nozzle thrust vectoring: gimbaling of a finned aerospike, the addition of a slot-type secondary port, and the addition of a hole-type secondary port¹. The focus of this thesis is the experimental investigation of the compound aerospike nozzle formed by the addition of a secondary port.

The hole-type secondary port redirects a portion of the combustion chamber gases before they have passed through the aerospike nozzle throat. The location of the hole-type secondary port and its geometry are evaluated in this thesis. Effects of hole size and chamber pressure are examined as well as effects of the secondary port on the aerospike nozzle flow. The importance of the secondary port inlet geometry is also observed.

¹ "Optimal Thrust Vectoring for an Annular Aerospike Nozzle," NASA STTR Grants: Phase II, Contract NND06AB82C, 06/06 – 08/08; Phase I, Contract NND05AA53C, 01/05 – 01/06.

Background

Aerospike development and testing conducted at General Electric Company and Rocketdyne since the early 1960s have demonstrated the potential of the aerospike nozzle. These early tests produced thrust levels up to 250,000 lbf. Later tests done in the 1970s and until 2001 were done with a linear aerospike configuration (Sutton, 2005).

The aerospike is known to have performance advantages over the conventional bell nozzle, particularly at off-design conditions. The altitude compensating effects of the aerospike design yield significant improvements in thrust at low altitude (Ruf & McMonnaughey, 1997).

Thrust vectoring control by some means is required to maintain flight trajectory and Erickson (1997) found thrust vectoring of a linear-type aerospike nozzle through differential throttling to be advantageous to gimbaling of the aerospike structure. Little if any research has been conducted in the past on thrust vectoring methods for annular aerospike nozzles. Thus, thrust vectoring research as well as hybrid rocket motor test capability at California Polytechnic State University, San Luis Obispo has provided an ideal setting to evaluate the thrust vectoring potential of the annular aerospike nozzle.

Research Objectives

The primary objective of this thesis is to evaluate the thrust vectoring performance of a hole-type compound aerospike nozzle. In order to be deemed effective, a thrust-vectoring nozzle must produce a turn angle equivalent to a 10° gimbaling of the thrust.

2. Facilities and Equipment

Engines Lab

The engine test facility in Engineering Building 13 at Cal Poly is equipped with a thrust vectoring test stand designed and developed during the early 1990s under grants from the NASA Dryden Flight Research Center. The facility has been upgraded and now accommodates both hot-fire testing and cold-flow testing. Clean, dry air at ambient temperature is used for testing, termed “*cold flow*”, and supplied to the test stand under pressure. Cold flow was used exclusively for tests reported in this thesis.

Extensive testing and calibration have been done during previous experiments (Rossi, 1994) proving the stand to be quite accurate for measuring forces and moments. Table 1 lists the measured forces and moments with their corresponding measurement error as well as the calculated pitch and yaw angles with their respective error values. Calculations showing the derivation of the forces and moments found in the **Table 1**, along with the physical dimensions of the test stand used for the calculations may be found in Rossi (1994).

Table 1. Error in test stand measurements.

Force	Error in force
F_x	+/- 0.20 lbf
F_y	+/- 0.13 lbf
F_z	+/- 0.34 lbf
Moment	Error in moment
M_x	+/- 1.81 in-lbf
M_y	+/- 2.20 in-lbf
M_z	+/- 0.52 in-lbf
Angle	Error in angle
δ_{pitch}	$\pm 0.5^\circ$
δ_{yaw}	$\pm 0.5^\circ$

Rapid Prototype Manufacturing

The rapid-prototype, or *RP*, process used to manufacture the test nozzle presents certain restrictions and limitations. Firstly and most immediately obvious is the resolution of the rendering of the models. The RP machine extrudes a small bead of molten ABS plastic as it builds each layer of the model. In particular, areas of high curvature make the layer thickness obvious. The rough surface finish of the models introduces small flow perturbations that are visible in Schlieren photographs. Another less noticeable result of the RP process is porosity, which can weaken the models and allow air to flow through the walls. The porosity must be taken into consideration when designing parts with thin-section features or small details. During testing, several instances of mechanical failures of the ABS models occurred.

Flow Visualization/Schlieren

For flow visualization, a two-mirror color Schlieren shadowgraph apparatus was used. It was found that a red-green filter provided the best images in terms of appearance. When carefully calibrated color Schlieren may be used for quantitative measurement, however, it should be noted that the Schlieren images used in this thesis were taken at different times under different conditions and are for qualitative flow visualization only.

Through most of the early testing, Schlieren video was recorded onto VHS tape by way of video camera. Still images were then captured from the VHS video recording using computer video processing hardware and software. Near

the end of the low-pressure testing phase, a high-definition digital video camera became available for capturing Schlieren images. The high definition camera provides much higher resolution images than the VHS-based system. The high definition camera provided most of the images presented in this thesis. Note that in each compound aerospike nozzle Schlieren photograph, a black radial line has been superimposed onto the photograph to indicate the axis of symmetry of the secondary port. The axial location of the superimposed line is somewhat arbitrary, however it is placed as close axially as possible to the secondary port axis of symmetry within the resolution that the word processing software would allow.

Air Supply

A 75 horsepower Ingersoll-Rand air compressor charges two large, outdoor holding tanks to 125 psig. The tanks provide approximately 2000 cubic feet of volume. The pressurized supply air is then piped into the test lab. Here, it passes through a shut-off valve then into an ASME specification orifice flow meter calibrated to measure flow rate passing into the test stand. Air flow into the test stand is throttled by a servo-controlled ball valve. The servo-controlled ball valve is in turn controlled by computer. **Figure 1** shows layout and components of the supply air system.

Test Stand

Once through the electronic ball valve, supply air enters the test stand. The test stand is instrumented with six miniature tension-compression load cells. Three load cells are oriented axially and three load cells are oriented radially to produce three force measurements and three moment measurements. Significant effort has been made to decouple the test stand from the inlet air pipes through the use of externally pressurized bellows couplers and a specially designed inlet plenum to eliminate momentum and pressure effects of the supply air flow. The test stand development effort resulted in a patent on the test stand (Carpenter & Gerhardt 1998). The plenum and test stand are shown in **Figure 2** and the six-component thrust stand is shown in **Figure 3**.

Data Acquisition

Pressure transducers and force transducers on the test stand are monitored by a Fluke *Helios Plus* Data Acquisition System. A computer records and stores these measurements. The raw data files are post-processed by Microsoft Excel macros written and refined during years of previous experiments to produce meaningful results. The output of the Excel macros are the results reported in this thesis.

Testing Procedure

A strict procedure was developed to test nozzles safely. Before any air is flowed, condensed moisture is drained from the holding tanks to prevent it from entering the test lab. Then, the servo ball valve is powered on as well as the data acquisition system and computer. Once the control equipment is running and the electronic valves are verified to be closed, the shutoff valve is opened allowing pressurized air to enter the system. Next, a test nozzle is mounted in the test stand and secured with four set screws. Immediately before the servo ball valve is activated, the computer data collection software is initialized to collect baseline measurements for later comparison. Now the servo-controlled ball valve is opened, allowing supply air to flow through the nozzle. Data is collected for 20-30 seconds at a rate of one data point per second across all channels after pressure stabilizes to allow enough readings for good averaging. The data collection is stopped just before the electronic valve is closed, shutting off air flow. Additional detail is documented in cold-flow testing done by Rossi (1994).

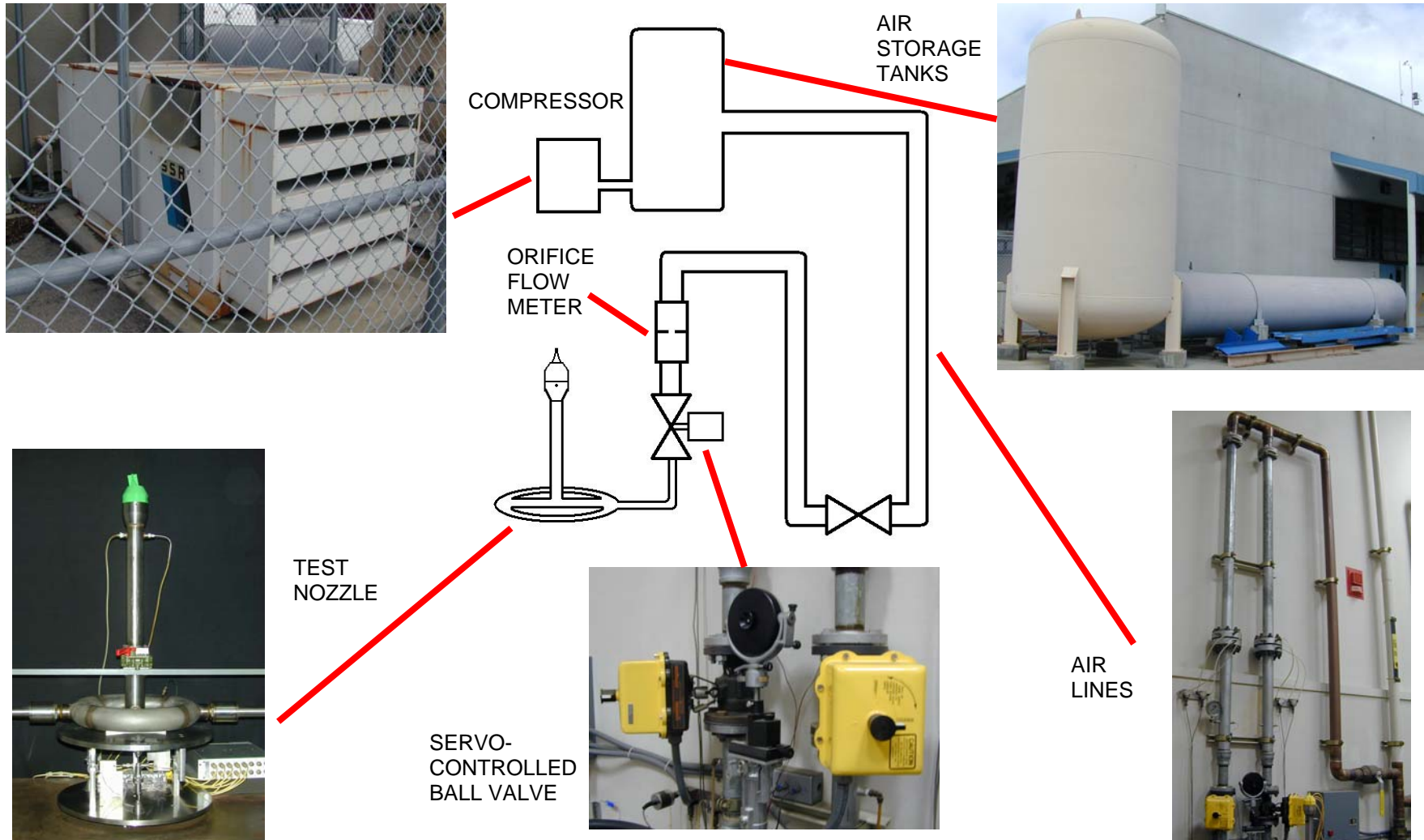


Figure 1. Layout of supply air system showing individual components.

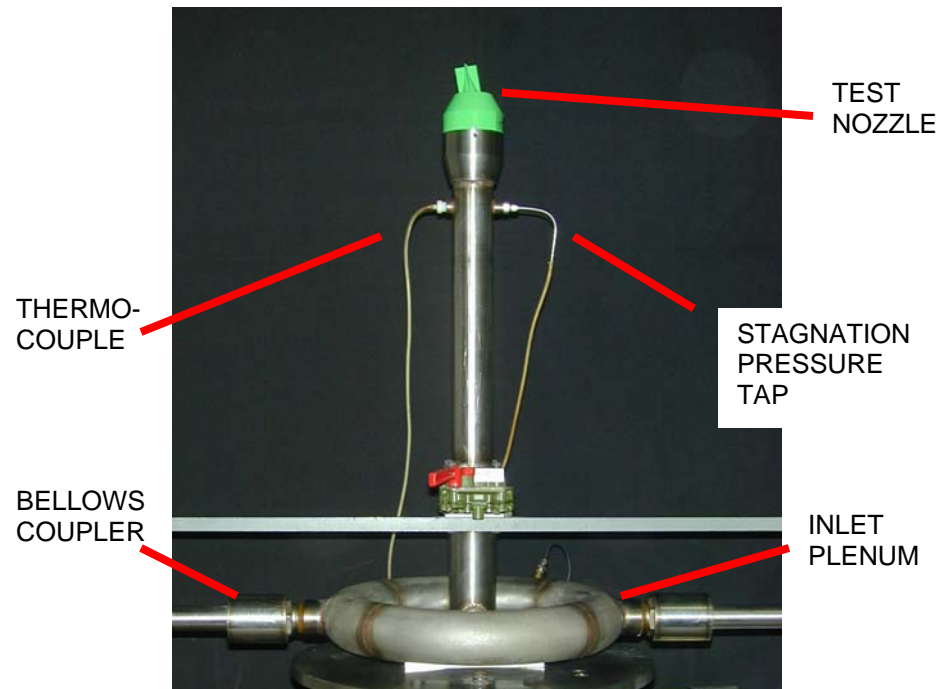


Figure 2. Test stand showing bellows, plenum, and a test nozzle mounted. Just below the nozzle can be seen stagnation pressure and temperature probes.

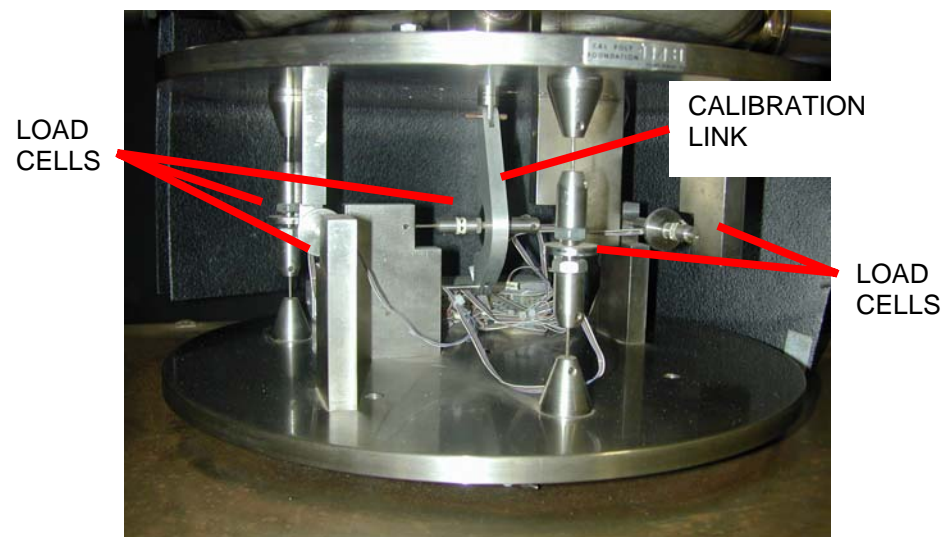


Figure 3. Load cells at base of test platform. Nozzle and plenum are supported entirely by these load cells. Hanging from the center can be seen a link from which weights are hung for calibration.

3. Nozzle Design

Aerospike Design/Theory

The specific geometry of the aerospike profile is governed by the expansion of the supersonic exhaust from the nozzle. A Fortran computer program was developed by NASA in 1964 to determine the aerospike cross-section profile and published in a technical memorandum (Lee & Thompson, 1964) and used herein. The program utilizes simplified one-dimensional isentropic Prandtl-Meyer wave expansion concepts. The program generates a list of radial and axial coordinate points defining the aerospike nozzle throat lip angle and aerospike cross-section profile from eight input parameters. The details of the Fortran program are described at length in the NASA technical memorandum. Two additional examples of aerospike cross-section approximation can be found by Rao (1961) and Greer (1960), which use similar techniques.

The aerospike nozzles used in these experiments were arbitrarily scaled to be of somewhat similar overall size to fit the test stand. The aerospike nozzles presented in this thesis are described by a dimensionless characteristic termed “nozzle pressure ratio” (NPR). Nozzle pressure ratio is the ratio of chamber pressure to ambient pressure. During data collection the NPR value was recorded as “Right NPR” to indicate it as being the NPR value recorded for the right hand inlet plenum of the dual plenum capable test stand. Since only the right hand inlet plenum was utilized during testing, “Right NPR” will simply be referred to as “NPR”.

In this thesis, all the nozzles tested were designed to operate at atmospheric pressure. Thus, if a nozzle is described as having a nozzle pressure ratio of 6 (i.e., NPR6), it is a nozzle designed for ideal operation at atmospheric pressure, a chamber pressure of 6 atmospheres and the exhaust flow is fully expanded to atmospheric pressure. Three NPRs were chosen for testing: NPR6, NPR20 and NPR50. NPR6 was chosen to provide a nozzle that could be tested at full design pressure of around 88 psig. Parenthetically, the large aerospike throat area of the NPR6 nozzles proved to be at the upper flow rate limit of the flow bench. The NPR20 design was chosen to provide preliminary data for future high-pressure and hot-fire testing planned during later phases of the STTR. The NPR50 was chosen to share the design parameter of solid-fuel aerospike rocket flight tests done by Trong Bui from NASA's Dryden Flight Research Center in March, 2004 (NASA 2004). The highest test NPR value recorded during testing was approximately 7.7 and thus the NPR20 and NPR50 nozzles are considered to be operating at over-expanded conditions. Technical drawings of the test nozzles are included in Appendix C.

Thrust Vectoring Design

Initial thrust-vectoring experiments with gimbaled aerospike nozzles (Rohlik, 2008) showed that the addition of fins to the aerospike were required for gimbaling to produce effective thrust vectoring. However, the annular geometry of the aerospike nozzle design makes thrust vectoring by gimbaling a finned aerospike significantly more complex than gimbaling a conventional nozzle. The

support of the aerospike in particular presents a challenge due to high mechanical and thermal stresses. A non-gimbaled aerospike would avoid these complexities and it was felt that a compound aerospike nozzle formed by the addition of a secondary port would provide a more effective and simple solution, and further tests were conducted.

4. Initial Testing

Initial Hole-Type Compound Aerospike Nozzle

Shown in **Figure 4** is a diagram to clarify the terms that will be used to describe the compound aerospike nozzle geometric features.

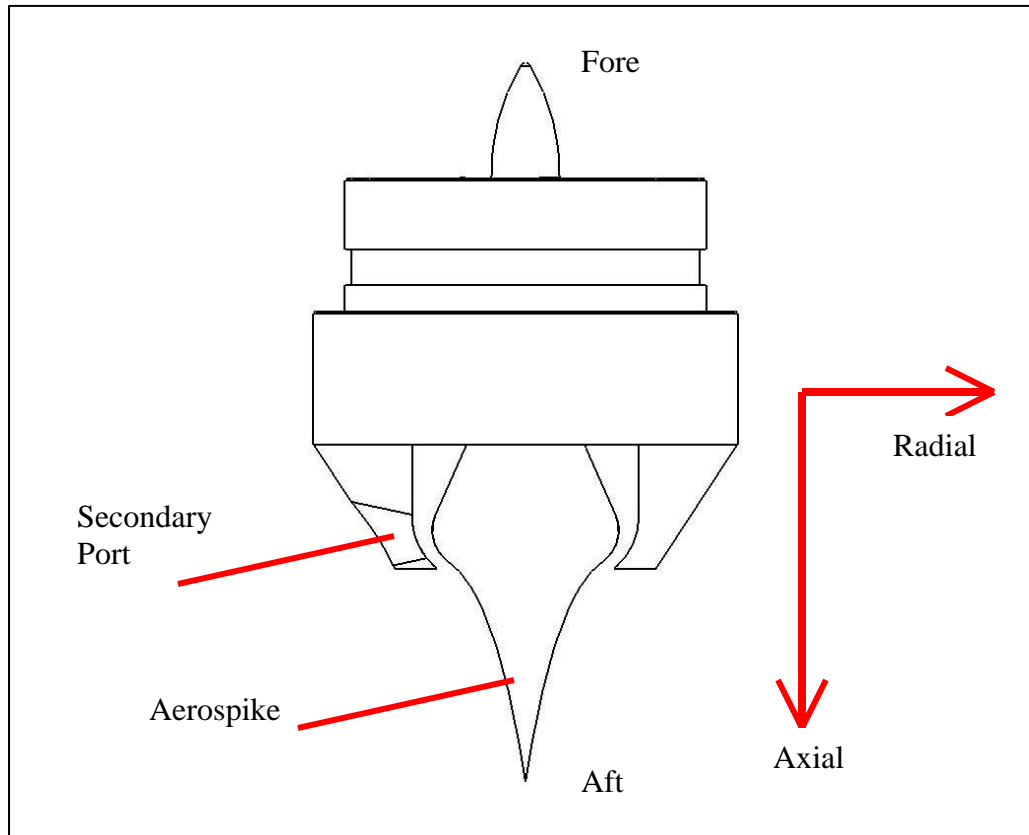


Figure 4. Diagram of terms describing compound aerospike nozzle geometry.

The initial configuration of hole-type compound aerospike nozzle, named “NPR20 Hole”, is shown in **Figure 5**. The axial location and geometry of the secondary port features were chosen somewhat arbitrarily. A Schlieren photograph and a cross-section drawing of NPR20 Hole are shown in **Figure 6**. The secondary port is axisymmetric with its central axis oriented radially with a

3.1° divergence half-angle. A technical drawing of NPR20 Hole is included in Appendix B to show geometric details of the nozzle.



Figure 5. Initial hole-type compound aerospike nozzle configuration.

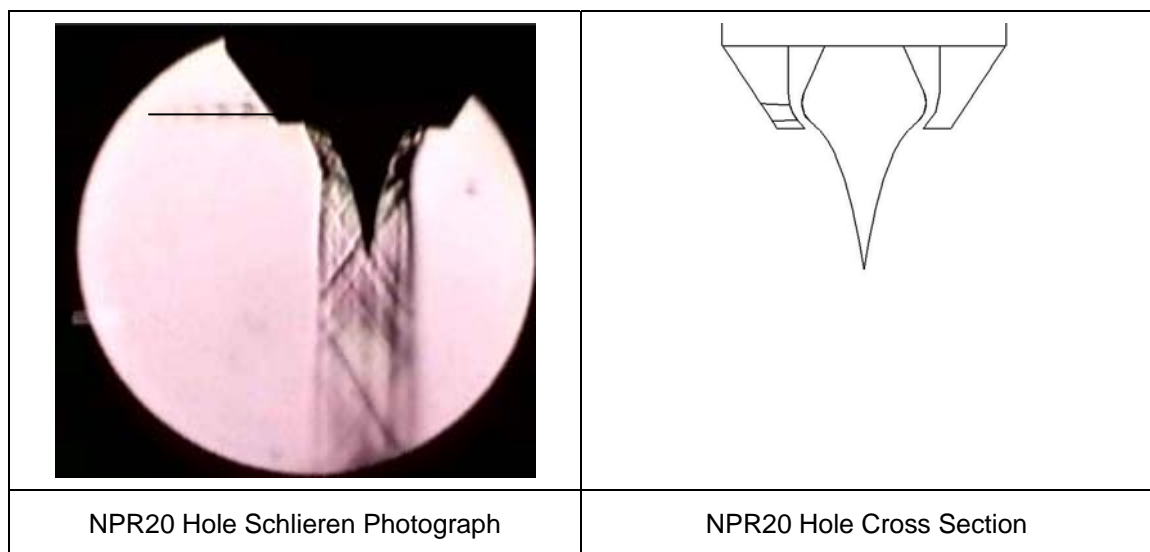


Figure 6. “NPR20 Hole” Schlieren photograph and cross-section drawing represents the initial configuration of hole-type aerospike compound nozzle. Secondary port is a 3.1° half-angle nozzle.

Visible in the Schlieren photograph of **Figure 6**, the secondary port is experiencing supersonic flow as evidenced by the pattern of shock waves. NPR20 Hole produced approximately 3.6° of resultant turn angle, which is well short of the 10° required for effective thrust vectoring. The resultant turn angle is calculated by the vector sum of forces produced by the aerospike nozzle and secondary port. Further details of resultant turn angle calculation is described in chapter seven "Nozzle Performance." It should be noted that the rough surface of the RP nozzle has introduced many small shock waves, giving the aerospike nozzle flow a "rough" appearance in the Schlieren photograph in **Figure 6**.

5. Pressure Distribution on Nozzle Wall

In order to characterize nozzle flow approaching the aerospike throat, four test runs were performed with an aerospike nozzle equipped with ten pressure taps to measure static pressure along the outside nozzle wall. Pressure tap “P1” was located 0.036 in. axially forward of the aerospike nozzle throat lip, with each successive pressure tap approximately 0.05 in. forward from the previous. The pressure tap instrumented nozzle is shown in **Figure 7**. Pressure tap data are presented in **Table 2** and these data are shown graphically in **Figure 8**. It can be observed that the static pressure measured at the nozzle wall decreases as the flow approaches the throat, which is expected as the velocity increases.



Figure 7. Pressure tap equipped NPR20 nozzle.

Table 2. Pressure distribution along nozzle wall.

	P1 (psig)	P2 (psig)	P3 (psig)	P4 (psig)	P5 (psig)	P6 (psig)	P7 (psig)	P8 (psig)	P9 (psig)	P10 (psig)
Axial Location (in)	0.039	0.076	0.118	0.163	0.210	0.260	0.309	0.359	0.409	0.459
RUN # 2105	58.8	79.6	80.8	83.7	84.8	87.3	87.6	88.2	89.6	87.7
RUN # 2106	59.2	80.0	81.3	84.3	85.0	87.7	88.2	88.4	89.8	87.9
RUN # 2107	59.4	80.2	81.0	84.0	85.2	87.7	87.9	88.5	89.9	87.9
RUN # 2108	59.6	80.1	80.8	84.2	85.3	87.6	88.1	88.4	89.8	87.6

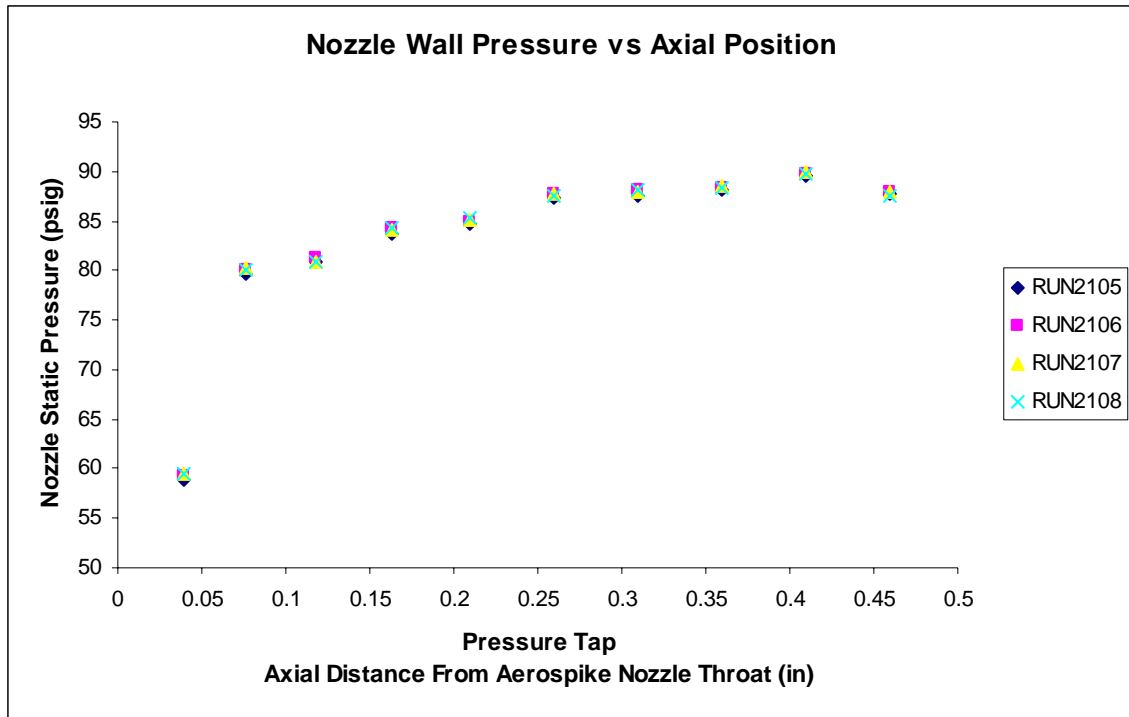


Figure 8. Nozzle Wall Static Pressure versus Axial Position Pressure Tap Results.

The absence of flow disturbances or a localized region of high pressure on the nozzle wall allows placement of the compound nozzle where geometric or other considerations allow. These pressure tap data also show that the static pressure of the flow as it approaches the throat is decreasing in relation to the total (chamber) pressure, especially nearing 0.05 in. upstream of the throat. The drop in static pressure indicates that the flow is developing kinetic energy. Chamber pressure during these tests measured about 104 psig, which translates to approximately Mach 0.57 at pressure tap “P2” and approximately Mach 0.85 at pressure tap “P1” which indicates that the flow is nearing the transonic range. It should be noted that these pressure readings are not meant to determine the actual velocity within the chamber, but instead to identify any regions of localized, unexpected high pressure (none were found).

6. Test Nozzles

After initial testing showed promising results for the hole-type compound aerospike nozzle configurations, an array of test nozzles was designed. At each of the three NPR values two compound aerospike nozzles were designed and built such that one had twice the secondary port throat area of the other (0.026 in.^2 vs 0.051 in.^2), while axial location of the radially oriented central axis was held constant. All secondary ports were designed to have a 12° half angle conical divergent section. Having the same secondary port geometries would allow direct comparison of the nozzles among themselves and at different NPRs. The array of compound aerospike nozzles along with the non-compound aerospike nozzle of each of the three NPR values is shown in **Table 3**. Schlieren photographs are shown in **Figure 9**, **Figure 10**, **Figure 11**, and **Figure 12**. Using the superimposed radial line as reference, it can be noted that the direction of the secondary port flow does not follow the secondary port axis of symmetry, and can be noted in many of the compound aerospike nozzles. The observation that the secondary port flow does not follow the axis of symmetry of the secondary port is further discussed in the Results section of this thesis.

Three NPR20 aerospike test nozzles were machined from aluminum and stainless steel. The aerospike nozzle “NPR20 Straight Metal” was made by Cal Poly ME Master Technician Jim Gerhardt, while the aerospike nozzles “NPR20 Straight Metal (Stan 1)” and “NPR20 Metal Port (Stan 2)” were fabricated by the author and are very similar to Mr. Gerhardt’s. Both of the authors nozzles were made at the same time and are identical with the exception of the hole-type

secondary port machined into the side of “NPR20 Metal Port (Stan 2)”. The intention of “NPR20 Metal Port (Stan 2)” was to duplicate “NPR20 Hole 3” however, a machining error resulted in an unknown secondary port throat diameter. The secondary port throat of “NPR20 Metal Port (Stan 2)” is particularly sharp and no effort was made to provide it with a radius. Photographs of the metal NPR20 test aerospike nozzles are shown in **Table 4**. Schlieren photographs of the three metal test aerospike nozzles are shown in **Figure 13**. The lack of flow perturbations caused by RP surface roughness in the aerospike nozzle flow can be noted in the Schlieren photographs of the metal nozzles. Also in the Schlieren photograph of compound aerospike nozzle “NPR20 Metal Port (Stan 2)” the axisymmetric, radial direction of the secondary port flow and the introduction of small flow perturbations into the aerospike nozzle flow can be seen. Metal nozzle results are further discussed in the Results section of this thesis.

Table 3. Photos of test nozzles.



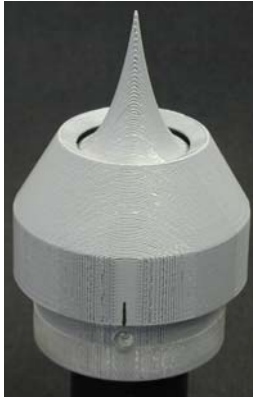







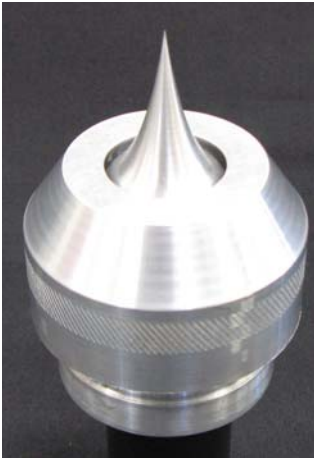
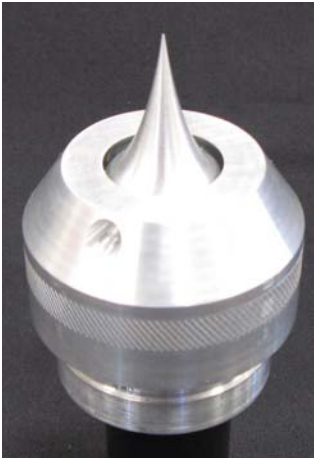
	NPR 6 Nozzles	NPR 20 Nozzles	NPR 50 Nozzles
Non-Compound Aerospike Nozzles			
	NPR6 Straight	NPR20 Straight	NPR50 Straight
Large Secondary Port Compound Aerospike Nozzles			
	NPR6 Hole 2	NPR20 Hole 2	NPR50 Hole 2
Small Secondary Port Compound Aerospike Nozzles			
	NPR6 Hole 3	NPR20 Hole 3	NPR50 Hole 3

Table 4. Photos of metal test aerospike nozzles

		
NPR20 Straight Metal	NPR20 Straight Metal (Stan 1)	NPR20 Metal Port (Stan 2)

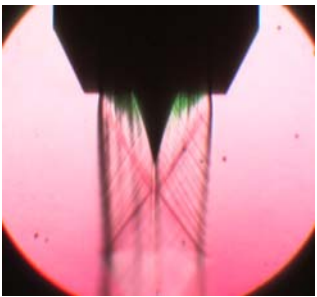

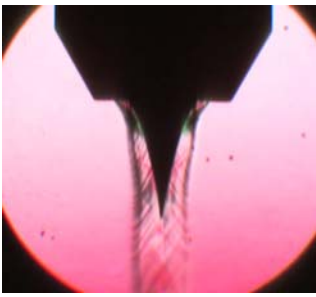
		
NPR6 Straight	NPR20 Straight	NPR50 Straight

Figure 9. Schlieren photographs of non-compound aerospike nozzles.

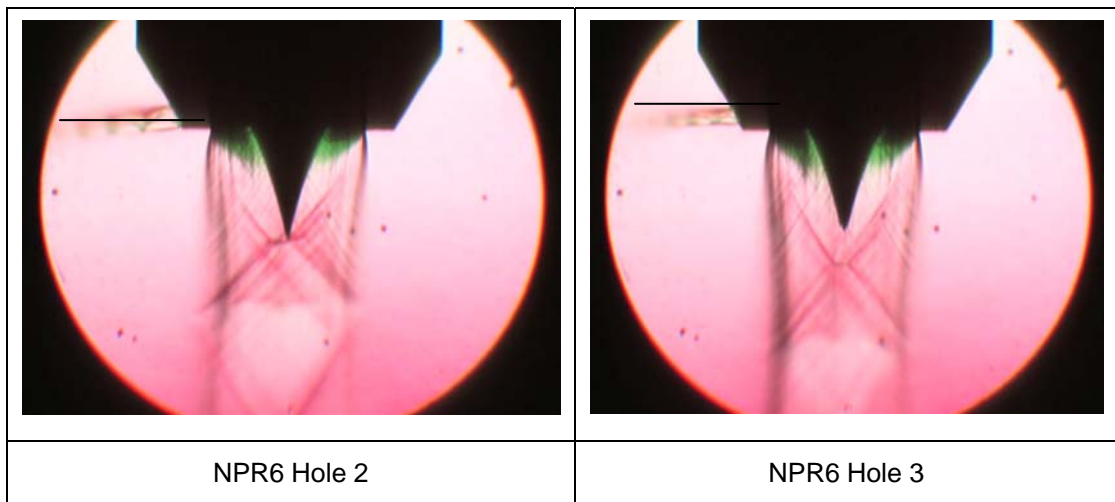


Figure 10. Schlieren photographs of NPR6 compound nozzles. Note non-radial flow direction of secondary port.

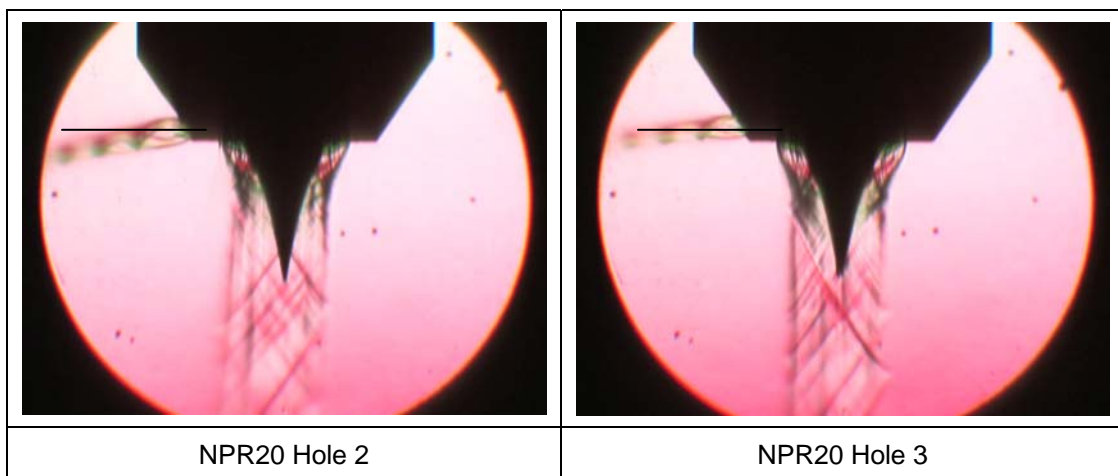


Figure 11. Schlieren photographs of NPR20 compound nozzles, no inlet radius. Note non-radial flow direction of secondary port.

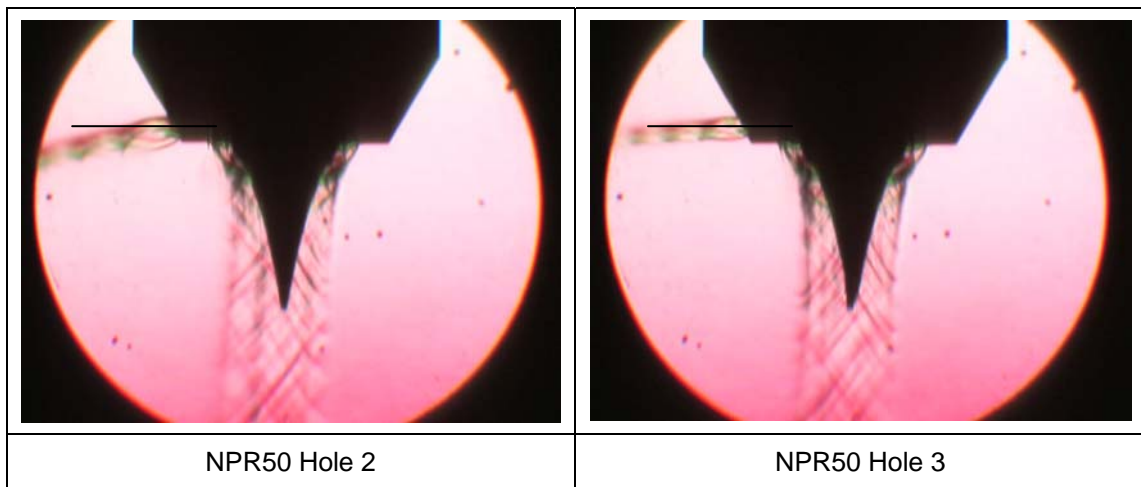


Figure 12. Schlieren photographs of NPR50 compound aerospike nozzles. Note the non-radial direction of secondary port flow.

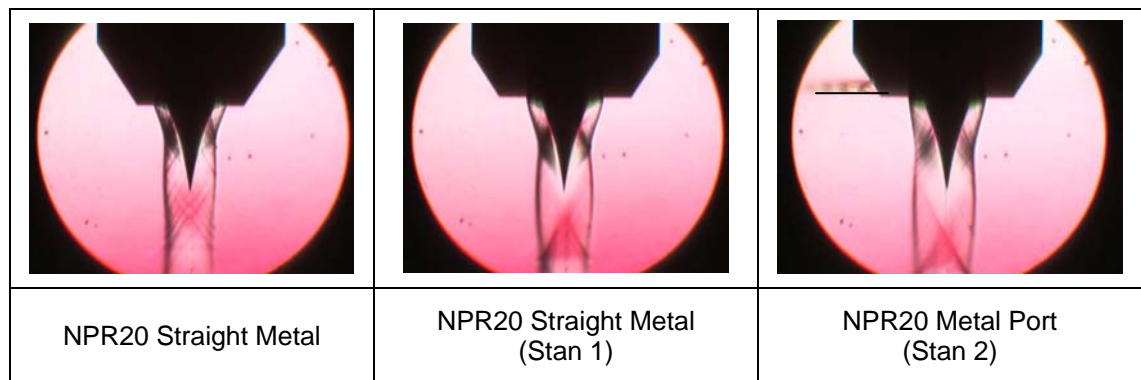


Figure 13. Schlieren photographs of NPR20 metal aerospike nozzles. Aerospike nozzle “NPR20 Straight Metal (Stan 1)” and compound aerospike nozzle “NPR20 Metal Port (Stan 2)” are of the same design and construction with the exception of the addition of a hole-type secondary port to “NPR20 Metal Port (Stan 2)”.

The intersection of the secondary port and the aerospike nozzle inner wall is of particular importance as the throat of the secondary port is defined by the geometry in this location. The secondary port inlet is also formed by a sharp edge. With the addition of aerodynamic disturbances near the throat of the secondary port, it is unknown how this will affect the transonic secondary port flow.

In order to observe the effect of minimizing the sharp inlet region of the secondary port, a set of test nozzles was made with a radius provided on the inlet of the secondary port. Nozzle “NPR20 Hole 3” was modified to have secondary port inlet radii of 0.025 in., 0.050 in., and 0.075 in. to become “NPR20 Hole 7”, “NPR20 Hole 5”, and “NPR20 Hole 6”, respectively. The outward appearance of these compound aerospike nozzles is identical, thus individual photos have been omitted for the sake of brevity. **Figure 14** shows the Schlieren photographs of the compound aerospike nozzles with secondary port inlet radii.

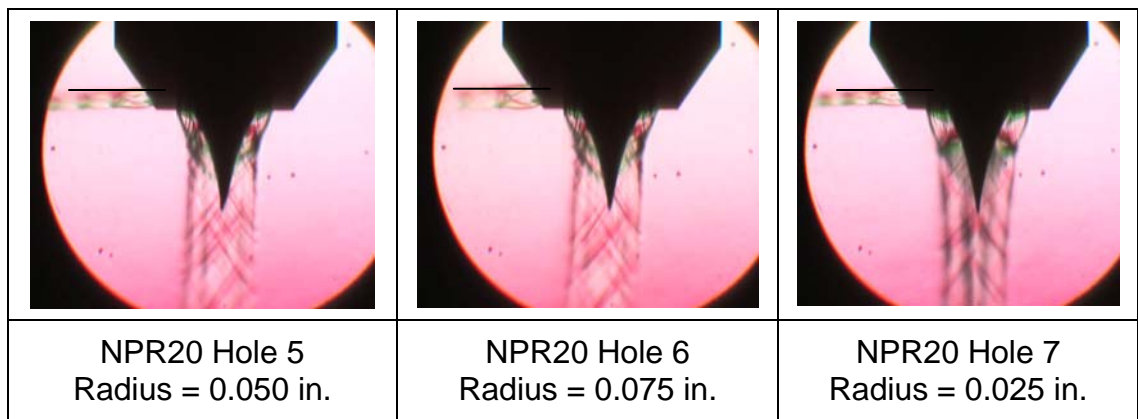


Figure 14. Schlieren photographs of NPR20 compound aerospike nozzles with secondary port inlet radii. Note improvement in radial direction of secondary port flow.

7. Nozzle Performance

Chamber Pressure Variations

For each compound and non-compound aerospike nozzle, a series of tests was performed in which the servo-controlled ball valve was used to throttle the air flow into the test stand. Throttled air flow resulted in a change in nozzle chamber pressure. Five increments of chamber pressure were tested that ranged from the smallest possible flow through the servo-controlled ball valve to fully open. The results of these experiments are shown in **Figure 15** as a graph of resultant turn angle versus chamber pressure (NPR). It should be noted that the servo-controlled ball valve positions were chosen without consideration of the resultant chamber pressure as the qualitative behavior of the compound aerospike nozzle in response to varying chamber pressure was the desired result of this experiment.

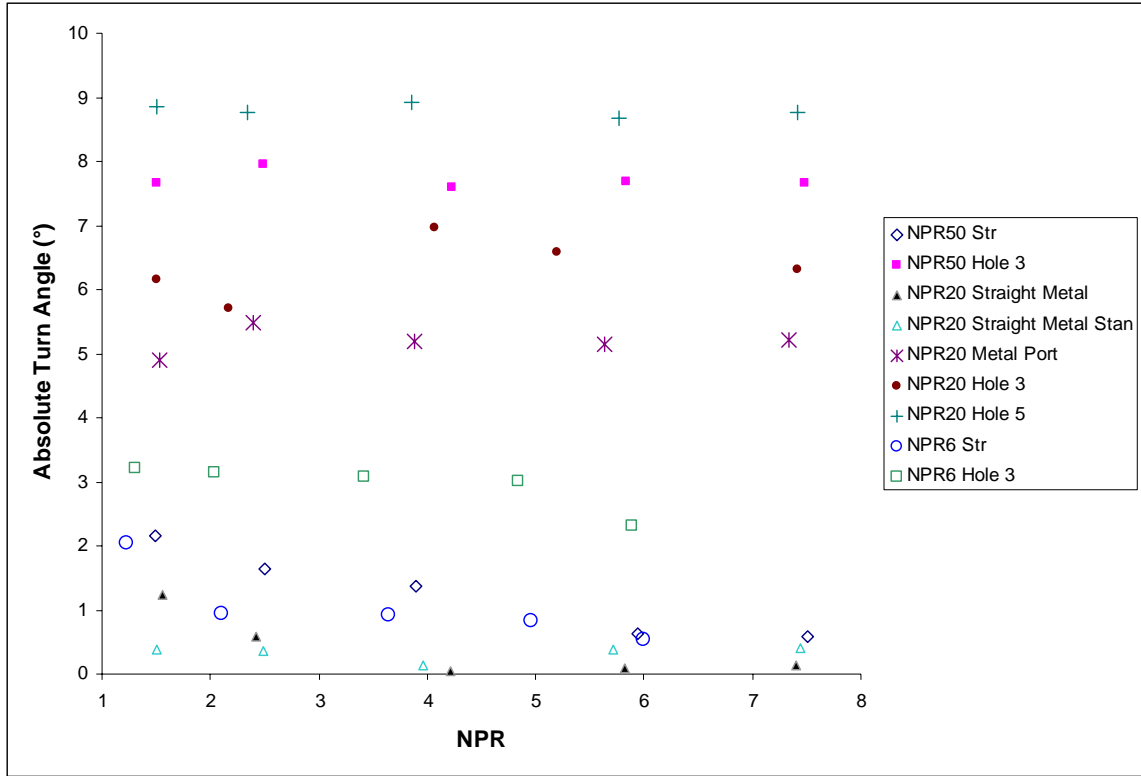


Figure 15. Absolute Turn Angle versus NPR, results of varying chamber pressure.

Turn Angle Prediction

Resultant turn angle (δ_r) is determined by the angle of the resultant vector sum of the aerospike axial force (F_z) and secondary port radial vectoring force (F_{vector}) and is calculated as follows:

$$\text{Equation 1. } \delta_r = \tan^{-1} \left(\frac{F_{vector}}{F_z} \right)$$

A diagram showing the orientation of the aerospike nozzles axial force (F_z) and secondary port radial vectoring force (F_{vector}) relative to the compound aerospike nozzle is shown in **Figure 16**.

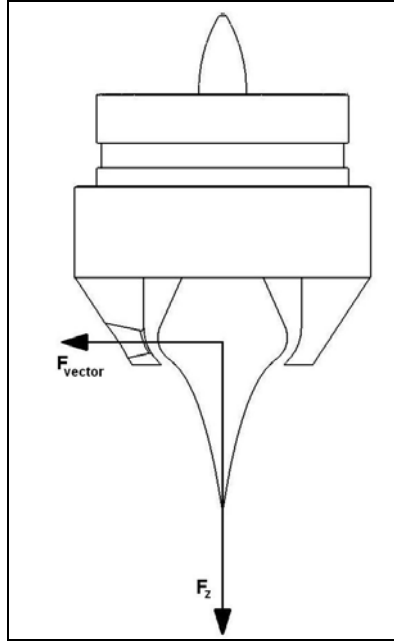


Figure 16. Diagram of compound aerospike nozzle forces (not to scale).

To estimate the resultant turn angle of the compound aerospike nozzles, the CAD models of the nozzles were used to measure secondary port throat area (A_t) and exit area (A_e). Using the measured areas together with the measured chamber pressure (P_1) and chamber temperature (T_1), the radial vectoring force produced by the secondary port (F_{calc}) can be calculated using the equations in Appendix A for each run and compared with the measured radial vectoring force (F_{vector}).

Using NPR values measured during the experiment that varied chamber pressure, the results of these calculations for secondary port radial vectoring force are shown in **Figure 17** through **Figure 20**. Similarly for the aerospike nozzle, using the throat area obtained from the CAD model the axial force produced by the aerospike nozzle (F_z) may be calculated for the actual test NPR values that were also used in calculating secondary port radial vectoring force.

The results of these calculations for aerospike axial force are shown in **Figure 21** through **Figure 24**. Also shown in each figure is a dashed line that represents the critical pressure above which choked flow may form. The critical pressure value (NPR = 1.89) was also used in the calculated turn set and is the lowest NPR value used in the calculations as any lower pressure will not result in supersonic flow.

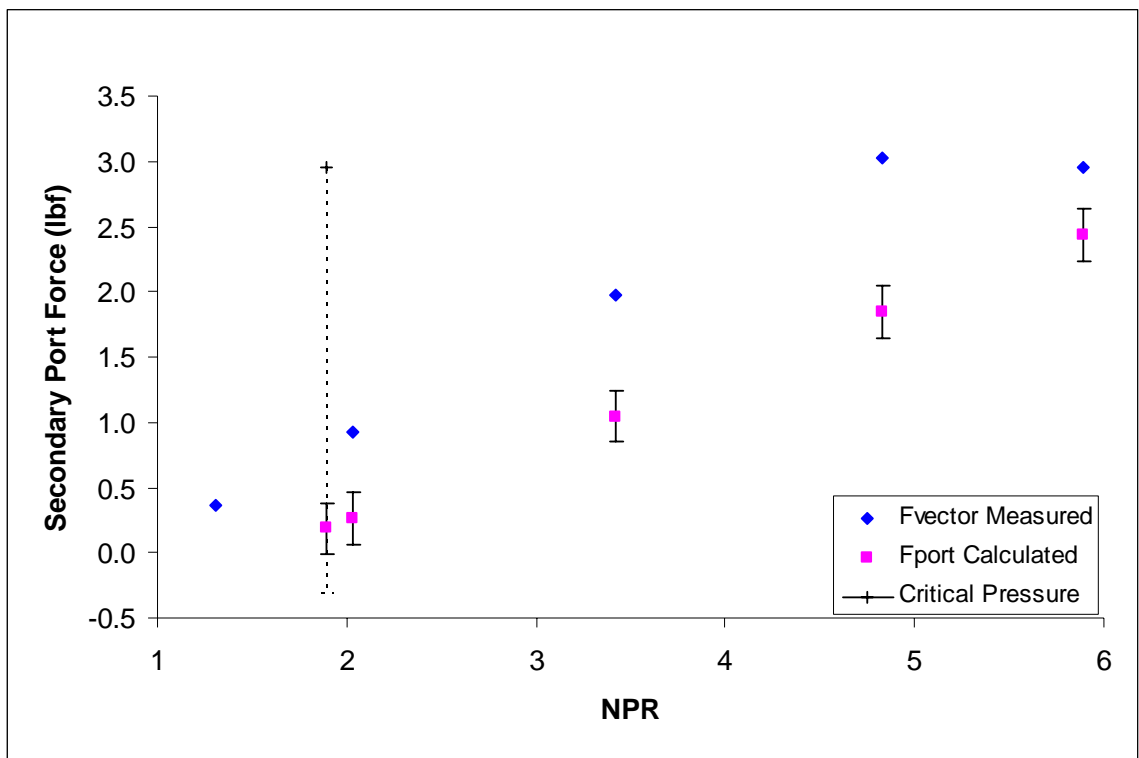


Figure 17. NPR6 Hole 3 Secondary Port Measured and Calculated Radial Vectoring Force versus NPR.

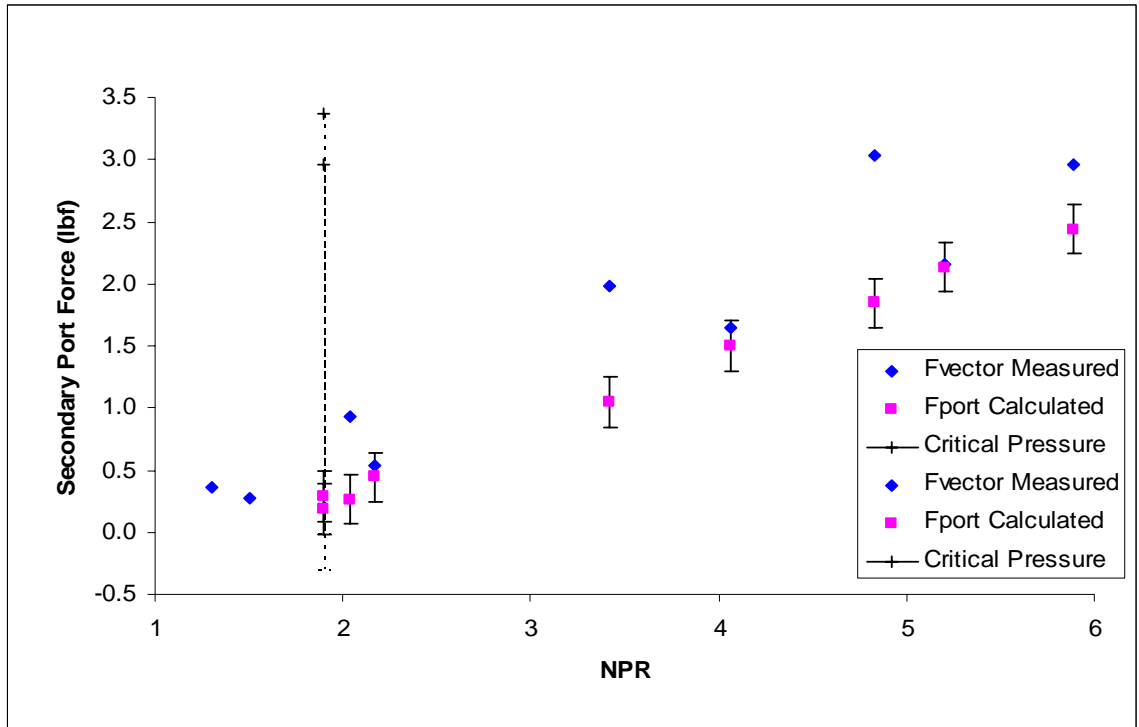


Figure 18. NPR20 Hole 3 Secondary Port Measured and Calculated Radial Vectoring Force versus NPR.

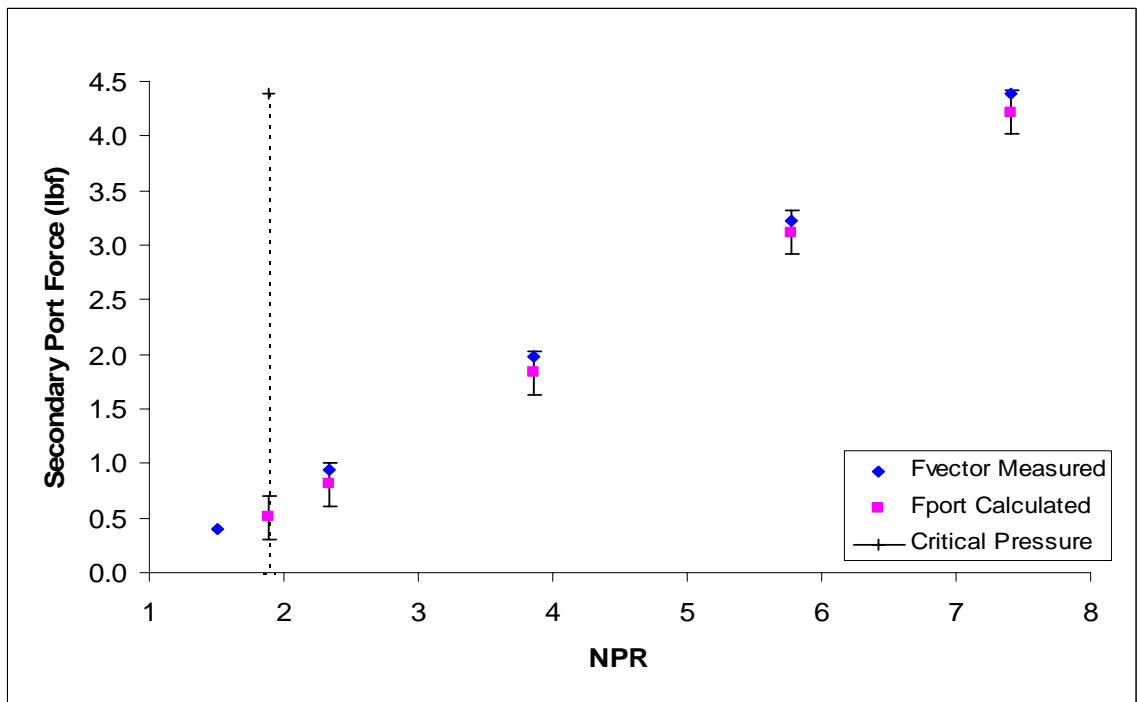


Figure 19. NPR20 Hole 5 Secondary Port Measured and Calculated Radial Vectoring Force versus NPR.

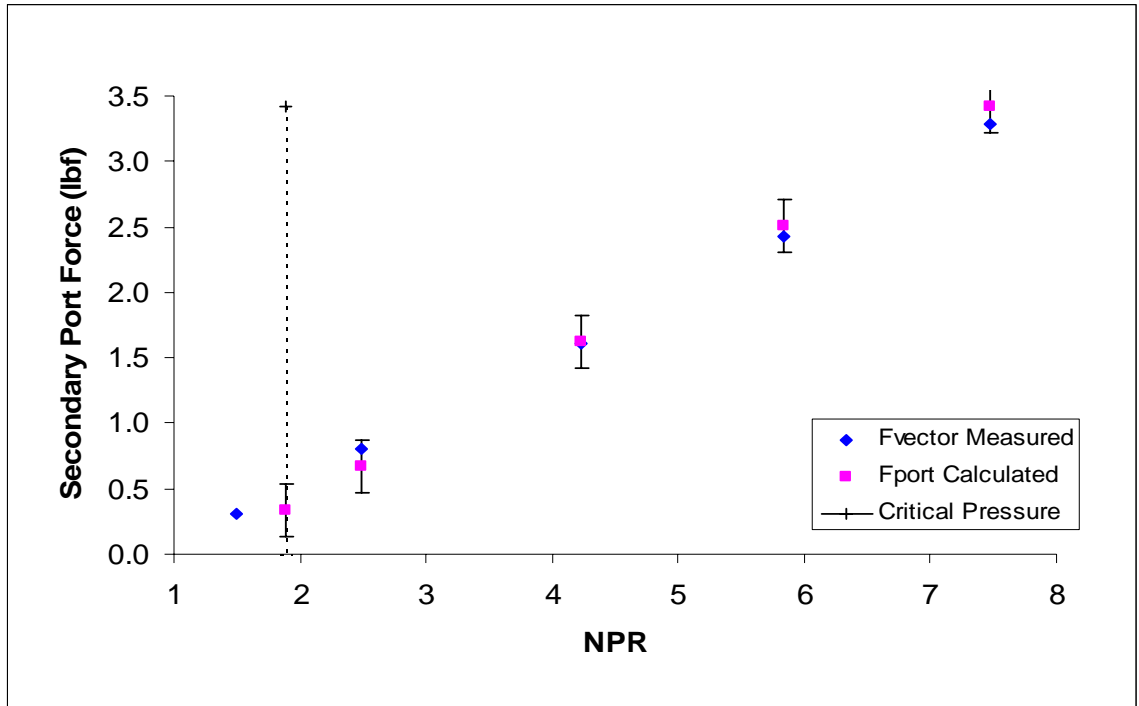


Figure 20. NPR50 Hole 3 Secondary Port Measured and Calculated Radial Vectoring Force versus NPR.

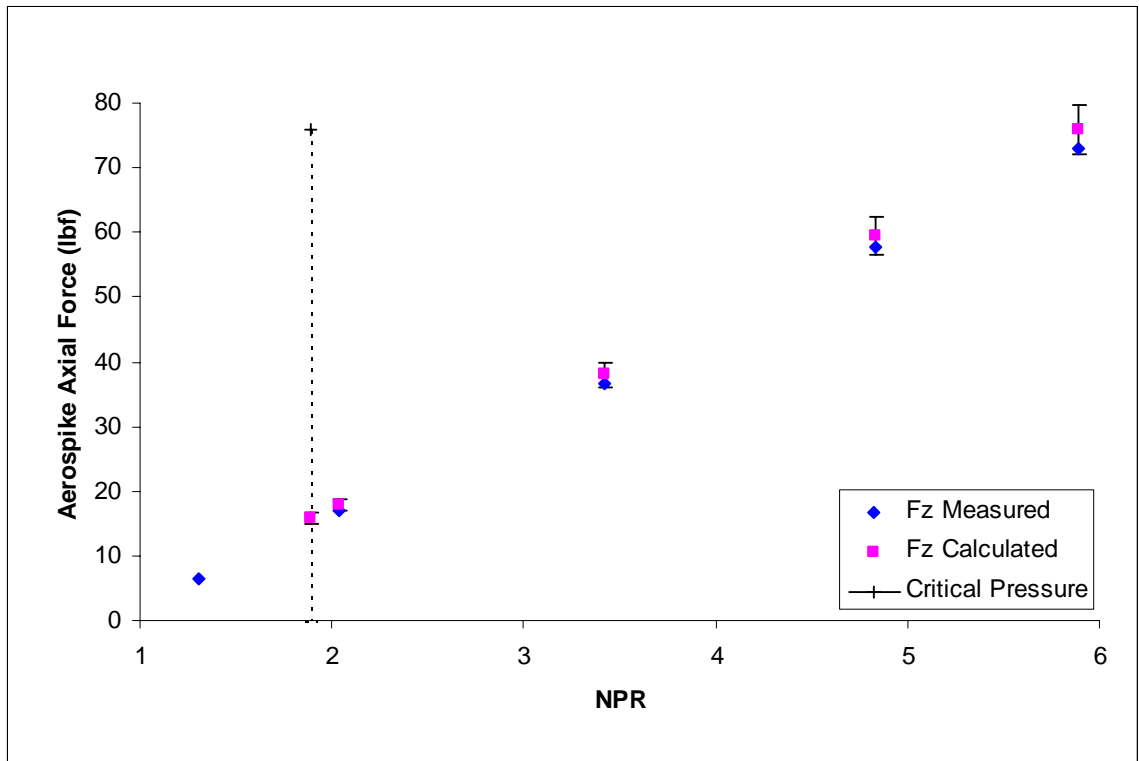


Figure 21. NPR6 Hole 3 Aerospike Nozzle Measured and Calculated Axial Force versus NPR.

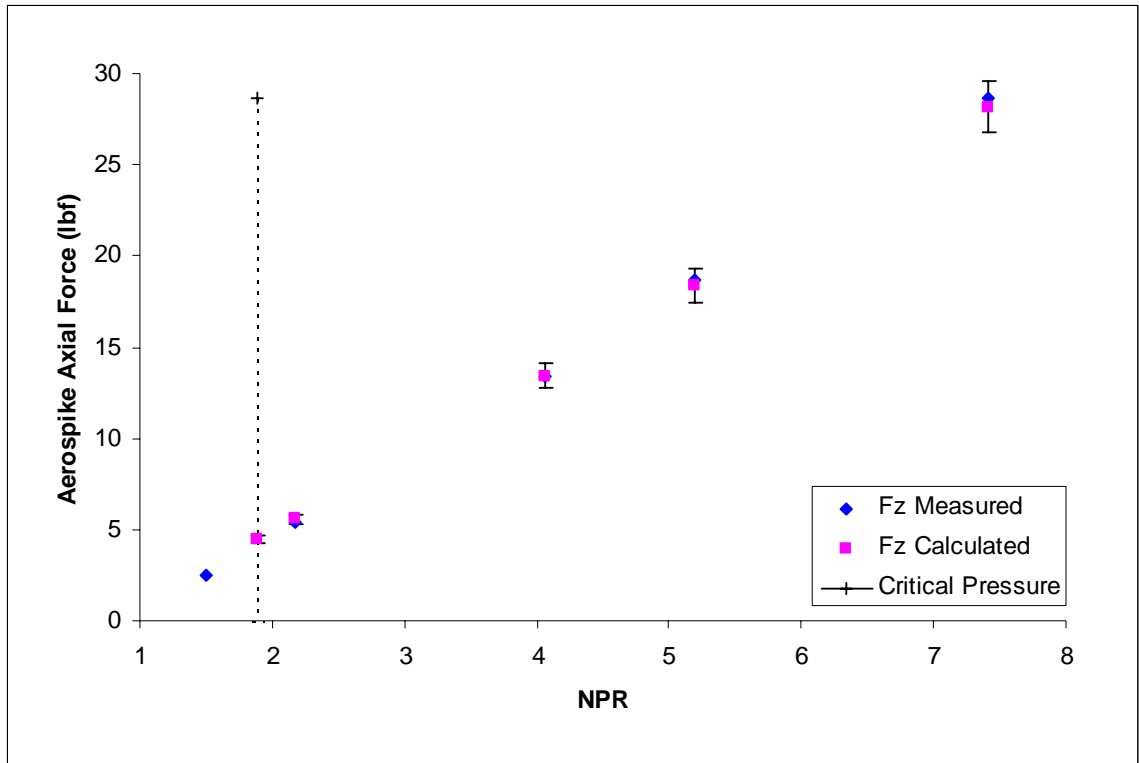


Figure 22. NPR20 Hole 3 Aerospike Nozzle Measured and Calculated Axial Force versus NPR.

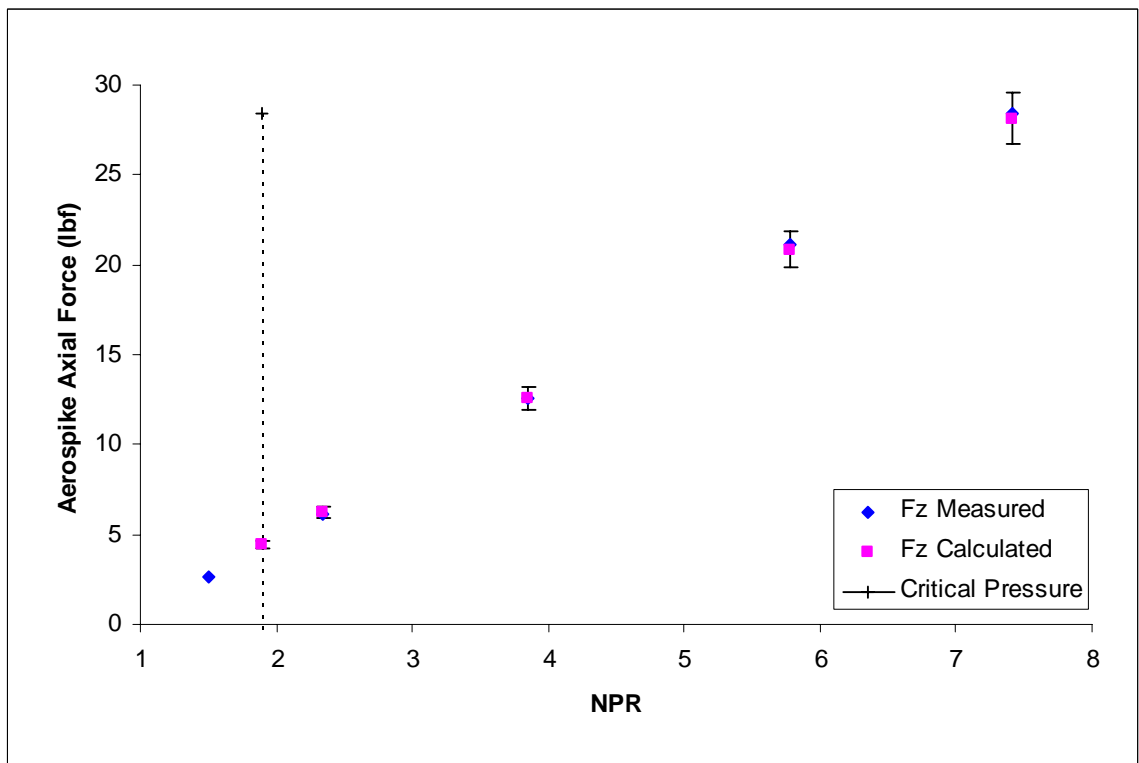


Figure 23. NPR20 Hole 5 Aerospike Nozzle Measured and Calculated Axial Force versus NPR.

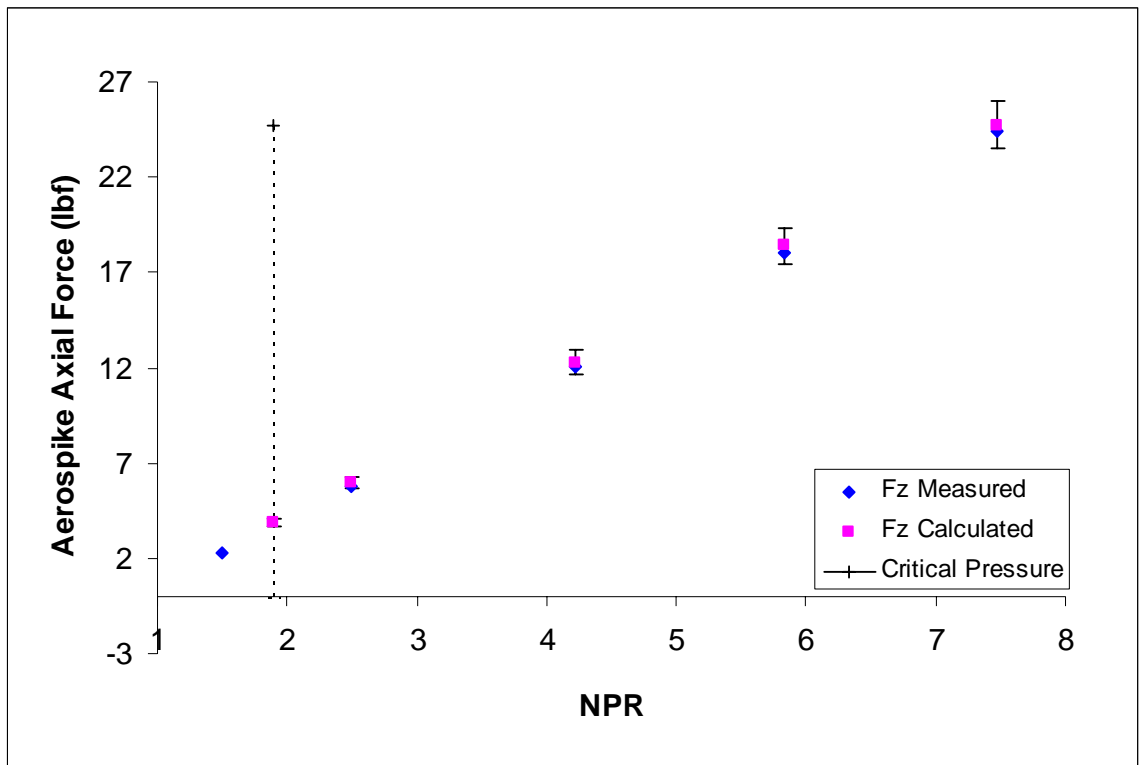


Figure 24. NPR50 Hole 3 Aerospike Nozzle Measured and Calculated Axial Force versus NPR.

To observe the effect of chamber pressure on compound aerospike nozzle resultant turn angle, resultant turn angle (δ_{calc}) was calculated for each NPR value recorded during the experiment that varied chamber pressure. The calculated aerospike compound nozzle resultant turn angle (δ_{calc}) is graphed against NPR alongside the measured absolute values of resultant turn angle (δ_r) for aerospike compound nozzles: NPR6 Hole 3, NPR20 Hole 3, NPR20 Hole 5, NPR50 Hole 3 and shown as **Figure 25**, **Figure 26**, **Figure 27**, and **Figure 28**, respectively.

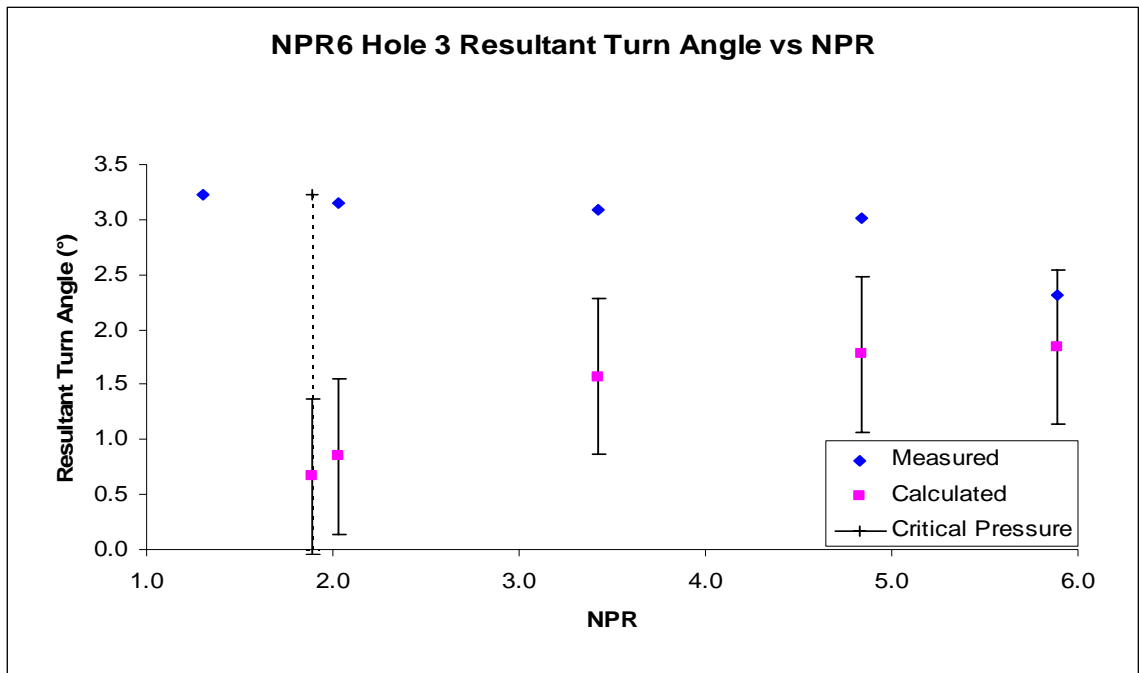


Figure 25. NPR6 Hole 3 Absolute Turn Angle versus NPR comparison of calculated and measured results.

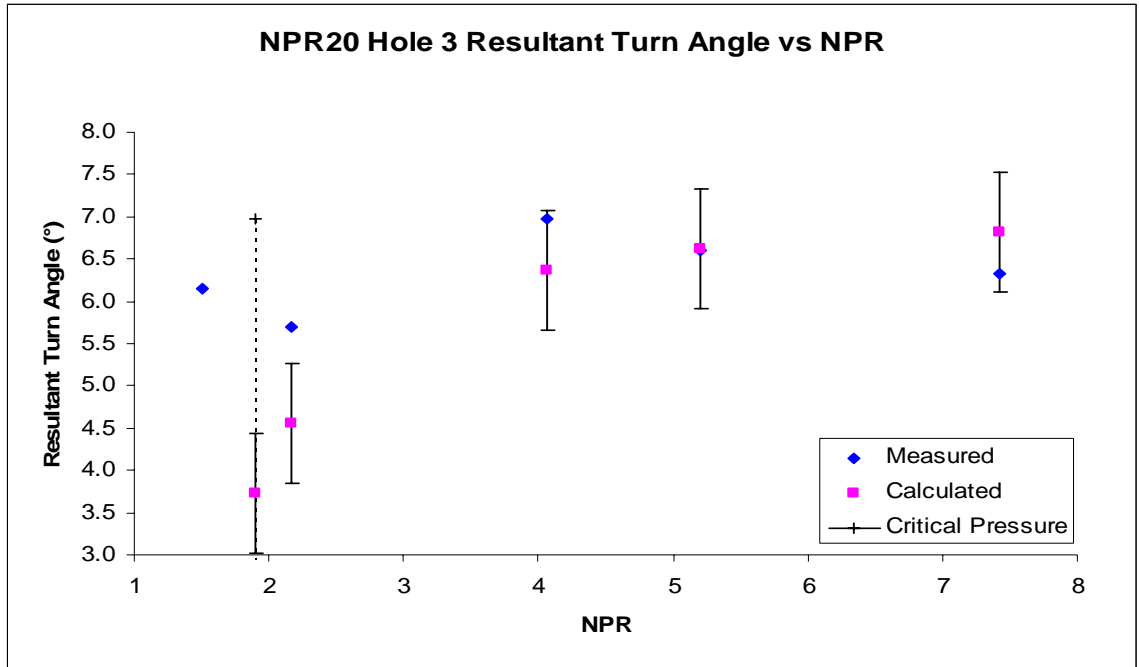


Figure 26. NPR20 Hole 3 Absolute Turn Angle versus NPR comparison of calculated and measured results.

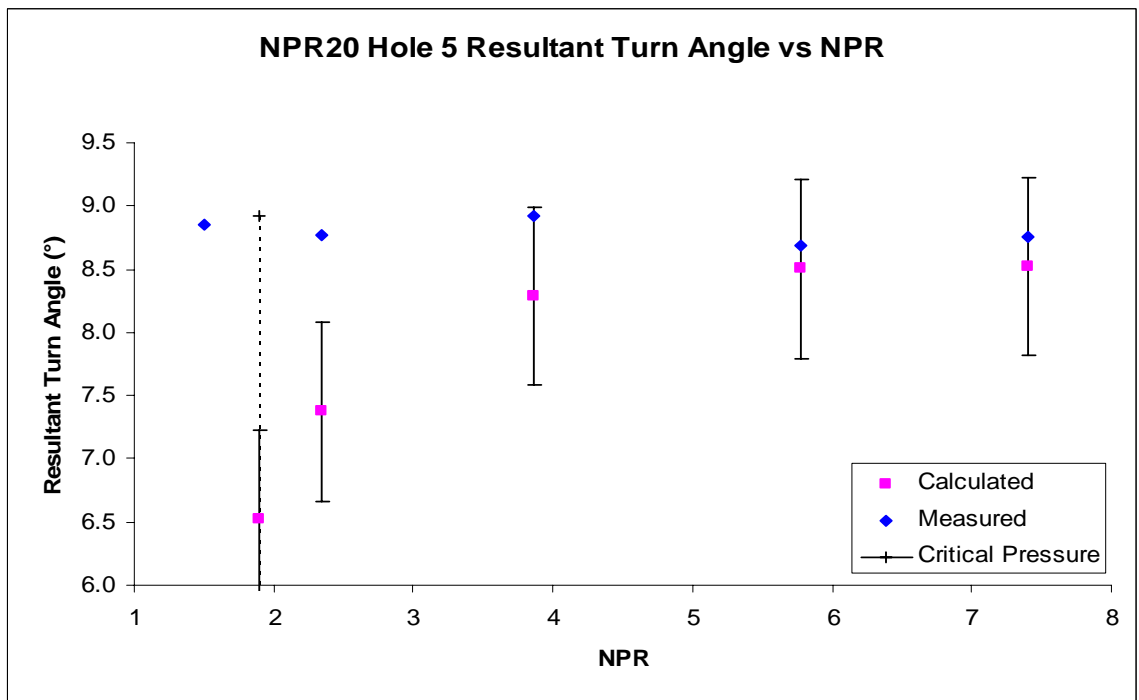


Figure 27. NPR20 Hole 5 Absolute Turn Angle versus NPR comparison of calculated and measured results.

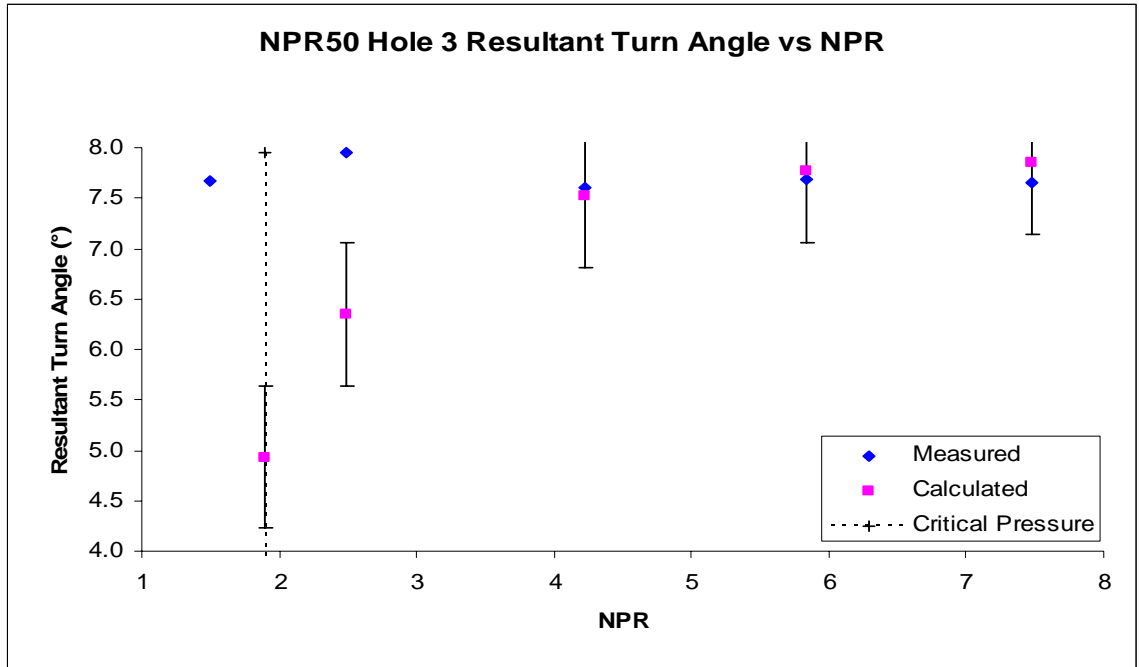


Figure 28. NPR50 Hole 3 Absolute Turn Angle versus NPR comparison of calculated and measured results.

For direct comparison, the calculated secondary port radial vectoring force (F_{calc}) is translated into calculated resultant turn angle (δ_{calc}) by using the calculated aerospike axial force ($F_{z\ Calc}$) and then compared to the measured aerospike axial force (F_z), measured secondary port vectoring force (F_{vector}) and measured resultant turn angle (δ_r). The results for these measured and calculated compound aerospike nozzle forces at each specific NPR value recorded during each test run are shown in **Table 5**.

Table 5. Calculated and measured compound nozzle forces and turn angles.

Run	Nozzle	A _e	A _t	T ₁	P ₁	F _{calc}	F _{z Calc}	F _{vector}	δ _r	δ _{calc}
		in ²	in ²	°F	psi	lbf	lbf	lbf	°	°
2169	NPR6 Hole 2	0.089	0.052	68.43	86.66	5.093	-76.199	5.400	4.229	3.824
2170	NPR6 Hole 2	0.089	0.052	69.21	80.86	4.665	-69.993	4.728	4.009	3.813
2171	NPR6 Hole 3	0.060	0.026	69.89	87.88	2.498	-77.444	3.434	2.644	1.847
2172	NPR6 Hole 3	0.060	0.026	71.59	82.25	2.282	-71.467	3.643	3.020	1.829
2177	NPR20 Hole 2	0.083	0.050	71.17	109.26	6.568	-28.312	5.453	10.777	13.060
2178	NPR20 Hole 2	0.083	0.050	71.59	108.92	6.543	-28.204	5.447	10.704	13.062
2179	NPR20 Hole 2	0.083	0.050	71.86	108.79	6.534	-28.170	5.335	10.587	13.059
2180	NPR20 Hole 3	0.052	0.026	72.05	108.86	3.358	-28.189	3.172	6.227	6.794
2181	NPR20 Hole 3	0.052	0.026	71.32	108.99	3.363	-28.222	3.120	6.132	6.796
2182	NPR20 Hole 3	0.052	0.026	71.50	109.01	3.364	-28.226	2.944	5.839	6.796
2219	NPR20 Hole 5	0.052	0.032	72.79	109.28	4.238	-28.297	4.330	8.509	8.518
2220	NPR20 Hole 5	0.052	0.032	71.50	108.92	4.224	-28.203	4.390	8.641	8.518
2221	NPR20 Hole 6	0.052	0.036	73.20	108.68	4.608	-28.096	4.868	9.710	9.315
2222	NPR20 Hole 6	0.052	0.036	73.42	109.70	4.659	-28.429	4.789	9.417	9.307
2223	NPR20 Hole 7	0.052	0.029	73.80	109.31	3.829	-28.304	4.373	8.699	7.703
2224	NPR20 Hole 7	0.052	0.029	74.51	109.15	3.822	-28.264	4.310	8.573	7.701
2191	NPR50 Hole 2	0.079	0.051	72.88	110.04	6.782	-24.800	5.189	11.755	15.294
2192	NPR50 Hole 2	0.079	0.051	73.18	110.22	6.795	-24.883	5.336	12.035	15.275
2193	NPR50 Hole 2	0.079	0.051	73.53	109.66	6.755	-24.716	5.275	12.015	15.286
2194	NPR50 Hole 3	0.048	0.026	73.59	109.71	3.415	-24.725	3.065	7.110	7.863
2195	NPR50 Hole 3	0.048	0.026	73.91	109.17	3.394	-24.604	3.206	7.496	7.855
2196	NPR50 Hole 3	0.048	0.026	73.18	110.77	3.454	-25.006	3.251	7.486	7.865
2197	NPR50 Hole 3	0.048	0.026	73.38	110.41	3.441	-24.926	3.153	7.275	7.860

8. Results and Conclusions

Summary of Results

Table 6 is a summary of results from the many experiments performed over the course of the research. Each row represents an average of all the data collected for that nozzle. The original data may be found in Appendix C.

Table 6. Tabulated summary of results.

Nozzle Description	NPR	F _x	F _y	F _z	W _p	W _i	F _i	F _r	F _r /F _i	F _z /F _i	W _p /W _i	δ _{pitch}	δ _{yaw}	δ _r
		lb _f	lb _f	lb _f	lb _m / s	lb _m / s	lb _f	lb _f				°	°	°
NPR6 Straight	5.995	-0.419	-0.561	-75.152	1.368	1.408	75.051	75.155	1.001	-1.001	0.971	0.428	0.319	-0.534
NPR6 Hole 1	3.614	-3.935	-0.206	-68.098	1.443	0.939	62.719	68.213	1.089	-1.087	1.543	0.177	3.317	-3.323
NPR6 Hole 2	5.742	-5.055	-0.220	-70.248	1.489	1.489	73.154	70.430	0.963	-0.960	1.000	0.173	4.112	-4.119
NPR6 Hole 3	5.851	-3.337	-0.215	-72.115	1.519	1.532	74.347	72.193	0.971	-0.970	0.991	0.170	2.656	-2.662
NPR20 Straight Metal	7.490	-0.014	-0.032	-25.484	0.489	0.548	25.352	25.484	1.006	-1.006	0.892	0.072	0.032	-0.144
NPR20 Straight	7.411	-0.021	-0.014	-27.548	0.546	0.542	28.331	27.549	0.974	-0.974	1.008	0.032	0.042	-0.451
NPR20 Hole	7.502	-1.776	-0.100	-27.829	0.572	0.550	29.694	27.885	0.939	-0.937	1.041	0.260	3.652	-3.658
NPR20 Hole 2	7.472	-5.411	0.079	-28.669	0.649	0.544	33.681	29.175	0.866	-0.851	1.193	-0.158	10.687	-10.689
NPR20 Hole 3	7.459	-3.139	0.113	-28.923	0.630	0.544	32.704	29.093	0.890	-0.885	1.158	-0.224	6.194	-6.199
NPR20 Hole 5	7.448	-4.358	0.280	-28.757	0.640	0.545	33.192	29.087	0.877	-0.867	1.174	-0.558	8.618	-8.636
NPR20 Hole 6	7.463	-4.828	0.226	-28.691	0.630	0.544	32.742	29.095	0.889	-0.876	1.158	-0.451	9.553	-9.563
NPR20 Hole 7	7.465	-4.336	0.211	-28.586	0.652	0.544	33.946	28.914	0.852	-0.842	1.200	-0.424	8.626	-8.636
NPR20 Straight Metal (Stan 1)	7.453	-0.098	-0.032	-29.831	0.582	0.546	30.126	29.832	0.991	-0.991	1.066	0.062	0.188	-0.200
NPR20 Straight Metal (Stan 2)	7.460	-0.053	0.050	-32.488	0.608	0.546	31.512	32.488	1.032	-1.032	1.114	-0.088	0.092	-0.164
NPR20 Metal Port (Stan 2)	7.331	-2.890	0.000	-31.668	0.655	0.542	33.641	31.799	0.945	-0.941	1.209	0.000	5.214	-5.214
NPR50 STR4	7.600	-0.029	-0.038	-23.266	0.475	0.483	24.840	23.268	0.937	-0.937	0.985	0.091	0.069	-0.614
NPR50 Straight Hole	7.616	-1.944	0.313	-23.445	0.511	0.480	26.841	23.527	0.877	-0.874	1.064	-0.766	4.740	-4.801
NPR50 Hole 2	7.539	-5.266	-0.045	-24.915	0.591	0.476	30.765	25.466	0.828	-0.810	1.239	0.102	11.934	-11.935
NPR50 Hole 3	7.529	-3.179	0.273	-24.556	0.543	0.478	28.203	24.762	0.878	-0.871	1.136	-0.636	7.376	-7.404

NOTE: “NPR20 Straight Metal (Stan 2)” was modified by the addition of a hole to become “NPR20 Metal Port (Stan 2)”.

Flow Behavior and Inlet Radius Results

Axisymmetric, uniform flow from the secondary port has been demonstrated. A radius on the secondary port inlet serves to minimize deflection of the secondary flow off of the radial axis of symmetry.

Schlieren photographs of many of the secondary ports show the secondary port flow angled slightly aft of the radial direction. With the addition of an inlet radius, it is immediately obvious from examining Schlieren photographs that the secondary port flow exhibits improved axial flow symmetry. The Schlieren photographs of radiused-inlet nozzles are shown in **Figure 14**.

The exact cause for the non-radial secondary port flow seen in the nozzles with sharp secondary port inlet edges is not known. It should be noted that all of the sharp inlet secondary port RP compound aerospike test nozzles exhibit some degree of non-radial, aft-deflection of the secondary port flow with larger secondary port throat diameters showing more deflection than the smaller secondary port throat diameters. However, the metal compound aerospike test nozzle “NPR20 Metal Port (Stan 2)” does not show any appreciable deflection of the secondary port flow off of the radial direction, despite the fact that the secondary port inlet is quite sharp.

There is the potential for a pressure gradient to exist across the secondary port inlet. Examination of the CAD models shows the largest NPR20 hole-type secondary port (“NPR20 Hole 2”) to have the secondary port aft throat edge 0.061 in. forward of the aerospike nozzle throat lip. Recalling the pressure tap discussion and results shown in **Figure 8**, at the aft edge of the secondary port throat chamber air velocity is beginning to increase. **Figure 29** shows the

location of the secondary port throat edges of NPR20 Hole 2 relative to the pressure tap data.

Static pressure readings in the chamber of 90 psig equates to a velocity of approximately Mach 0.43 based on the stagnation pressure reading of approximately 104 psig taken immediately forward of the compound aerospike nozzle attachment on the thrust stand. The location of the stagnation pressure tap can be seen on the right in **Figure 7**. The highest pressure from stagnation of any flow entering the secondary port is 104 psig for a difference of 14 psi relative to the 90 psig static chamber pressure reading. Whether or not 14 psi of stagnation pressure gradient within the secondary port is sufficient to redirect the secondary port flow off of the radial axis (as evidenced in the Schlieren photographs in **Figure 10** through **Figure 12**) has not been evaluated and is beyond the scope of this work.

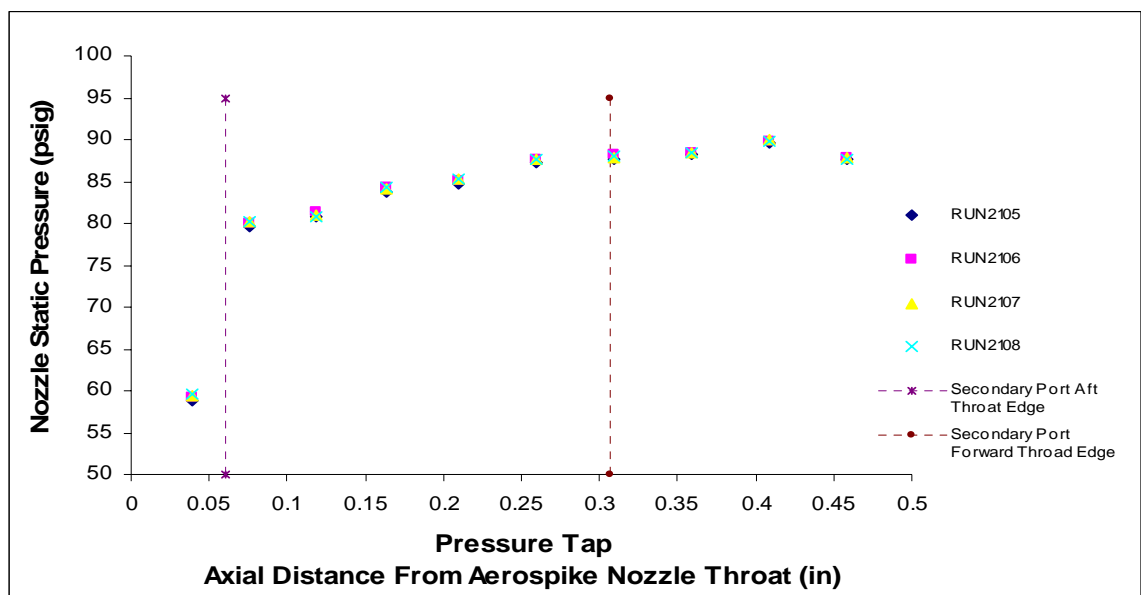


Figure 29. NPR20 Hole 2 pressure distribution at inlet of secondary port. Dashed lines show location of secondary port throat aft and forward edges. Note the possibility of a pressure gradient across the secondary port throat.

Metal Nozzles Results

Special attention should be paid to the shock patterns of the Schlieren photographs in **Figure 30** of “NPR20 Straight Metal (Stan 1)” and “NPR20 Metal Port (Stan 2)”. It appears that “NPR20 Metal Port (Stan 2)” has incurred additional disturbances with a greater number of shock waves visible midway aft on the aerospike. It also appears that the aerospike nozzle flow is no longer radially symmetrical. It is unknown whether these disturbances are the result of the sharp secondary port entrance or from the radially asymmetrical flow of air through the aerospike nozzle throat, as air was diverted out of the secondary port. The Schlieren images of NPR20 Straight Metal (Stan 1) and NPR20 Metal Port (Stan 2) are shown again in larger format in **Figure 30** to show details and are identical to Schlieren photographs shown in **Figure 13**.

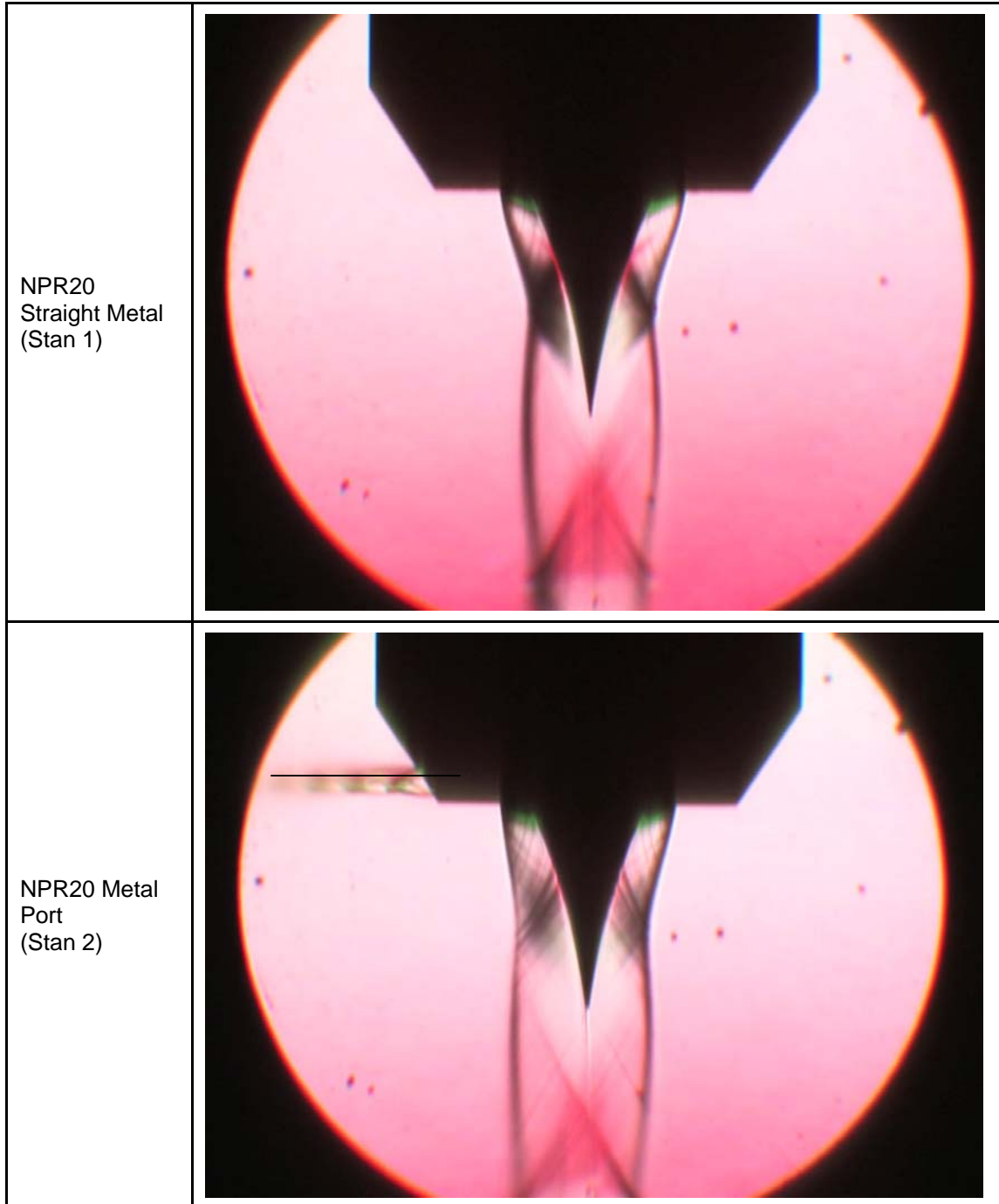


Figure 30. Schlieren photographs of two NPR20 metal nozzles. The two are of the same design and construction with the exception of the hole-type secondary port on “NPR20 Metal Port (Stan 2)”. Note the additional aerospike nozzle flow perturbations on NPR20 Metal Port (Stan 2).

Chamber Pressure and Turn Angle Results

Effective turn angle capability of the hole-type compound nozzle has been demonstrated in both NPR20 and NPR50 nozzles that produced up to 10.7° and 11.9° of turn, respectively. Sufficient inlet radius to provide radial flow is also necessary for good performance predictability.

Test results shown in **Figure 15** indicate that measured turn angle is largely independent of chamber pressure. When compared to calculated turn angle results, the observed linear behavior of turn angle to changing chamber pressure is contrary to what is expected as the thrust produced by both the aerospike nozzle and the secondary port vary linearly with chamber pressure and show good correlation to calculated results. However, nozzle “NPR20 Hole 3” does exhibit a small degree of predicted drop in turn angle as chamber pressure was reduced.

Examination of the graphs of calculated versus measured aerospike nozzle axial force and secondary port radial force shown in **Figure 17** through **Figure 24** show excellent linearity and correlation between measured and calculated results except for NPR 6 Hole 3 secondary port radial force shown in Figure 17, which shows large differences in measured and calculated results.

The excellent correlation between measured and calculated results for aerospike nozzle axial force shown in **Figure 21** through **Figure 24** indicates that the secondary port has no measurable effect on aerospike nozzle performance.

It is suspected that geometrical error resulting from the rapid prototyping process is a significant contributor to poor correlation between measured and calculated results. Thin features and sharp edges are often poorly replicated

during the RP process. The secondary port inlet area in particular is formed by a sharp edge in all but those nozzles with inlet radii. Actual measurement of the secondary port throat diameter to verify the dimension proved impossible.

Compound aerospike nozzles with secondary port inlet radii show good results in terms of predictability as well as flow symmetry. Comparisons between calculated and measured compound aerospike nozzle resultant turn angles on a run-by-run basis are shown in **Table 5** are shown graphically as **Figure 31** through **Figure 33**. Excellent correlation between measured and calculated data can be found in the nozzles with inlet radii (NPR20 Hole 5, 6, and 7) in **Figure 32**. The good correlation observed in nozzles equipped with secondary port inlet radii further reinforces the importance of a smooth inlet region for performance predictability and flow symmetry as also seen in the Schlieren photographs.

Interestingly, the nozzle with the best predictability (NPR20 Hole 5) is designed with the mid-sized secondary port inlet radii (0.050 in.). Without higher resolution nozzles and a test array of inlet radii models, it is uncertain if there is indeed an ideal relationship between secondary port throat size and inlet radius.

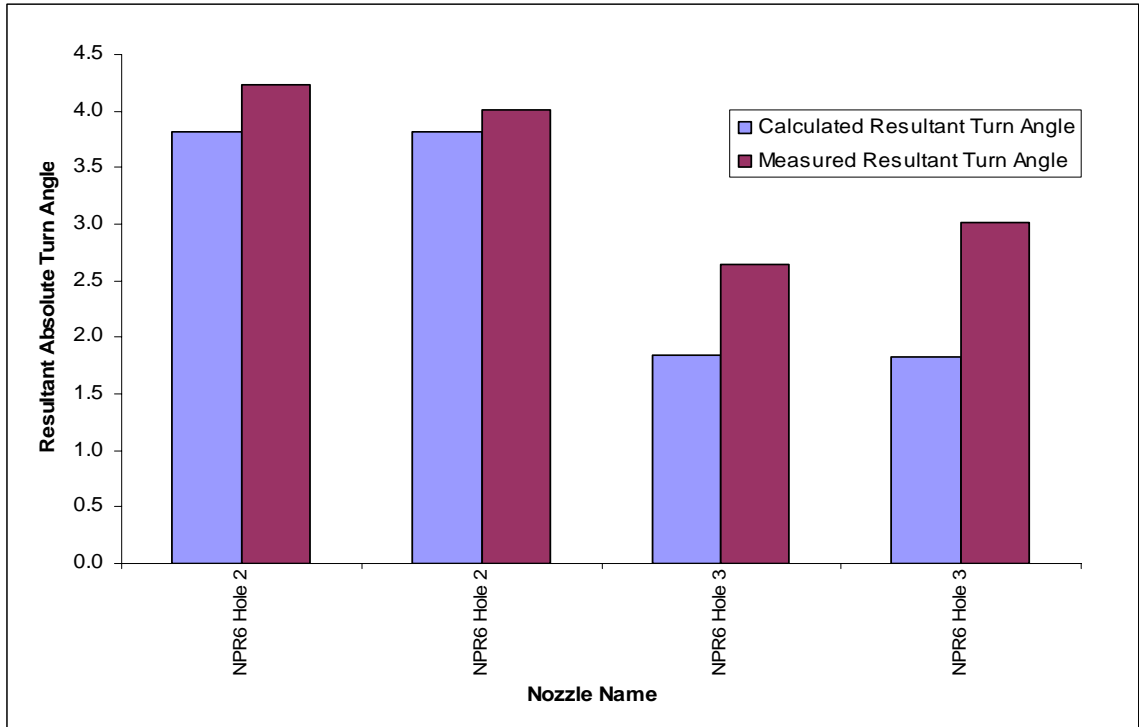


Figure 31. Comparison between calculated and measured turn angles for NPR6 nozzles on a run-by-run level.

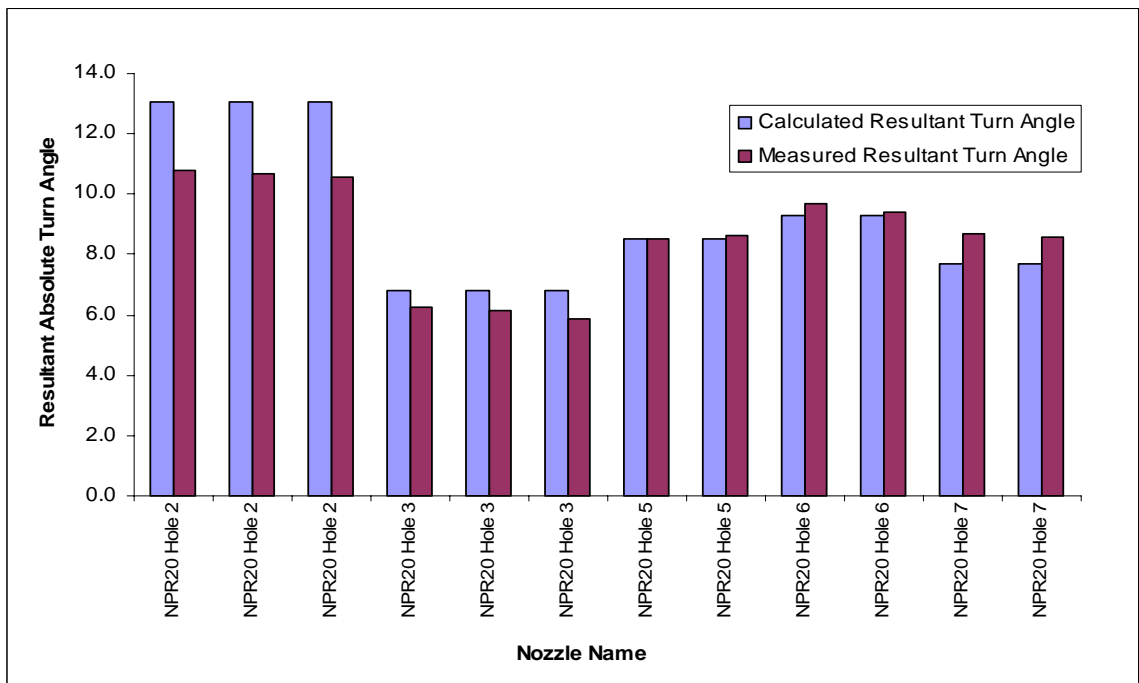


Figure 32. Comparison between calculated and measured turn angles for NPR20 nozzles on a run-by-run level.

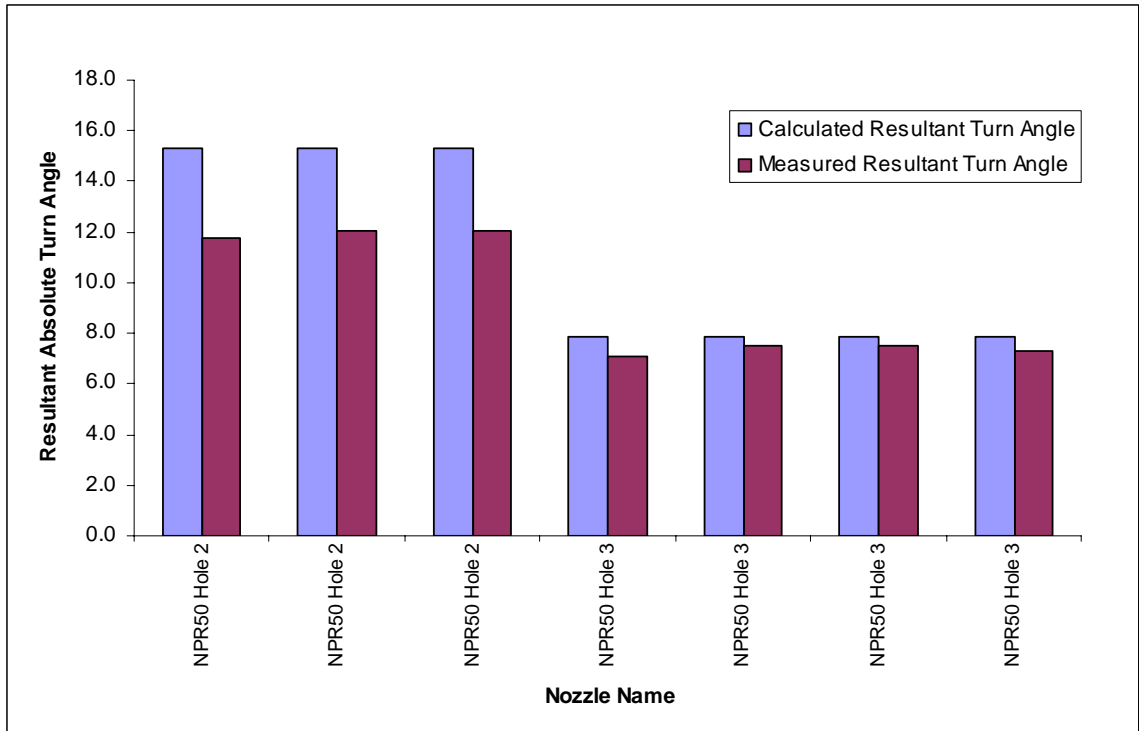


Figure 33. Comparison between calculated and measured turn angles for NPR50 nozzles on a run-by-run level.

Conclusions

A hole-type compound aerospike nozzle was found to provide effective thrust vectoring. The addition of a secondary port did not affect aerospike nozzle axial force. The addition of an inlet radius on the secondary port provided significant improvements in the development of axisymmetric flow. Compound aerospike nozzle axial force and radial vectoring forces showed excellent correlation between measured and calculated results.

The cause of non-axisymmetric secondary port flow observed in Schlieren photographs is not known. Possible causes include the presence of a pressure gradient across the secondary port throat, flow attachment to the diverging section of the secondary port, and turning of flow through shock waves at the secondary port throat.

The poor resolution of the RP nozzle models leaves significant uncertainties in the geometry of the models at this scale. While the nozzles presented in this thesis may be sufficient for qualitative assessment, larger models or higher resolution during the RP process would be necessary for further development.

Bibliography

Carpenter, T.W., and Gerhardt, J.A. "Nozzle Flow Thrust Vector Measurement."
U.S. Patent 6 032 545, 1998.

Erickson, C., "Thrust Vector Control Selection in Aerospike Engines,"
*Proceedings of the 33rd AIAA/ASME/SAE/ASEE Joint Propulsion
Conference & Exhibit*, AIAA, Seattle, WA, 1997, AIAA Paper 1997-3307.

Greer, H., "Rapid Method for Plug Nozzle Design," ARJ Journal, Nov. 1960, pp.
560-561.

Hall, P.E., "Validation and Performance Evaluation of a Dual Flow Thrust Stand,"
Master's Thesis, California Polytechnic State University, 1994.

Lee, C.C., and Thompson, D.D., "Fortran Program for Plug Nozzle Design,"
NASA TM X-53019, 1964.

NASA Dryden Flight Research Center (2004), "Aerospike Engine Flight Test
Successful," [Online]. Available at
<http://www.nasa.gov/centers/dryden/news/NewsReleases/2004/04-23.html>
(accessed 26 January 2009). Posted News Release.

Nasuti, F., and Onofri, M., "Analysis of In-Flight Behavior of Truncated Plug Nozzles" *Proceedings of the 33rd AIAA/ASME/SAE/ASEE Joint Propulsion Conference & Exhibit*, AIAA, Seattle, WA, 1997, AIAA Paper 2000-3289.

Rao, G.V.R., "Spike Nozzle Contour for Optimum Thrust" *Proceedings of the Fourth AFBMD/STL Symposium on Advances in Ballistic Missile and Space Technology*, vol. 1, Pergamon Press, New York, 1961, pp. 92-101.

Rohlik, N., "Thrust vector optimization of 10 degree gimbaled finned aerospike nozzles," Master's Thesis, California Polytechnic State University, 2008.

Rossi, R. A., "Undelected Dual Flow Thrust Vectoring Nozzle Performance," Master's Thesis, California Polytechnic State University, 1994.

Ruf, J.H., and McMonnaughey, P.K., "The Plume Physics Behind Aerospike Nozzle Altitude Compensation and Slipstream Effect," *Proceedings of the 33rd AIAA/ASME/SAE/ASEE Joint Propulsion Conference & Exhibit*, AIAA, Seattle, WA, 1997, AIAA Paper 97-3218.

Sutton, G. P., "History of Liquid Propellant Rocket Engines," AIAA, Reston, VA, Nov. 2005, pp. 94-96.

Appendix A: Equations

Thrust: $F_{vector} = \dot{m}V_e + (p_e - p_o)A_e$

Exit Velocity: $V_e = M_e \sqrt{kRT_e}$

Mass Flow Rate: $\dot{m} = A_t p_1 \frac{k \sqrt{\left[\frac{2}{k+1} \right]^{\frac{k+1}{k-1}}}}{\sqrt{kRT_1}}$

Resultant Turn Angle: $\delta_r = \tan^{-1}\left(\frac{F_{vector}}{F_z}\right)$

Appendix B: Nozzle Geometry

The technical drawings shown in **Figure 34** through **Figure 48** reveal the specific geometry of each nozzle as it was introduced to the RP machine and represents all nozzles discussed in the text.

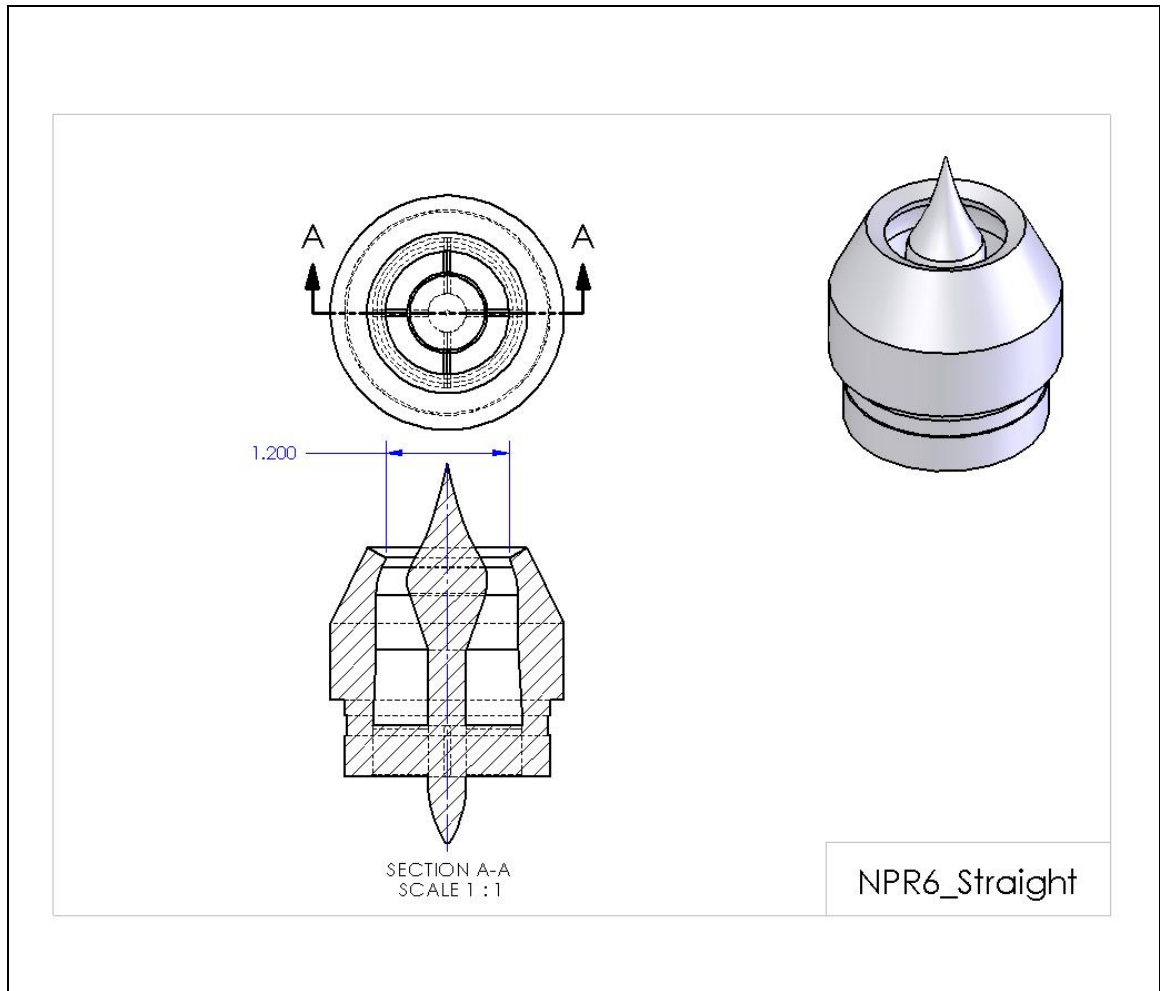


Figure 34. NPR6 Straight design drawing.

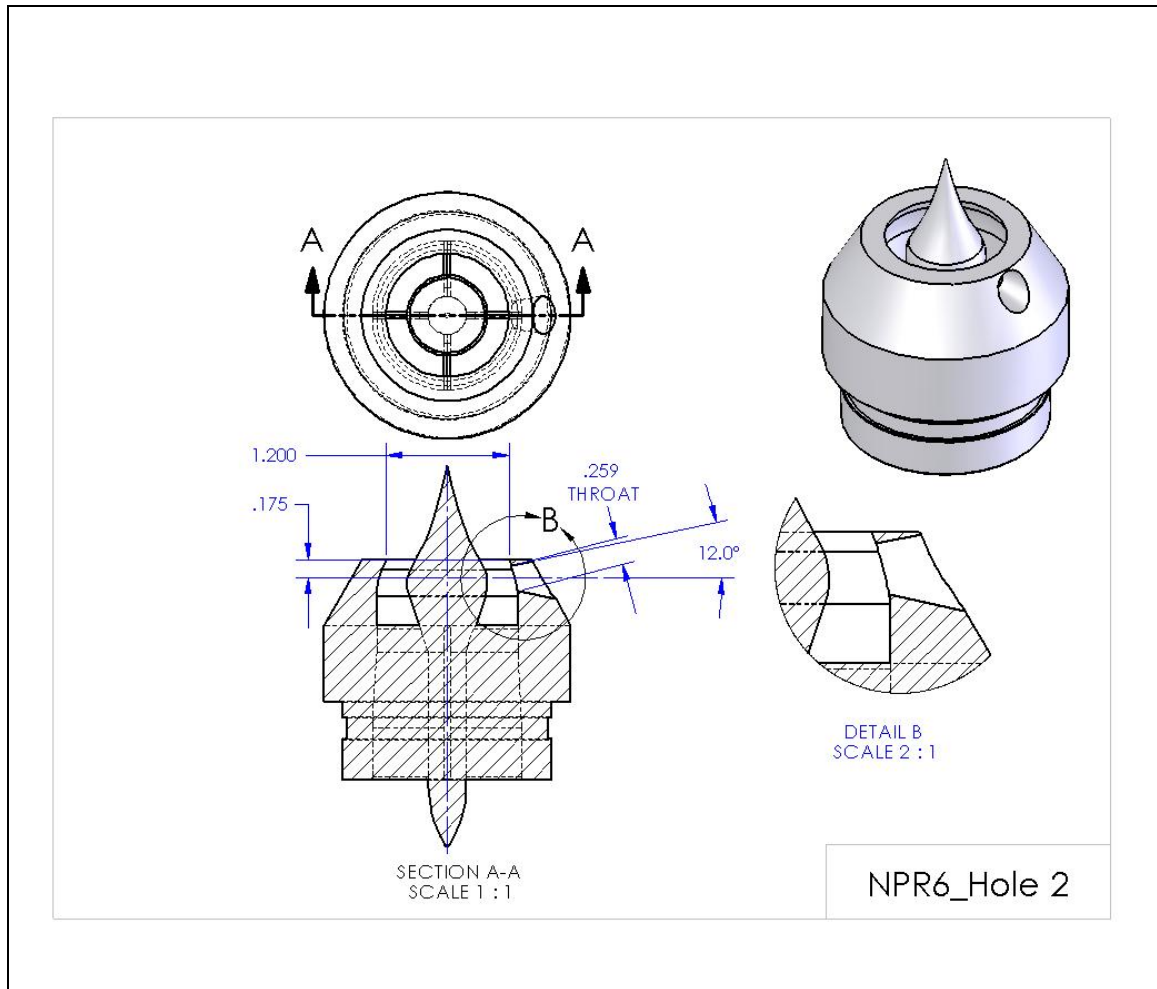


Figure 35. NPR6 Hole 2 design drawing.

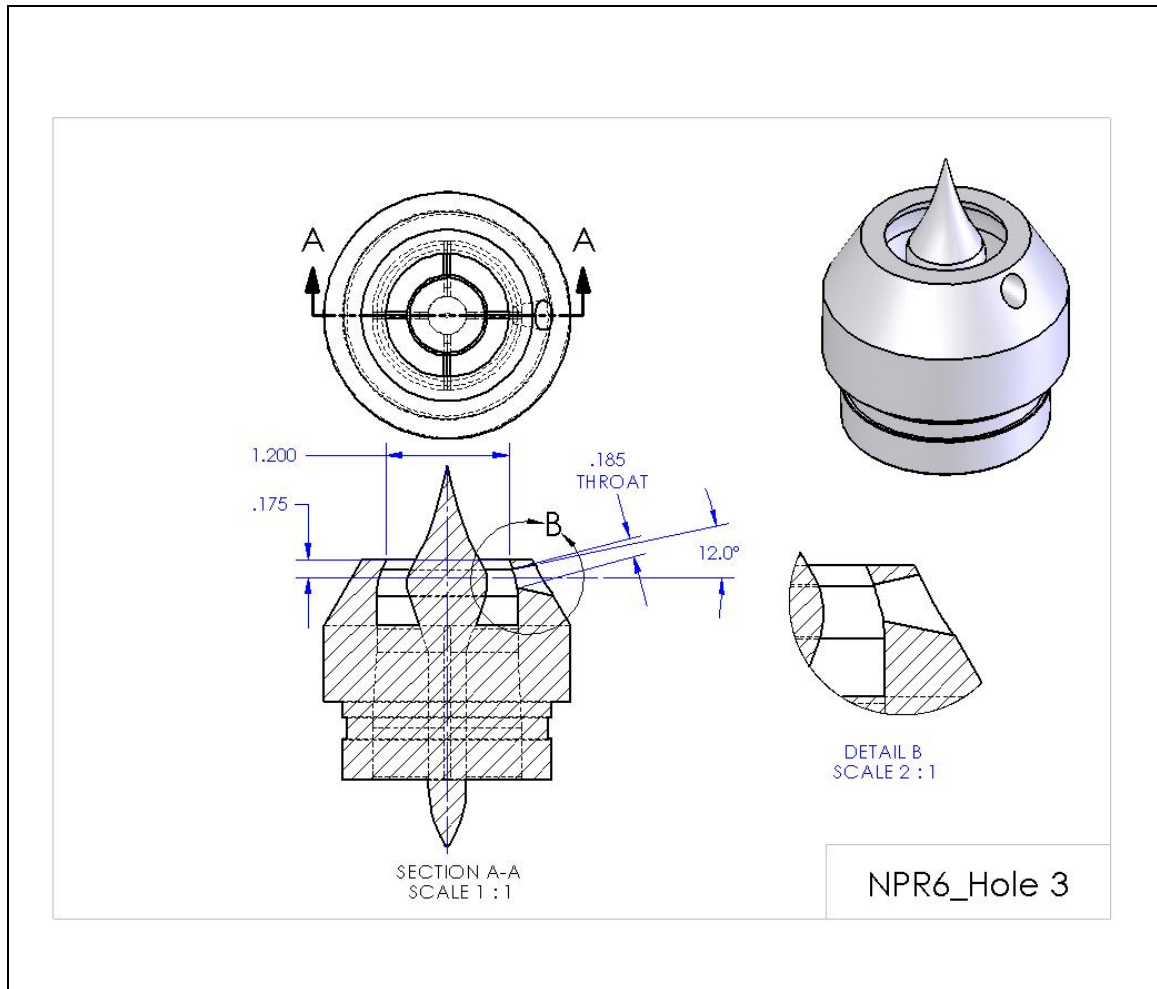


Figure 36. NPR6 Hole 3 design drawing.

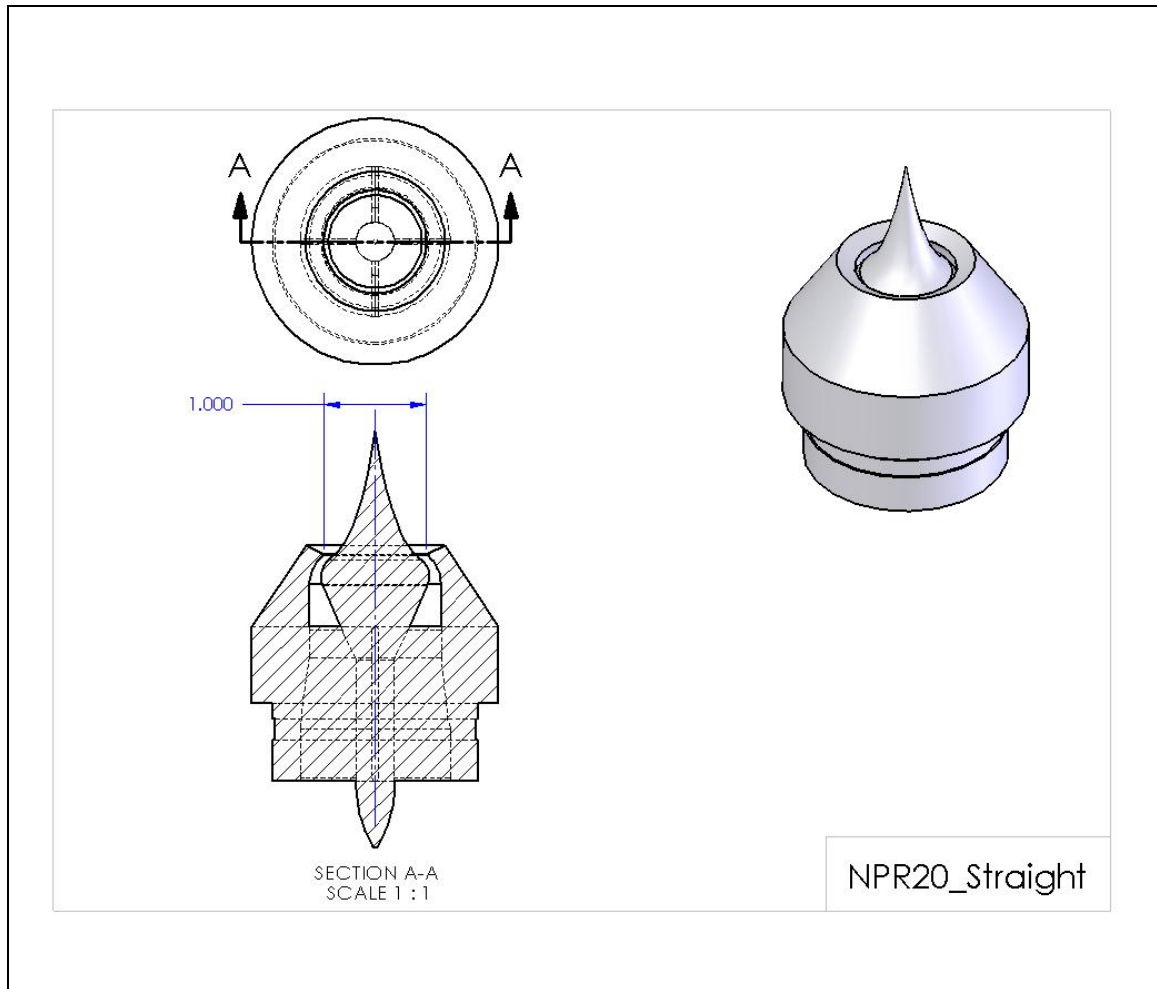


Figure 37. NPR20 Straight design drawing.

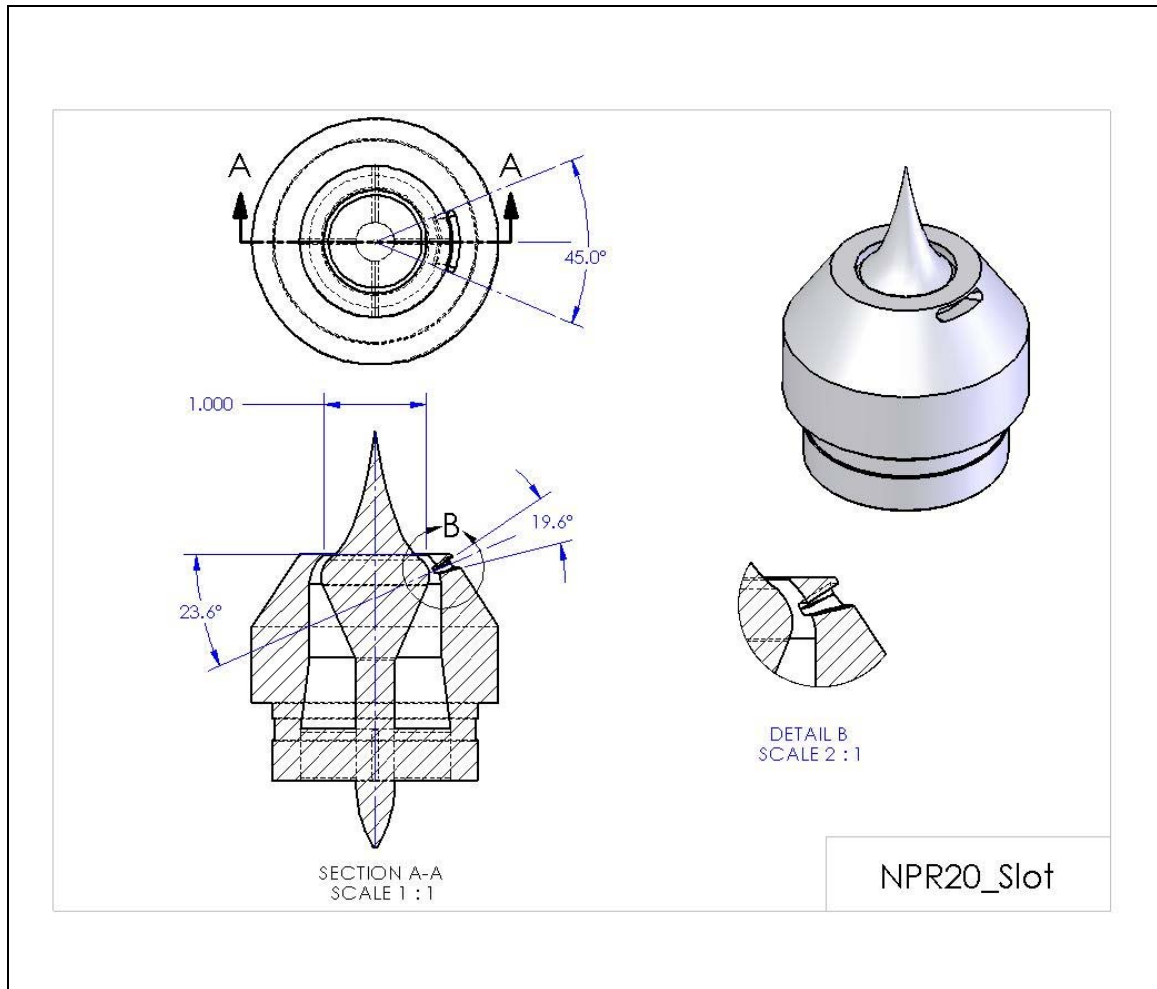


Figure 38. NPR20 Slot design drawing.

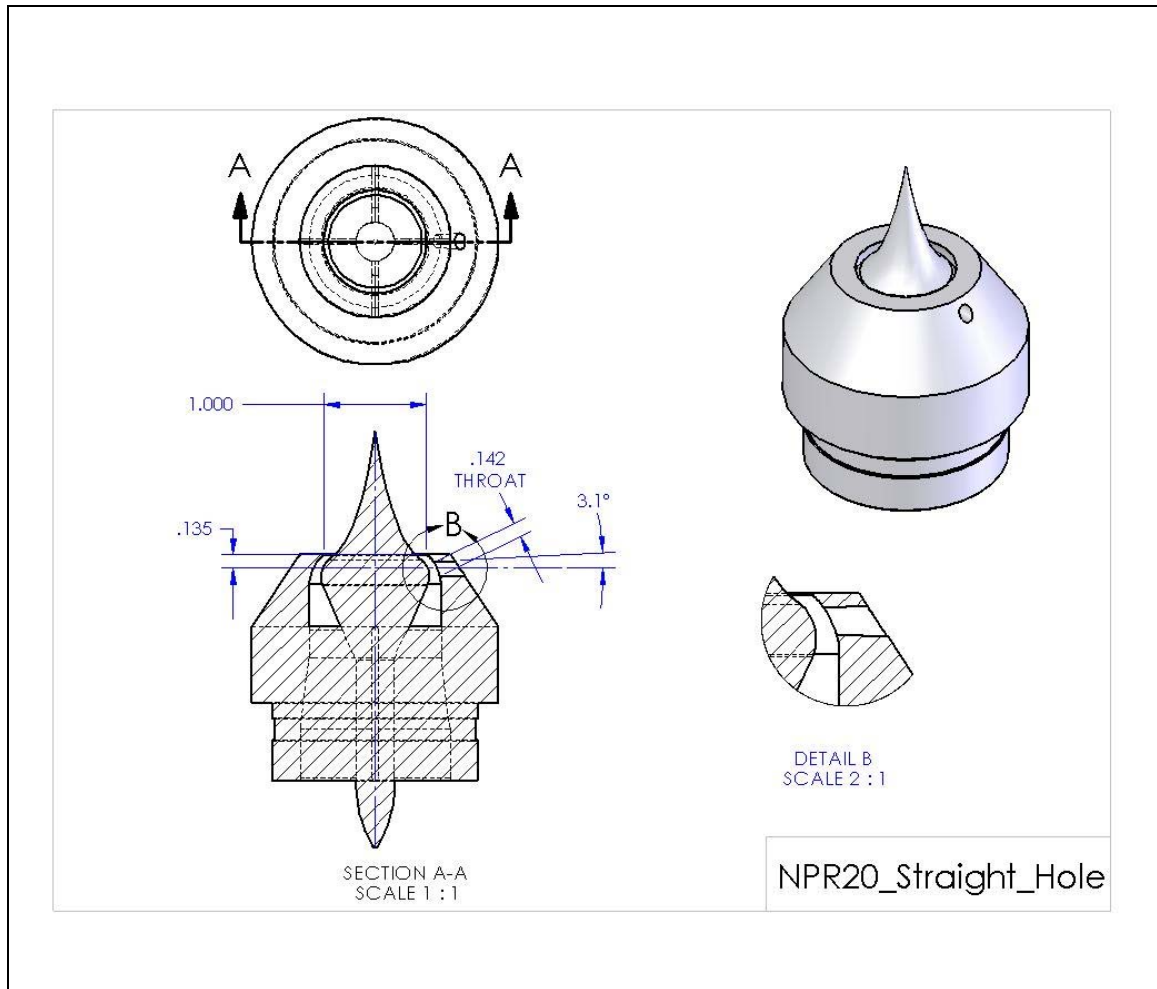


Figure 39. NPR20 Straight Hole design drawing.

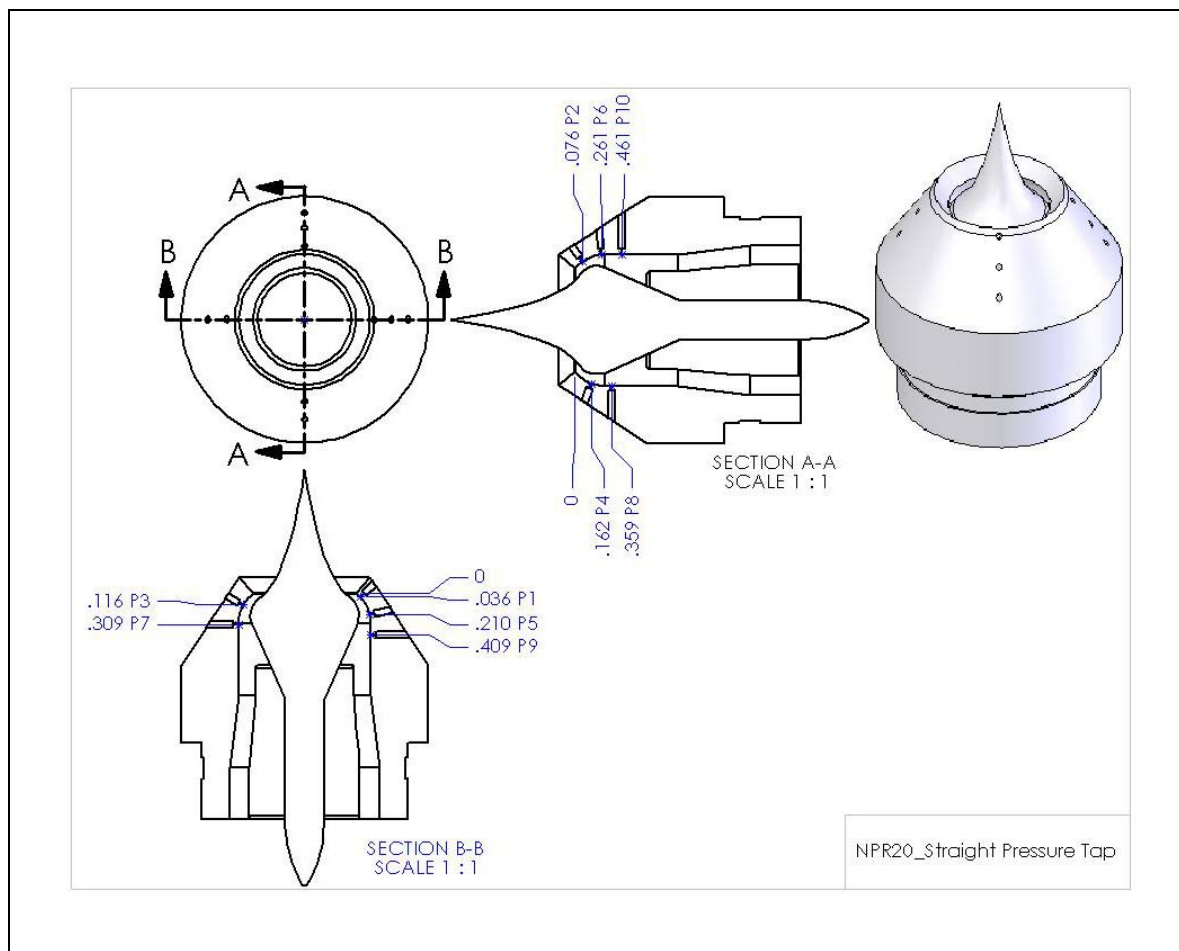


Figure 40. NPR20 Straight Pressure Tap design drawing.

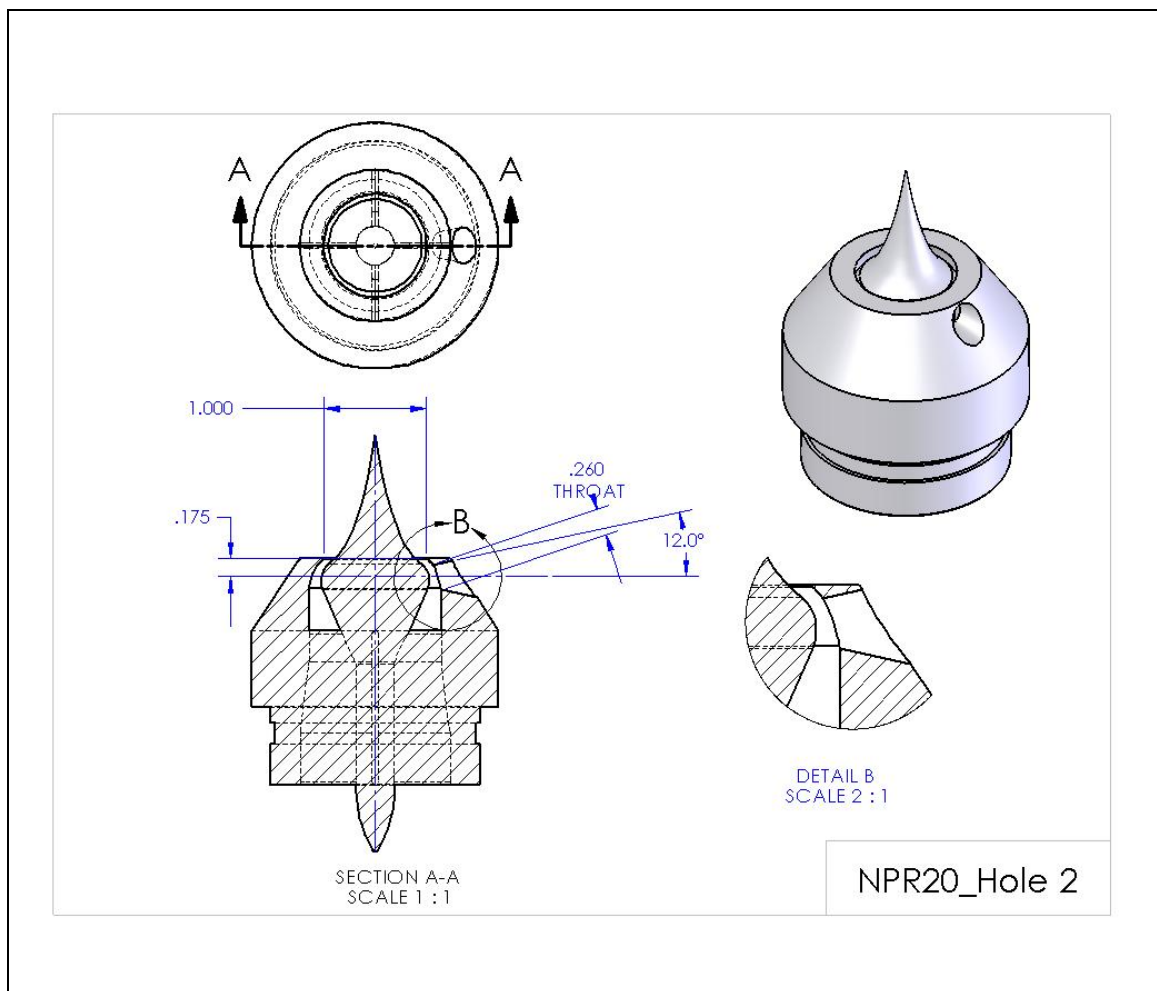


Figure 41. NPR20 Hole 2 design drawing.

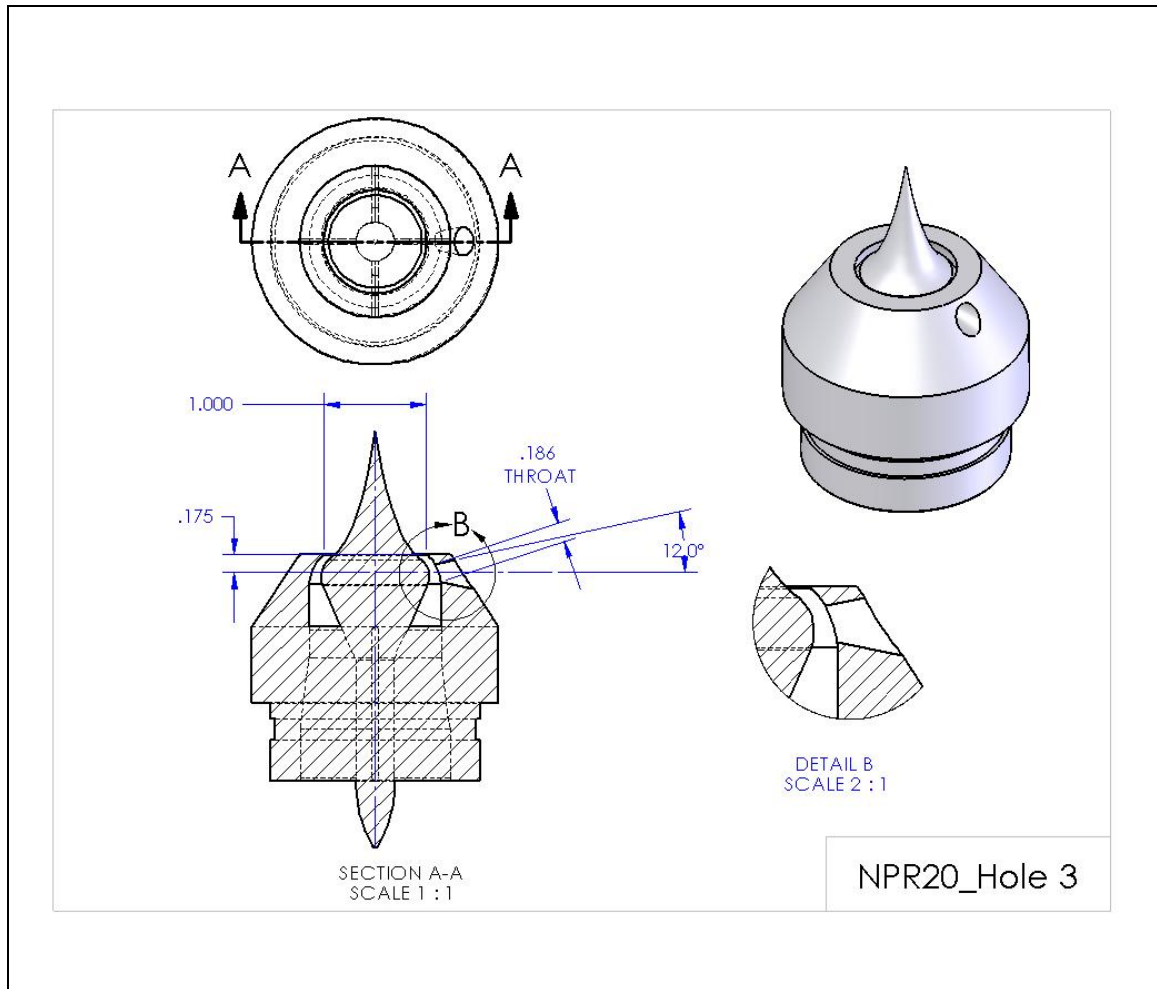


Figure 42. NPR20 Hole 3 design drawing.

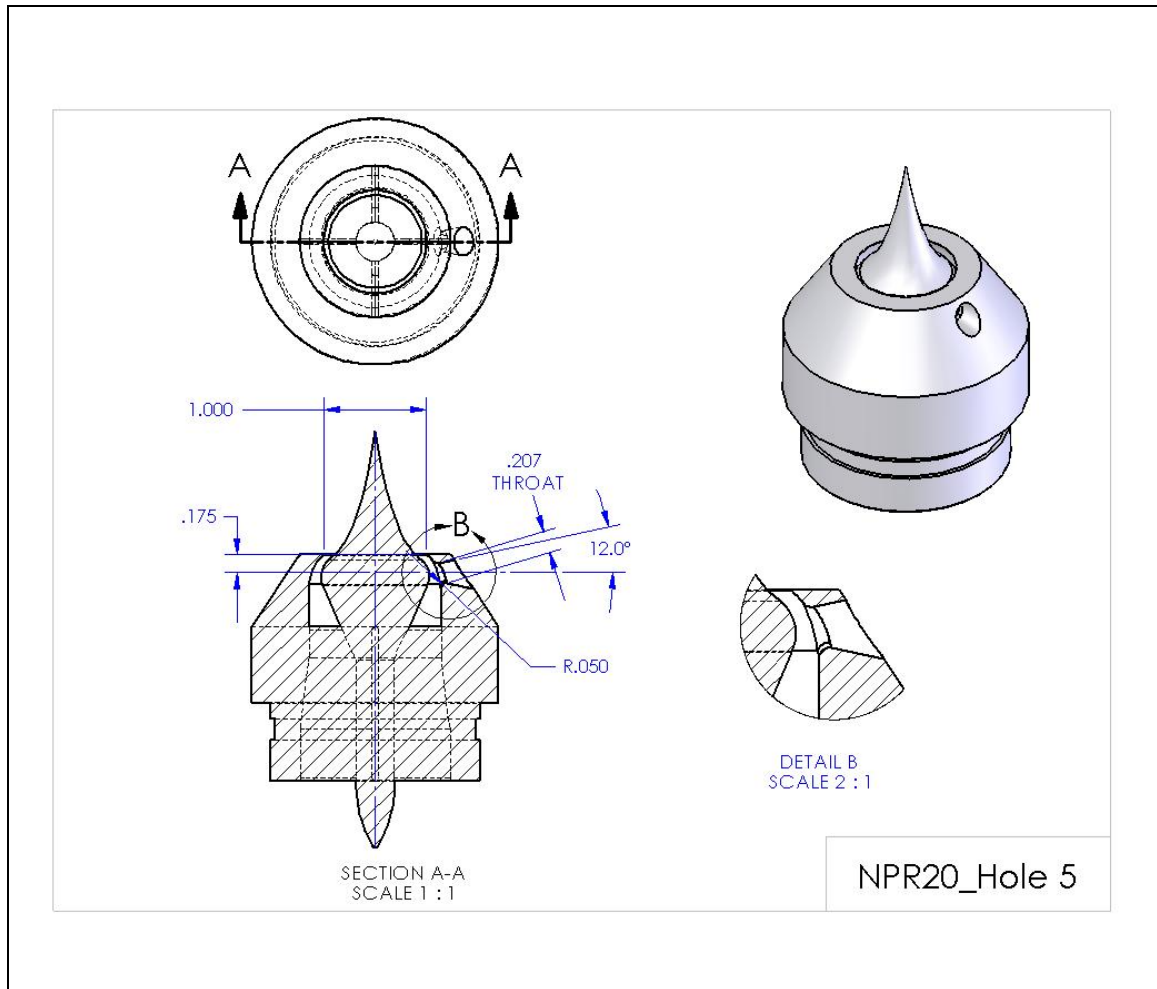


Figure 43. NPR20 Hole 5 design drawing.

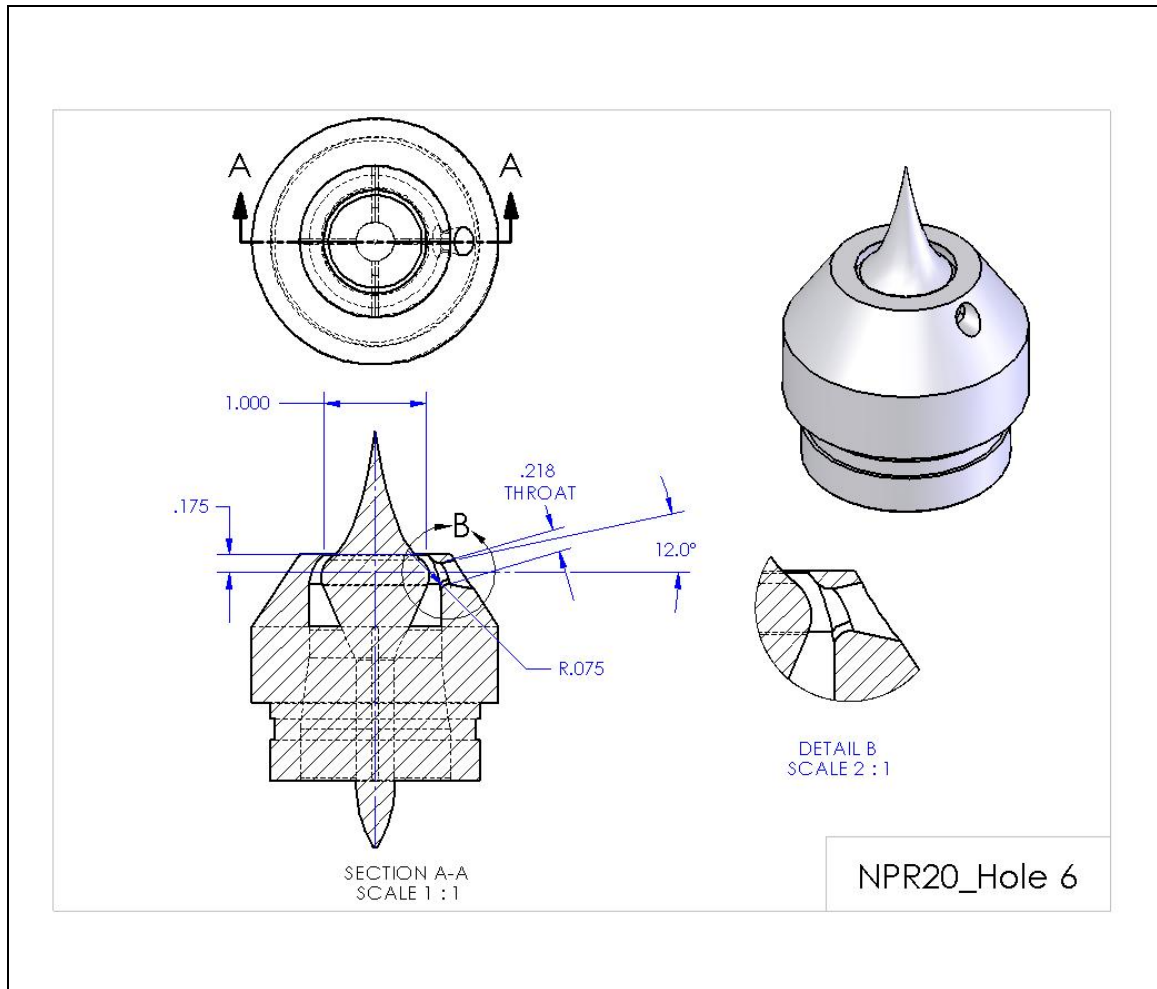


Figure 44. NPR20 Hole 6 design drawing.

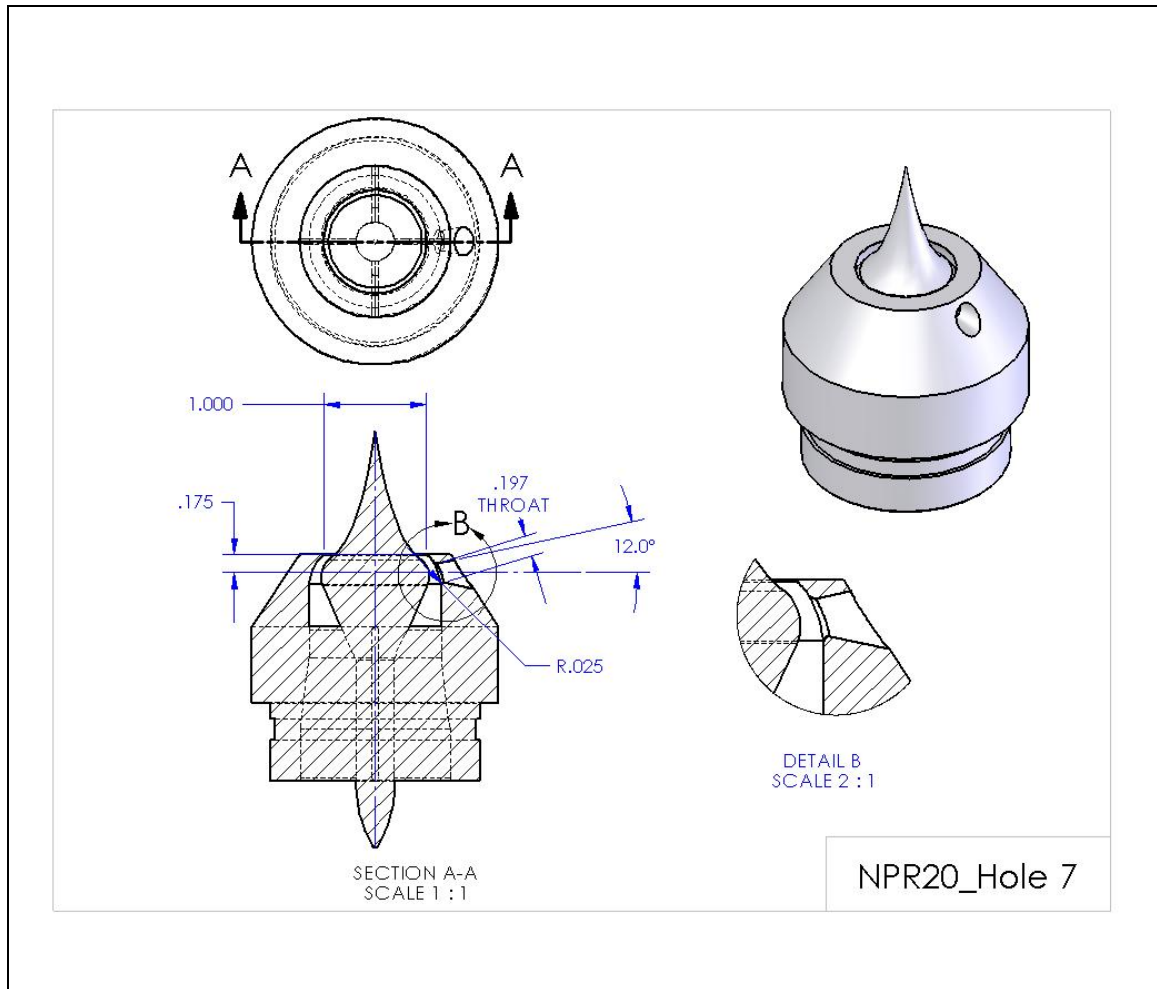


Figure 45. NPR20 Hole 7 design drawing.

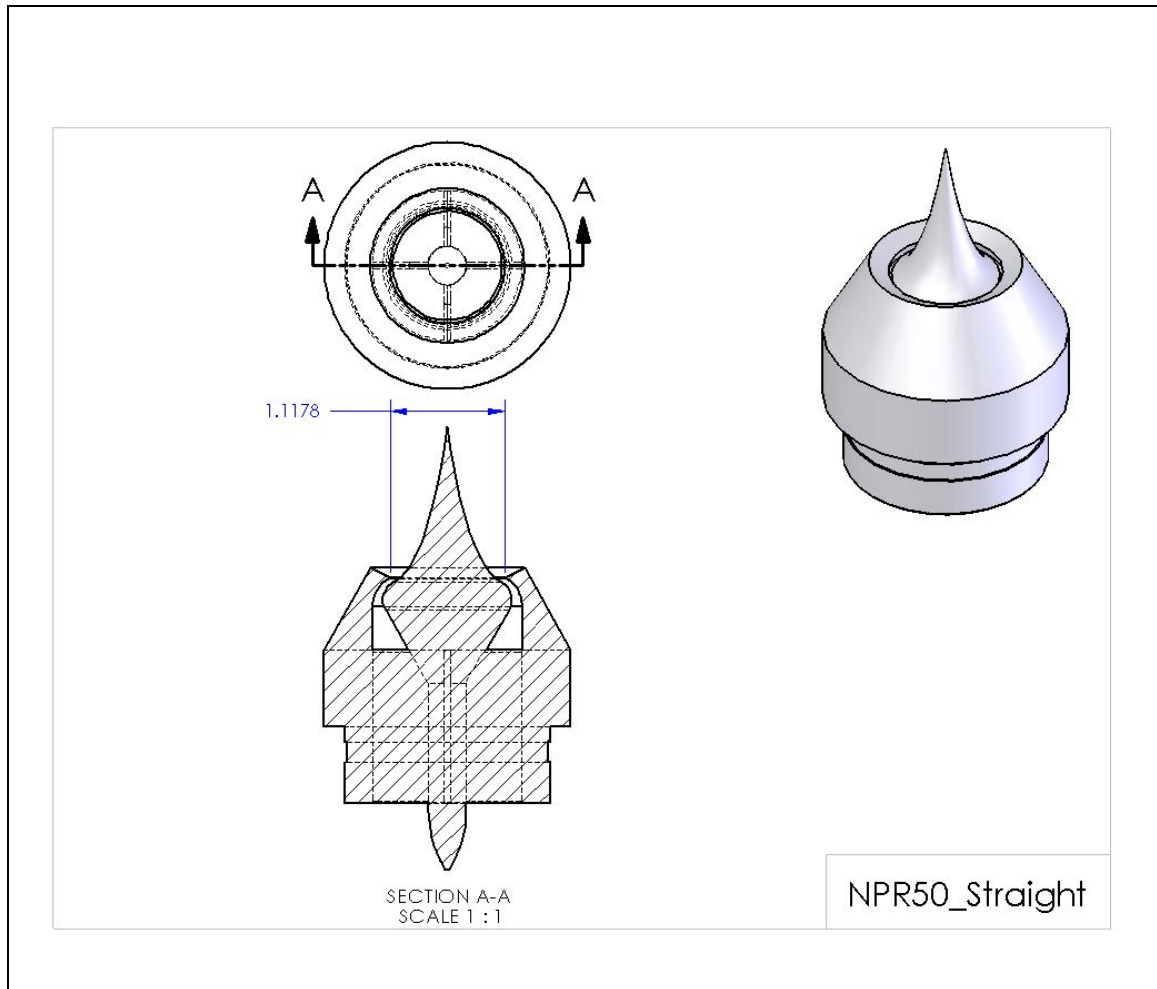


Figure 46. NPR50 Straight design drawing.

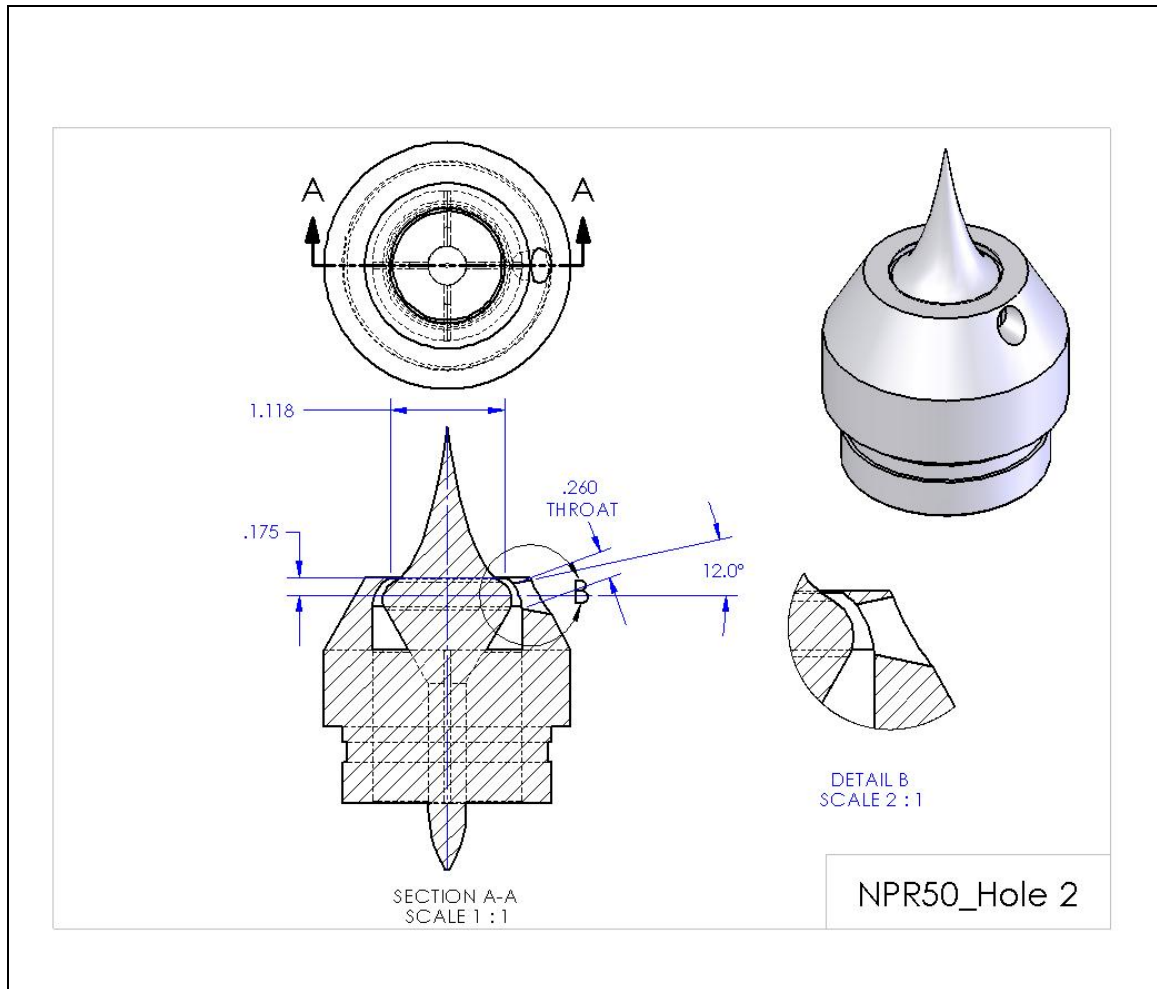


Figure 47. NPR50 Hole 2 design drawing.

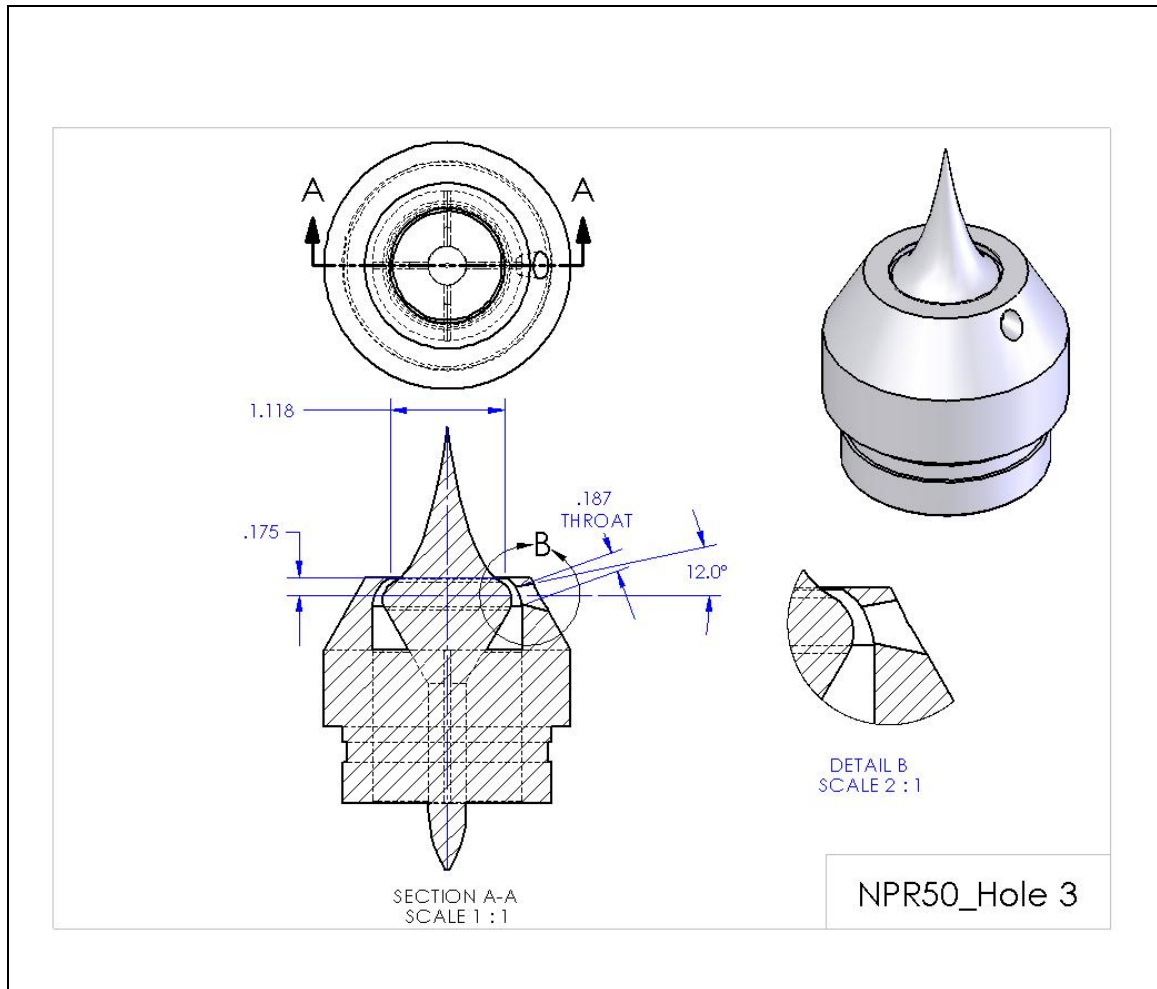


Figure 48. NPR50 Hole 3 design drawing.

Appendix C: Original Data

Run Number	Nozzle Type	Notes	Right NPR	Corrected R1	Corrected R2	Corrected R3	Corrected R4	Corrected R5	Corrected R6	Fx	Fy	Fz
				lbf	lbf	lbf	lbf	lbf	lbf	lbf	lbf	lbf
NPR6												
RUN2115	NPR6 Hole 1		3.908	23.151	32.814	12.956	-3.594	-0.359	-0.483	-3.594	-0.124	-68.921
RUN2116	NPR6 Hole 1		3.718	24.048	33.707	13.230	-3.996	-0.510	-0.658	-3.996	-0.148	-70.986
RUN2117	NPR6 Hole 1		3.217	21.881	30.989	11.518	-4.214	-0.116	-0.462	-4.214	-0.346	-64.388
RUN2169	NPR6 Hole 2		5.941	24.394	37.866	10.772	-5.383	0.082	-0.347	-5.383	-0.429	-73.033
RUN2170	NPR6 Hole 2		5.543	22.511	34.915	10.037	-4.728	-0.031	-0.043	-4.728	-0.011	-67.463
RUN2171	NPR6 Hole 3		6.025	24.694	31.950	17.719	-3.425	-0.005	-0.247	-3.425	-0.242	-74.362
RUN2172	NPR6 Hole 3		5.639	22.668	30.295	16.086	-3.640	0.209	0.059	-3.640	-0.151	-69.049
RUN2291	NPR6 Str	A = 0.020	5.995	23.760	24.807	26.585	-0.419	0.199	-0.363	-0.419	-0.561	-75.152
RUN2292	NPR6 Str	A = 0.016	4.960	18.803	19.671	20.665	-0.541	0.354	-0.318	-0.541	-0.673	-59.140
RUN2293	NPR6 Str	A = 0.012	3.648	12.355	13.704	13.949	-0.618	0.180	0.020	-0.618	-0.159	-40.008
RUN2294	NPR6 Str	A = 0.008	2.099	5.519	5.960	6.583	-0.138	0.101	-0.164	-0.138	-0.265	-18.062
RUN2295	NPR6 Str	A = 0.006	1.229	1.636	1.853	1.743	-0.187	0.020	0.013	-0.187	-0.007	-5.232
RUN2296	NPR6 Hole 3	A = 0.020	5.890	23.771	31.478	17.683	-2.946	0.155	-0.097	-2.946	-0.252	-72.932

Run Number	Nozzle Type	Mx	My	Mz	Wp	Wi	Fi	Fr	F _{vector}	Fr/Fi	Fz/Fi	Wp/Wi	pitch	yaw	r
		in-lbf	in-lbf	in-lbf	lbm/s	lbm/s	lbf	lbf	lbf						
NPR6															
RUN2115	NPR6 Hole 1	-1.327	-86.046	-3.371	1.445	1.016	64.398	69.015	3.597	1.072	-1.070	1.422	0.103	2.985	-2.987
RUN2116	NPR6 Hole 1	-2.897	-88.727	-4.670	1.503	0.966	65.973	71.099	3.998	1.078	-1.076	1.555	0.119	3.222	-3.224
RUN2117	NPR6 Hole 1	-3.135	-84.367	-2.315	1.381	0.836	57.787	64.526	4.228	1.117	-1.114	1.652	0.308	3.744	-3.757
RUN2169	NPR6 Hole 2	-0.376	-117.401	-1.063	1.541	1.541	76.205	73.232	5.400	0.961	-0.958	1.000	0.337	4.215	-4.229
RUN2170	NPR6 Hole 2	-0.178	-107.794	-0.295	1.438	1.436	70.104	67.629	4.728	0.965	-0.962	1.001	0.010	4.009	-4.009
RUN2171	NPR6 Hole 3	0.700	-61.664	-1.012	1.562	1.560	77.589	74.442	3.434	0.959	-0.958	1.001	0.187	2.637	-2.644
RUN2172	NPR6 Hole 3	2.612	-61.564	1.070	1.434	1.458	70.318	69.145	3.643	0.983	-0.982	0.983	0.125	3.017	-3.020
RUN2291	NPR6 Str	9.682	7.707	-0.657	1.368	1.408	75.051	75.155	0.700	1.001	-1.001	0.971	0.428	0.319	-0.534
RUN2292	NPR6 Str	6.825	4.306	0.143	1.115	1.162	59.004	59.146	0.863	1.002	-1.002	0.960	0.652	0.524	-0.836
RUN2293	NPR6 Str	7.355	1.058	0.801	0.635	0.665	40.040	40.014	0.638	0.999	-0.999	0.955	0.228	0.885	-0.914
RUN2294	NPR6 Str	3.763	2.700	-0.255	0.521	0.548	17.848	18.065	0.299	1.012	-1.012	0.951	0.841	0.439	-0.948
RUN2295	NPR6 Str	0.813	-0.476	0.131	0.255	0.321	4.790	5.236	0.187	1.093	-1.092	0.796	0.080	2.050	-2.052
RUN2296	NPR6 Hole 3	4.045	-59.770	0.231	1.560	1.577	75.133	72.992	2.957	0.972	-0.971	0.990	0.198	2.313	-2.321

Run Number	Nozzle Type	Notes	Right NPR	Corrected R1	Corrected R2	Corrected R3	Corrected R4	Corrected R5	Corrected R6	Fx	Fy	Fz
				lbf	lbf	lbf	lbf	lbf	lbf	lbf	lbf	lbf
RUN2297	NPR6 Hole 3	A = 0.016	4.834	18.771	25.591	13.293	-3.031	-0.021	-0.037	-3.031	-0.015	-57.656
RUN2298	NPR6 Hole 3	A = 0.012	3.420	12.088	16.484	8.152	-1.978	-0.065	0.005	-1.978	0.070	-36.724
RUN2299	NPR6 Hole 3	A = 0.008	2.034	5.494	7.482	3.901	-0.927	-0.034	-0.089	-0.927	-0.055	-16.877
RUN2300	NPR6 Hole 3	A = 0.006	1.304	2.069	2.746	1.517	-0.353	-0.013	0.037	-0.353	0.050	-6.332
NPR 20												
RUN2016	NPR20 Straight Metal		7.501	8.582	8.304	9.022	-0.057	0.099	0.057	-0.057	-0.042	-25.909
RUN2017	NPR20 Straight Metal		7.482	8.531	8.140	9.449	-0.012	0.024	0.027	-0.012	0.003	-26.120
RUN2018	NPR20 Straight Metal		7.505	8.550	8.187	8.589	0.018	0.026	0.030	0.018	0.004	-25.326
RUN2019	NPR20 Straight Metal	rotated 90 degrees cw	7.547	8.487	8.600	9.295	-0.127	0.107	0.044	-0.127	-0.063	-26.383
RUN2020	NPR20 Straight Metal	rotated 90 degrees cw	7.517	8.448	8.516	8.671	-0.025	0.077	0.033	-0.025	-0.044	-25.635
RUN2021	NPR20 Straight Metal	rotated 90 degrees cw	7.523	8.352	8.455	8.673	0.011	0.089	-0.003	0.011	-0.092	-25.480
RUN2022	NPR20 Straight Metal	rotated 90 degrees cw	7.473	8.339	8.466	8.874	-0.099	0.026	0.021	-0.099	-0.005	-25.680
RUN2023	NPR20 Straight Metal	rotated 90 degrees cw	7.514	8.314	8.426	9.000	-0.054	0.136	0.009	-0.054	-0.127	-25.740

Run Number	Nozzle Type	Mx	My	Mz	Wp	Wi	Fi	Fr	F _{vector}	Fr/Fi	Fz/Fi	Wp/Wi	pitch	yaw	r
		in-lbf	in-lbf	in-lbf	lbm/s	lbm/s	lbf	lbf	lbf						
RUN2297	NPR6 Hole 3	3.355	-53.287	-0.231	1.018	1.013	59.738	57.735	3.031	0.966	-0.965	1.005	0.015	3.009	-3.009
RUN2298	NPR6 Hole 3	1.151	-36.103	-0.241	0.603	0.615	37.619	36.777	1.979	0.978	-0.976	0.980	-0.109	3.083	-3.085
RUN2299	NPR6 Hole 3	0.986	-15.518	-0.493	0.532	0.541	17.531	16.902	0.929	0.964	-0.963	0.984	0.185	3.145	-3.151
RUN2300	NPR6 Hole 3	0.313	-5.328	0.096	0.295	0.340	6.279	6.342	0.356	1.010	-1.008	0.869	-0.449	3.188	-3.219
NPR 20															
RUN2016	NPR20 Straight Metal	0.404	3.112	0.626	0.488	0.549	25.266	25.909	0.071	1.025	-1.025	0.887	0.093	0.126	-0.157
RUN2017	NPR20 Straight Metal	1.319	5.673	0.205	0.479	0.548	24.789	26.120	0.012	1.054	-1.054	0.873	-0.008	0.025	-0.027
RUN2018	NPR20 Straight Metal	-0.811	1.743	0.225	0.506	0.550	26.208	25.326	0.018	0.966	-0.966	0.920	-0.009	-0.041	-0.042
RUN2019	NPR20 Straight Metal	2.301	3.011	0.603	0.478	0.552	24.843	26.383	0.142	1.062	-1.062	0.866	0.138	0.276	-0.309
RUN2020	NPR20 Straight Metal	0.728	0.673	0.438	0.504	0.550	26.153	25.635	0.051	0.980	-0.980	0.916	0.098	0.057	-0.113
RUN2021	NPR20 Straight Metal	1.060	0.945	0.345	0.483	0.550	25.070	25.480	0.092	1.016	-1.016	0.877	0.207	-0.024	-0.208
RUN2022	NPR20 Straight Metal	1.656	1.768	0.189	0.500	0.547	25.957	25.680	0.099	0.989	-0.989	0.916	0.011	0.222	-0.222
RUN2023	NPR20 Straight Metal	1.996	2.490	0.581	0.488	0.549	25.343	25.740	0.139	1.016	-1.016	0.888	0.284	0.121	-0.308

Run Number	Nozzle Type	Notes	Right NPR	Corrected R1	Corrected R2	Corrected R3	Corrected R4	Corrected R5	Corrected R6	Fx	Fy	Fz
				lbf	lbf	lbf	lbf	lbf	lbf	lbf	lbf	lbf
RUN2024	NPR20 Straight Metal	rotated 90 degrees cw	7.461	8.357	8.434	6.922	-0.080	0.074	0.036	-0.080	-0.038	-23.713
RUN2025	NPR20 Straight Metal	rotated 180 degrees cw	7.499	8.539	8.168	9.222	0.029	0.017	0.031	0.029	0.013	-25.929
RUN2026	NPR20 Straight Metal	rotated 180 degrees cw	7.490	8.545	8.154	8.747	0.025	0.113	0.090	0.025	-0.023	-25.447
RUN2027	NPR20 Straight Metal	rotated 180 degrees cw	7.512	8.552	8.239	8.875	-0.041	0.071	0.100	-0.041	0.029	-25.666
RUN2028	NPR20 Straight Metal	rotated 270 degrees cw	7.485	8.521	8.388	7.417	-0.026	0.079	0.036	-0.026	-0.043	-24.327
RUN2029	NPR20 Straight Metal	rotated 270 degrees cw	7.500	8.471	8.289	8.715	0.010	0.104	0.062	0.010	-0.042	-25.476
RUN2030	NPR20 Straight Metal	rotated 270 degrees cw	7.490	8.460	8.156	8.349	0.029	0.076	0.048	0.029	-0.028	-24.966
RUN2039	NPR20 Straight		7.392	9.372	8.223	10.176	0.217	0.049	0.085	0.217	0.036	-27.770
RUN2040	NPR20 Straight		7.518	9.575	8.491	9.667	0.178	0.019	0.029	0.178	0.010	-27.734
RUN2041	NPR20 Straight	rotated 90 degrees CW	7.063	7.998	8.657	8.899	0.039	0.131	-0.078	0.039	-0.209	-25.553
RUN2042	NPR20 Straight	rotated 90 degrees CW	7.485	8.611	9.276	10.257	0.038	0.145	-0.072	0.038	-0.217	-28.144
RUN2043	NPR20 Straight	rotated 180 degrees CW	7.413	9.040	9.745	9.385	-0.220	0.103	0.035	-0.220	-0.068	-28.170
RUN2044	NPR20 Straight	rotated 180 degrees CW	7.486	9.103	9.840	8.826	-0.259	0.076	0.046	-0.259	-0.029	-27.769

Run Number	Nozzle Type	Mx	My	Mz	Wp	Wi	Fi	Fr	F _{vector}	Fr/Fi	Fz/Fi	Wp/Wi	pitch	yaw	r
		in-lbf	in-lbf	in-lbf	lbm/s	lbm/s	lbf	lbf	lbf						
RUN2024	NPR20 Straight Metal	-3.392	-6.551	0.442	0.471	0.546	24.408	23.713	0.089	0.972	-0.971	0.863	0.091	0.194	-0.214
RUN2025	NPR20 Straight Metal	0.783	4.565	0.192	0.488	0.548	25.337	25.929	0.032	1.023	-1.023	0.890	-0.029	-0.065	-0.071
RUN2026	NPR20 Straight Metal	-0.470	2.569	0.810	0.512	0.547	26.567	25.447	0.034	0.958	-0.958	0.935	0.052	-0.057	-0.077
RUN2027	NPR20 Straight Metal	0.026	2.754	0.683	0.501	0.549	26.056	25.666	0.050	0.985	-0.985	0.913	-0.064	0.090	-0.111
RUN2028	NPR20 Straight Metal	-3.093	-4.210	0.460	0.504	0.547	26.164	24.327	0.050	0.930	-0.930	0.921	0.101	0.060	-0.117
RUN2029	NPR20 Straight Metal	0.155	1.846	0.662	0.456	0.548	23.690	25.476	0.043	1.075	-1.075	0.832	0.095	-0.023	-0.098
RUN2030	NPR20 Straight Metal	-1.037	0.835	0.496	0.486	0.547	25.256	24.966	0.040	0.989	-0.989	0.889	0.064	-0.067	-0.093
RUN2039	NPR20 Straight	-0.864	8.462	0.533	0.540	0.541	27.956	27.771	0.220	0.993	-0.993	0.997	-0.074	-0.448	-0.454
RUN2040	NPR20 Straight	-2.481	5.097	0.195	0.538	0.550	27.949	27.734	0.178	0.992	-0.992	0.978	-0.020	-0.367	-0.368
RUN2041	NPR20 Straight	3.900	1.047	0.213	0.544	0.516	27.957	25.554	0.213	0.914	-0.914	1.053	0.470	-0.087	-0.478
RUN2042	NPR20 Straight	5.778	4.254	0.290	0.560	0.547	29.127	28.145	0.220	0.966	-0.966	1.024	0.441	-0.078	-0.448
RUN2043	NPR20 Straight	2.627	-1.556	0.553	0.507	0.542	26.304	28.171	0.230	1.071	-1.071	0.936	0.138	0.448	-0.468
RUN2044	NPR20 Straight	1.151	-4.394	0.489	0.547	0.547	28.446	27.771	0.260	0.976	-0.976	1.000	0.060	0.534	-0.537

Run Number	Nozzle Type	Notes	Right NPR	Corrected R1	Corrected R2	Corrected R3	Corrected R4	Corrected R5	Corrected R6	Fx	Fy	Fz
				lbf	lbf	lbf	lbf	lbf	lbf	lbf	lbf	lbf
RUN2045	NPR20 Straight	rotated 270 degrees CW	7.541	10.123	8.976	8.483	-0.032	-0.064	0.125	-0.032	0.190	-27.581
RUN2046	NPR20 Straight	rotated 270 degrees CW	7.392	9.780	8.817	9.066	-0.132	0.000	0.175	-0.132	0.176	-27.662
RUN2160	NPR20 Straight Metal		7.455	8.500	8.214	8.747	0.106	0.097	0.038	0.106	-0.060	-25.461
RUN2161	NPR20 Straight Metal		7.450	8.487	8.375	8.827	-0.050	0.070	0.059	-0.050	-0.012	-25.689
RUN2162	NPR20 Straight Metal		7.494	8.591	8.422	8.775	0.027	0.064	0.060	0.027	-0.003	-25.787
RUN2163	NPR20 Straight Metal (Stan 1)		7.465	9.955	9.856	10.272	-0.053	0.100	0.068	-0.053	-0.031	-30.084
RUN2164	NPR20 Straight Metal (Stan 1)		7.458	9.816	9.806	10.112	-0.097	0.052	0.010	-0.097	-0.042	-29.734
RUN2165	NPR20 Straight Metal (Stan 1)		7.453	9.877	9.767	10.192	-0.080	0.081	0.054	-0.080	-0.026	-29.836
RUN2166	NPR20 Straight Metal (Stan 2)		7.459	11.060	10.343	11.250	-0.089	0.061	0.081	-0.089	0.020	-32.654
RUN2167	NPR20 Straight Metal (Stan 2)		7.469	11.099	10.484	10.923	-0.085	0.057	0.091	-0.085	0.034	-32.506
RUN2168	NPR20 Straight Metal (Stan 2)		7.451	11.026	10.322	10.956	0.016	0.037	0.132	0.016	0.095	-32.303
RUN2177	NPR20 Hole 2		7.492	9.948	25.421	-6.722	-5.452	0.010	0.112	-5.452	0.102	-28.647
RUN2178	NPR20 Hole 2		7.467	9.858	25.661	-6.701	-5.447	0.068	0.043	-5.447	-0.025	-28.818

Run Number	Nozzle Type	Mx	My	Mz	Wp	Wi	Fi	Fr	F _{vector}	Fr/Fi	Fz/Fi	Wp/Wi	pitch	yaw	r
		in-lbf	in-lbf	in-lbf	lbf	lbf	lbf	lbf	lbf						
RUN2045	NPR20 Straight	-6.967	-2.137	0.246	0.574	0.551	29.914	27.582	0.192	0.922	-0.922	1.043	-0.394	0.065	-0.399
RUN2046	NPR20 Straight	-4.193	1.079	0.700	0.558	0.540	28.992	27.663	0.220	0.954	-0.954	1.035	-0.364	0.273	-0.455
RUN2160	NPR20 Straight Metal	-0.095	2.309	0.541	0.467	0.546	24.166	25.461	0.121	1.054	-1.054	0.855	0.134	-0.238	-0.273
RUN2161	NPR20 Straight Metal	0.569	1.956	0.515	0.498	0.546	25.743	25.689	0.051	0.998	-0.998	0.912	0.026	0.111	-0.114
RUN2162	NPR20 Straight Metal	0.039	1.533	0.497	0.510	0.549	26.407	25.787	0.027	0.977	-0.977	0.929	0.007	-0.060	-0.060
RUN2163	NPR20 Straight Metal (Stan 1)	0.545	1.804	0.671	0.596	0.547	30.861	30.084	0.062	0.975	-0.975	1.090	0.060	0.101	-0.117
RUN2164	NPR20 Straight Metal (Stan 1)	0.715	1.327	0.249	0.582	0.546	30.126	29.734	0.106	0.987	-0.987	1.066	0.082	0.187	-0.204
RUN2165	NPR20 Straight Metal (Stan 1)	0.515	1.841	0.540	0.591	0.546	30.577	29.836	0.084	0.976	-0.976	1.082	0.051	0.153	-0.161
RUN2166	NPR20 Straight Metal (Stan 2)	-1.317	3.929	0.565	0.587	0.546	30.424	32.654	0.091	1.073	-1.073	1.076	-0.035	0.155	-0.159
RUN2167	NPR20 Straight Metal (Stan 2)	-1.977	1.900	0.592	0.603	0.547	31.246	32.507	0.091	1.040	-1.040	1.103	-0.059	0.150	-0.161
RUN2168	NPR20 Straight Metal (Stan 2)	-1.934	2.749	0.678	0.635	0.545	32.866	32.304	0.097	0.983	-0.983	1.164	-0.169	-0.028	-0.171
RUN2177	NPR20 Hole 2	-2.996	139.276	0.491	0.651	0.545	33.826	29.161	5.453	0.862	-0.847	1.194	-0.204	10.775	10.777
RUN2178	NPR20 Hole 2	-1.890	140.222	0.446	0.635	0.543	32.986	29.328	5.447	0.889	-0.874	1.169	0.050	10.704	10.704

Run Number	Nozzle Type	Notes	Right NPR	Corrected R1	Corrected R2	Corrected R3	Corrected R4	Corrected R5	Corrected R6	Fx	Fy	Fz
				lbf	lbf	lbf	lbf	lbf	lbf	lbf	lbf	lbf
RUN2179	NPR20 Hole 2		7.458	10.061	25.125	-6.644	-5.332	-0.037	0.123	-5.332	0.159	-28.542
RUN2180	NPR20 Hole 3		7.463	10.046	18.557	0.471	-3.172	0.024	0.061	-3.172	0.037	-29.073
RUN2181	NPR20 Hole 3		7.472	10.062	18.469	0.505	-3.118	0.037	0.124	-3.118	0.088	-29.035
RUN2182	NPR20 Hole 3		7.473	10.252	17.777	0.758	-2.940	0.003	0.160	-2.940	0.156	-28.787
RUN2204	NPR20 Straight Metal		7.488	8.461	8.454	8.779	-0.024	0.127	0.067	-0.024	-0.059	-25.694
RUN2205	NPR20 Straight Metal (Stan 1)		7.446	9.911	9.779	10.062	-0.056	0.085	0.086	-0.056	0.001	-29.752
RUN2219	NPR20 Hole 5	Inlet Radius = 0.050	7.469	10.580	21.971	-3.610	-4.319	-0.083	0.231	-4.319	0.314	-28.940
RUN2220	NPR20 Hole 5	Inlet Radius = 0.050	7.467	10.671	21.839	-3.624	-4.382	-0.100	0.166	-4.382	0.266	-28.886
RUN2221	NPR20 Hole 6	Inlet Radius = 0.075	7.428	10.254	23.375	-5.181	-4.863	-0.037	0.184	-4.863	0.221	-28.449
RUN2222	NPR20 Hole 6	Inlet Radius = 0.075	7.498	10.517	23.411	-4.995	-4.793	-0.054	0.177	-4.793	0.231	-28.933
RUN2223	NPR20 Hole 7	Inlet Radius = 0.025	7.471	10.199	21.769	-3.387	-4.369	0.006	0.194	-4.369	0.189	-28.582
RUN2224	NPR20 Hole 7	Inlet Radius = 0.025	7.460	10.272	21.665	-3.347	-4.304	-0.078	0.156	-4.304	0.234	-28.591
RUN2230	NPR20 Hole 3		7.468	10.172	18.647	0.242	-3.296	0.016	0.162	-3.296	0.146	-29.061

Run Number	Nozzle Type	Mx	My	Mz	Wp	Wi	Fi	Fr	F _{vector}	Fr/Fi	Fz/Fi	Wp/Wi	pitch	yaw	r
		in-lbf	in-lbf	in-lbf	lbm/s	lbm/s	lbf	lbf	lbf						
RUN2179	NPR20 Hole 2	-4.104	-137.654	0.344	0.659	0.543	34.232	29.036	5.335	0.848	-0.834	1.215	-0.320	10.583	-10.587
RUN2180	NPR20 Hole 3	-2.662	-78.367	0.341	0.647	0.543	33.592	29.246	3.172	0.871	-0.865	1.191	-0.074	6.227	-6.227
RUN2181	NPR20 Hole 3	-2.878	-77.838	0.644	0.618	0.544	32.098	29.203	3.120	0.910	-0.905	1.137	-0.173	6.130	-6.132
RUN2182	NPR20 Hole 3	-4.925	-73.745	0.653	0.627	0.544	32.548	28.937	2.944	0.889	-0.884	1.152	-0.311	5.830	-5.839
RUN2204	NPR20 Straight Metal	0.780	1.408	0.776	0.489	0.543	25.490	25.694	0.064	1.008	-1.008	0.900	0.132	0.054	-0.143
RUN2205	NPR20 Straight Metal (Stan 1)	0.047	1.226	0.684	0.578	0.540	30.075	29.752	0.056	0.989	-0.989	1.069	-0.002	0.108	-0.108
RUN2219	NPR20 Hole 5	-6.999	-110.842	0.595	0.665	0.545	34.567	29.262	4.330	0.847	-0.837	1.221	-0.621	8.487	-8.509
RUN2220	NPR20 Hole 5	-7.820	-110.331	0.261	0.615	0.544	31.956	29.218	4.390	0.914	-0.904	1.129	-0.528	8.625	-8.641
RUN2221	NPR20 Hole 6	-5.784	-123.731	0.588	0.622	0.541	32.334	28.862	4.868	0.893	-0.880	1.149	-0.445	9.700	-9.710
RUN2222	NPR20 Hole 6	-6.544	-123.084	0.492	0.637	0.546	33.151	29.328	4.798	0.885	-0.873	1.166	-0.456	9.406	-9.417
RUN2223	NPR20 Hole 7	-5.040	-109.002	0.800	0.652	0.544	33.947	28.914	4.373	0.852	-0.842	1.199	-0.378	8.691	-8.699
RUN2224	NPR20 Hole 7	-5.563	-108.376	0.309	0.652	0.543	33.944	28.914	4.310	0.852	-0.842	1.201	-0.469	8.560	-8.573
RUN2230	NPR20 Hole 3	-3.638	-79.747	0.711	0.629	0.543	32.773	29.248	3.299	0.892	-0.887	1.158	-0.287	6.470	-6.476

Run Number	Nozzle Type	Notes	Right NPR	Corrected R1	Corrected R2	Corrected R3	Corrected R4	Corrected R5	Corrected R6	Fx	Fy	Fz
				lbf	lbf	lbf	lbf	lbf	lbf	lbf	lbf	lbf
RUN2081	NPR20 Hole		7.526	8.947	14.772	4.141	-1.780	0.083	-0.046	-1.780	-0.129	-27.861
RUN2082	NPR20 Hole		7.496	8.877	14.533	4.388	-1.789	0.067	-0.004	-1.789	-0.072	-27.798
RUN2083	NPR20 Hole		7.484	8.823	14.717	4.287	-1.759	0.086	-0.014	-1.759	-0.100	-27.827
RUN2084	NPR20 Hole	rotated 90 degrees CW	7.485	15.530	6.592	5.919	-0.186	-0.804	0.889	-0.186	1.693	-28.040
RUN2085	NPR20 Hole	rotated 90 degrees CW	7.488	15.494	6.694	5.978	-0.217	-0.833	0.921	-0.217	1.754	-28.166
RUN2086	NPR20 Hole	rotated 90 degrees CW	7.497	15.533	6.589	5.800	-0.221	-0.833	0.937	-0.221	1.771	-27.922
RUN2256	NPR20 Str Metal	A = 0.020	7.403	8.275	8.312	8.661	0.056	0.035	0.027	0.056	-0.008	-25.248
RUN2257	NPR20 Str Metal	A = 0.016	5.825	6.102	6.234	6.499	-0.027	0.024	0.037	-0.027	0.013	-18.834
RUN2258	NPR20 Str Metal	A = 0.012	4.218	4.124	4.190	4.415	0.004	0.018	0.007	0.004	-0.011	-12.729
RUN2259	NPR20 Str Metal	A = 0.008	2.416	1.832	1.914	1.819	-0.035	0.002	-0.042	-0.035	-0.044	-5.565
RUN2260	NPR20 Str Metal	A = 0.006	1.551	0.729	0.879	0.813	-0.047	0.003	-0.019	-0.047	-0.022	-2.421
RUN2261	NPR20 Str Metal Stan	A = 0.020	7.444	9.610	10.099	10.044	-0.203	0.086	0.024	-0.203	-0.062	-29.752
RUN2262	NPR20 Str Metal Stan	A = 0.016	5.714	7.107	7.206	7.361	-0.139	0.057	0.004	-0.139	-0.053	-21.674

Run Number	Nozzle Type	Mx	My	Mz	Wp	Wi	Fi	Fr	F _{vector}	Fr/Fi	Fz/Fi	Wp/Wi	pitch	yaw	r
		in-lbf	in-lbf	in-lbf	lbm/s	lbm/s	lbf	lbf	lbf						
RUN2081	NPR20 Hole	2.549	-46.065	0.149	0.579	0.552	30.062	27.918	1.785	0.929	-0.927	1.050	0.265	3.657	-3.666
RUN2082	NPR20 Hole	2.915	-43.960	0.252	0.569	0.549	29.498	27.856	1.791	0.944	-0.942	1.035	0.148	3.683	-3.685
RUN2083	NPR20 Hole	3.394	-45.195	0.290	0.569	0.548	29.523	27.882	1.762	0.944	-0.943	1.038	0.206	3.618	-3.623
RUN2084	NPR20 Hole	-46.373	-2.915	0.343	0.574	0.549	29.760	28.092	1.703	0.944	-0.942	1.046	-3.455	0.380	-3.476
RUN2085	NPR20 Hole	-45.787	-3.102	0.354	0.578	0.549	29.955	28.222	1.768	0.942	-0.940	1.053	-3.564	0.441	-3.591
RUN2086	NPR20 Hole	-46.691	-3.420	0.416	0.578	0.549	29.959	27.979	1.784	0.934	-0.932	1.051	-3.629	0.454	-3.657
RUN2256	NPR20 Str Metal	1.057	1.514	0.247	0.469	0.548	24.129	25.248	0.056	1.046	-1.046	0.857	0.018	-0.127	-0.128
RUN2257	NPR20 Str Metal	1.323	1.149	0.246	0.371	0.431	18.188	18.834	0.030	1.036	-1.036	0.862	-0.039	0.082	-0.091
RUN2258	NPR20 Str Metal	0.894	0.974	0.102	0.267	0.312	12.091	12.730	0.012	1.053	-1.053	0.857	0.049	-0.020	-0.053
RUN2259	NPR20 Str Metal	0.174	-0.415	-0.162	0.149	0.179	5.483	5.565	0.057	1.015	-1.015	0.836	0.454	0.365	-0.583
RUN2260	NPR20 Str Metal	0.581	-0.287	-0.068	0.082	0.115	2.202	2.421	0.052	1.099	-1.099	0.717	0.519	1.120	-1.234
RUN2261	NPR20 Str Metal Stan	2.307	-0.238	0.437	0.563	0.550	28.991	29.753	0.212	1.026	-1.026	1.023	0.120	0.390	-0.408
RUN2262	NPR20 Str Metal Stan	0.884	0.672	0.245	0.426	0.422	20.779	21.674	0.149	1.043	-1.043	1.008	0.139	0.368	-0.393

Run Number	Nozzle Type	Notes	Right NPR	Corrected R1	Corrected R2	Corrected R3	Corrected R4	Corrected R5	Corrected R6	Fx	Fy	Fz
				lbf	lbf	lbf	lbf	lbf	lbf	lbf	lbf	lbf
RUN2263	NPR20 Str Metal Stan	A = 0.012	3.956	4.400	4.552	4.633	-0.029	0.003	-0.004	-0.029	-0.007	-13.585
RUN2264	NPR20 Str Metal Stan	A = 0.008	2.491	2.283	2.410	2.484	-0.029	0.043	0.010	-0.029	-0.034	-7.177
RUN2265	NPR20 Str Metal Stan	A = 0.006	1.503	0.777	0.920	0.893	-0.009	0.014	-0.001	-0.009	-0.015	-2.589
RUN2266	NPR20 Metal Port	A = 0.020	7.331	10.761	18.602	2.305	-2.890	0.069	0.069	-2.890	0.000	-31.668
RUN2267	NPR20 Metal Port	A = 0.016	5.631	7.846	13.535	1.572	-2.065	-0.033	0.005	-2.065	0.038	-22.952
RUN2268	NPR20 Metal Port	A = 0.012	3.880	4.838	8.454	0.961	-1.294	-0.040	0.036	-1.294	0.076	-14.253
RUN2269	NPR20 Metal Port	A = 0.008	2.389	2.423	4.252	0.561	-0.696	0.006	0.000	-0.696	-0.005	-7.236
RUN2270	NPR20 Metal Port	A = 0.006	1.534	0.958	1.675	0.272	-0.249	-0.022	-0.033	-0.249	-0.011	-2.905
RUN2271	NPR20 Hole 3	A = 0.020	7.420	9.997	18.551	0.109	-3.171	0.007	0.145	-3.171	0.138	-28.657
RUN2272	NPR20 Hole 3	A = 0.016	5.200	6.471	12.091	0.090	-2.153	-0.053	0.048	-2.153	0.101	-18.651
RUN2273	NPR20 Hole 3	A = 0.012	4.065	4.625	8.912	-0.097	-1.644	0.003	-0.026	-1.644	-0.029	-13.439
RUN2274	NPR20 Hole 3	A = 0.008	2.168	1.836	3.467	0.086	-0.538	-0.026	-0.009	-0.538	0.016	-5.389
RUN2275	NPR20 Hole 3	A = 0.006	1.502	0.791	1.550	0.139	-0.267	0.004	-0.005	-0.267	-0.008	-2.480

Run Number	Nozzle Type	Mx	My	Mz	Wp	Wi	Fi	Fr	F _{vector}	Fr/Fi	Fz/Fi	Wp/Wi	pitch	yaw	r
		in-lbf	in-lbf	in-lbf	lbm/s	lbm/s	lbf	lbf	lbf						
RUN2263	NPR20 Str Metal Stan	0.960	0.349	-0.002	0.310	0.292	13.808	13.585	0.030	0.984	-0.984	1.059	0.030	0.123	-0.126
RUN2264	NPR20 Str Metal Stan	0.821	0.318	0.212	0.175	0.184	6.527	7.177	0.044	1.100	-1.100	0.949	0.270	0.229	-0.354
RUN2265	NPR20 Str Metal Stan	0.647	-0.115	0.053	0.100	0.111	2.573	2.590	0.018	1.006	-1.006	0.896	0.336	0.195	-0.389
RUN2266	NPR20 Metal Port	-1.535	-70.615	0.556	0.655	0.542	33.641	31.799	2.890	0.945	-0.941	1.209	0.000	5.214	-5.214
RUN2267	NPR20 Metal Port	-1.462	-51.835	-0.113	0.512	0.416	24.912	23.045	2.066	0.925	-0.921	1.229	-0.094	5.141	-5.142
RUN2268	NPR20 Metal Port	-0.654	-32.469	-0.013	0.339	0.287	15.064	14.312	1.296	0.950	-0.946	1.183	-0.307	5.188	-5.197
RUN2269	NPR20 Metal Port	-0.083	-15.992	0.024	0.208	0.177	7.609	7.269	0.696	0.955	-0.951	1.178	0.041	5.494	-5.494
RUN2270	NPR20 Metal Port	0.080	-6.081	-0.222	0.106	0.113	2.805	2.916	0.249	1.040	-1.036	0.935	0.219	4.903	-4.908
RUN2271	NPR20 Hole 3	-3.337	-79.909	0.605	0.631	0.548	32.508	28.832	3.174	0.887	-0.882	1.152	-0.276	6.314	-6.320
RUN2272	NPR20 Hole 3	-1.906	-52.000	-0.019	0.453	0.384	21.689	18.776	2.156	0.866	-0.860	1.179	-0.310	6.586	-6.593
RUN2273	NPR20 Hole 3	-1.087	-39.039	-0.091	0.347	0.300	15.558	13.540	1.645	0.870	-0.864	1.155	0.122	6.976	-6.977
RUN2274	NPR20 Hole 3	-0.295	-14.651	-0.141	ERROR	0.160	ERROR	5.416	0.538	ERROR	ERROR	ERROR	-0.172	5.700	-5.702
RUN2275	NPR20 Hole 3	0.270	-6.111	-0.003	0.093	0.111	2.407	2.494	0.267	1.036	-1.030	0.840	0.190	6.147	-6.150

Run Number	Nozzle Type	Notes	Right NPR	Corrected R1	Corrected R2	Corrected R3	Corrected R4	Corrected R5	Corrected R6	Fx	Fy	Fz
				lbf	lbf	lbf	lbf	lbf	lbf	lbf	lbf	lbf
RUN2281	NPR20 Hole 5	A = 0.020	7.409	10.202	21.729	-3.487	-4.374	-0.105	0.156	-4.374	0.261	-28.444
RUN2282	NPR20 Hole 5	A = 0.016	5.774	7.504	16.170	-2.575	-3.214	-0.059	0.163	-3.214	0.222	-21.098
RUN2283	NPR20 Hole 5	A = 0.012	3.857	4.560	9.728	-1.673	-1.975	-0.078	0.053	-1.975	0.131	-12.615
RUN2284	NPR20 Hole 5	A = 0.008	2.338	2.307	4.693	-0.890	-0.939	-0.059	0.024	-0.939	0.083	-6.111
RUN2285	NPR20 Hole 5	A = 0.006	1.506	0.973	1.933	-0.310	-0.403	-0.025	0.002	-0.403	0.027	-2.595
NPR 50												
RUN2031	NPR50 STR4		7.571	7.547	8.150	7.823	-0.055	0.073	-0.005	-0.055	-0.078	-23.520
RUN2032	NPR50 STR4		7.552	7.449	8.044	8.121	-0.144	0.103	-0.017	-0.144	-0.119	-23.614
RUN2033	NPR50 STR4	rotated 90 degrees CW	7.594	8.267	8.010	6.534	-0.205	-0.045	0.123	-0.205	0.168	-22.812
RUN2034	NPR50 STR4	rotated 90 degrees CW	7.640	8.177	8.213	6.302	-0.274	0.000	0.159	-0.274	0.160	-22.692
RUN2035	NPR50 STR4	rotated 180 degrees CW	7.617	8.597	6.848	8.158	0.184	-0.076	0.183	0.184	0.259	-23.604
RUN2036	NPR50 STR4	rotated 180 degrees CW	7.599	8.636	6.880	8.245	0.020	-0.088	0.160	0.020	0.248	-23.761
RUN2037	NPR50 STR4	rotated 270 degrees CW	7.582	7.346	7.010	8.125	0.311	0.091	-0.024	0.311	-0.115	-22.481

Run Number	Nozzle Type	Mx	My	Mz	Wp	Wi	Fi	Fr	F _{vector}	Fr/Fi	Fz/Fi	Wp/Wi	pitch	yaw	r
		in-lbf	in-lbf	in-lbf	lbm/s	lbm/s	lbf	lbf	lbf						
RUN2281	NPR20 Hole 5	-5.405	-109.263	0.202	0.641	0.546	33.053	28.779	4.381	0.871	-0.861	1.173	-0.526	8.741	-8.757
RUN2282	NPR20 Hole 5	-3.533	-81.222	0.417	0.498	0.426	24.452	21.343	3.222	0.873	-0.863	1.171	-0.603	8.663	-8.683
RUN2283	NPR20 Hole 5	-2.665	-49.398	-0.101	0.323	0.284	14.384	12.769	1.979	0.888	-0.877	1.135	-0.594	8.897	-8.916
RUN2284	NPR20 Hole 5	-2.025	-24.191	-0.140	0.190	0.172	6.897	6.183	0.943	0.897	-0.886	1.103	-0.776	8.739	-8.772
RUN2285	NPR20 Hole 5	-0.805	-9.721	-0.090	0.105	0.111	2.724	2.627	0.404	0.964	-0.953	0.945	-0.588	8.832	-8.851
NPR 50															
RUN2031	NPR50 STR4	2.196	-1.416	0.271	0.461	0.478	24.041	23.520	0.095	0.978	-0.978	0.964	0.189	0.135	-0.232
RUN2032	NPR50 STR4	3.168	0.336	0.344	0.487	0.477	25.388	23.615	0.187	0.930	-0.930	1.021	0.289	0.348	-0.453
RUN2033	NPR50 STR4	-4.975	-6.395	0.311	0.489	0.479	25.569	22.814	0.265	0.892	-0.892	1.022	-0.421	0.514	-0.665
RUN2034	NPR50 STR4	-4.595	-8.282	0.637	0.456	0.489	23.792	22.694	0.317	0.954	-0.954	0.933	-0.403	0.691	-0.800
RUN2035	NPR50 STR4	-5.470	5.678	0.430	0.475	0.487	24.784	23.606	0.318	0.952	-0.952	0.976	-0.630	-0.445	-0.771
RUN2036	NPR50 STR4	-5.370	5.914	0.287	0.463	0.486	24.119	23.763	0.248	0.985	-0.985	0.952	-0.597	-0.048	-0.599
RUN2037	NPR50 STR4	1.104	4.831	0.265	0.478	0.484	24.934	22.483	0.331	0.902	-0.902	0.987	0.293	-0.792	-0.844

Run Number	Nozzle Type	Notes	Right NPR	Corrected R1	Corrected R2	Corrected R3	Corrected R4	Corrected R5	Corrected R6	Fx	Fy	Fz
				lbf	lbf	lbf	lbf	lbf	lbf	lbf	lbf	lbf
RUN2038	NPR50 STR4	rotated 270 degrees CW	7.587	7.336	7.117	8.071	0.225	0.116	-0.001	0.225	-0.117	-22.523
RUN2121	NPR50 STR4		7.733	7.235	8.576	8.138	-0.177	0.196	-0.030	-0.177	-0.226	-23.949
RUN2122	NPR50 STR4		7.678	7.168	8.374	8.217	-0.040	0.226	-0.034	-0.040	-0.259	-23.760
RUN2123	NPR50 STR4		7.541	7.000	8.243	8.110	-0.075	0.199	0.029	-0.075	-0.170	-23.353
RUN2191	NPR50 Hole 2		7.543	8.030	24.308	-7.403	-5.187	0.141	0.015	-5.187	-0.126	-24.935
RUN2192	NPR50 Hole 2		7.556	8.287	24.264	-7.523	-5.336	0.128	0.105	-5.336	-0.023	-25.028
RUN2193	NPR50 Hole 2		7.518	8.359	23.874	-7.450	-5.275	0.069	0.085	-5.275	0.016	-24.783
RUN2194	NPR50 Hole 3		7.521	8.986	17.117	-1.531	-3.047	-0.103	0.228	-3.047	0.331	-24.573
RUN2195	NPR50 Hole 3		7.484	8.932	17.074	-1.640	-3.197	-0.054	0.193	-3.197	0.247	-24.366
RUN2196	NPR50 Hole 3		7.594	9.124	17.165	-1.549	-3.236	-0.090	0.225	-3.236	0.314	-24.740
RUN2197	NPR50 Hole 3		7.569	9.079	17.203	-1.584	-3.140	-0.084	0.202	-3.140	0.286	-24.698
RUN2118	NPR50 Straight Hole		7.614	8.892	12.997	1.556	-1.986	-0.097	0.232	-1.986	0.330	-23.445
RUN2119	NPR50 Straight Hole		7.663	9.046	12.959	1.629	-1.986	-0.078	0.232	-1.986	0.310	-23.634

Run Number	Nozzle Type	Mx	My	Mz	Wp	Wi	Fi	Fr	F _{vector}	Fr/Fi	Fz/Fi	Wp/Wi	pitch	yaw	r
		in-lbf	in-lbf	in-lbf	lbm/s	lbm/s	lbf	lbf	lbf						
RUN2038	NPR50 STR4	1.290	4.132	0.458	0.466	0.484	24.307	22.525	0.253	0.927	-0.927	0.961	0.297	-0.572	-0.644
RUN2121	NPR50 STR4	5.609	-1.901	0.663	0.487	0.487	25.733	23.951	0.287	0.931	-0.931	1.002	0.540	0.422	-0.685
RUN2122	NPR50 STR4	5.637	-0.678	0.769	0.464	0.483	24.499	23.761	0.263	0.970	-0.970	0.962	0.626	0.096	-0.633
RUN2123	NPR50 STR4	5.880	-0.577	0.913	0.502	0.474	26.400	23.354	0.186	0.885	-0.885	1.059	0.417	0.184	-0.456
RUN2191	NPR50 Hole 2	2.112	-137.402	0.621	0.608	0.477	31.667	25.469	5.189	0.804	-0.787	1.275	0.290	11.751	-11.755
RUN2192	NPR50 Hole 2	0.415	-137.734	0.930	0.584	0.478	30.433	25.590	5.336	0.841	-0.822	1.223	0.053	12.035	-12.035
RUN2193	NPR50 Hole 2	-0.733	-135.724	0.614	0.580	0.475	30.195	25.338	5.275	0.839	-0.821	1.220	-0.036	12.015	-12.015
RUN2194	NPR50 Hole 3	-5.965	-80.802	0.497	0.537	0.475	27.981	24.764	3.065	0.885	-0.878	1.131	-0.772	7.069	-7.110
RUN2195	NPR50 Hole 3	-6.077	-81.087	0.558	0.543	0.473	28.266	24.576	3.206	0.869	-0.862	1.149	-0.582	7.474	-7.496
RUN2196	NPR50 Hole 3	-6.579	-81.085	0.540	0.548	0.480	28.611	24.952	3.251	0.872	-0.865	1.143	-0.728	7.451	-7.486
RUN2197	NPR50 Hole 3	-6.348	-81.404	0.471	0.531	0.478	27.668	24.898	3.153	0.900	-0.893	1.109	-0.663	7.245	-7.275
RUN2118	NPR50 Straight Hole	-8.077	-49.571	0.539	0.516	0.480	27.075	23.531	2.013	0.869	-0.866	1.073	-0.805	4.841	-4.907
RUN2119	NPR50 Straight Hole	-8.759	-49.092	0.614	0.496	0.483	26.105	23.720	2.010	0.909	-0.905	1.027	-0.751	4.802	-4.860

Run Number	Nozzle Type	Notes	Right NPR	Corrected R1	Corrected R2	Corrected R3	Corrected R4	Corrected R5	Corrected R6	Fx	Fy	Fz
				lbf	lbf	lbf	lbf	lbf	lbf	lbf	lbf	lbf
RUN2120	NPR50 Straight Hole		7.570	8.876	12.744	1.634	-1.861	-0.080	0.221	-1.861	0.301	-23.255
RUN2241	NPR50 Str	A = 0.020	7.511	6.815	8.416	7.895	-0.119	0.175	-0.027	-0.119	-0.201	-23.126
RUN2242	NPR50 Str	A = 0.016	5.941	5.119	6.297	6.139	-0.039	0.144	-0.042	-0.039	-0.186	-17.555
RUN2243	NPR50 Str	A = 0.012	3.894	2.803	3.904	3.499	-0.163	0.102	-0.081	-0.163	-0.182	-10.205
RUN2244	NPR50 Str	A = 0.008	2.497	1.409	2.087	1.913	-0.098	0.067	-0.053	-0.098	-0.120	-5.409
RUN2245	NPR50 Str	A = 0.006	1.496	0.446	0.841	0.871	-0.028	0.043	-0.034	-0.028	-0.077	-2.158
RUN2246	NPR50 Hole 3	A = 0.020	7.479	8.849	17.338	-1.784	-3.274	-0.044	0.141	-3.274	0.185	-24.402
RUN2247	NPR50 Hole 3	A = 0.016	5.835	6.512	12.732	-1.212	-2.428	-0.076	0.087	-2.428	0.163	-18.032
RUN2248	NPR50 Hole 3	A = 0.012	4.226	4.401	8.466	-0.769	-1.608	-0.086	0.060	-1.608	0.146	-12.097
RUN2249	NPR50 Hole 3	A = 0.008	2.494	2.214	3.995	-0.466	-0.798	-0.057	0.022	-0.798	0.079	-5.743
RUN2250	NPR50 Hole 3	A = 0.006	1.501	0.869	1.541	-0.106	-0.308	-0.014	0.022	-0.308	0.036	-2.305

Run Number	Nozzle Type	Mx	My	Mz	Wp	Wi	Fi	Fr	F _{vector}	Fr/Fi	Fz/Fi	Wp/Wi	pitch	yaw	r
		in-lbf	in-lbf	in-lbf	lbf/s	lbf/s	lbf	lbf	lbf						
RUN2120	NPR50 Straight Hole	-8.436	-48.138	0.565	0.520	0.477	27.342	23.331	1.885	0.853	-0.851	1.091	-0.741	4.576	-4.635
RUN2241	NPR50 Str	6.704	-2.258	0.592	0.476	0.484	24.514	23.128	0.234	0.943	-0.943	0.984	0.499	0.296	-0.580
RUN2242	NPR50 Str	5.496	-0.686	0.405	0.359	0.383	17.654	17.556	0.190	0.994	-0.994	0.939	0.607	0.127	-0.621
RUN2243	NPR50 Str	4.493	-1.756	0.085	0.243	0.251	10.736	10.208	0.245	0.951	-0.951	0.970	1.023	0.916	-1.373
RUN2244	NPR50 Str	2.952	-0.753	0.054	0.149	0.161	5.546	5.411	0.155	0.976	-0.975	0.924	1.266	1.040	-1.638
RUN2245	NPR50 Str	2.048	0.129	0.035	0.084	0.096	2.140	2.159	0.082	1.009	-1.008	0.865	2.033	0.743	-2.164
RUN2246	NPR50 Hole (small)	-5.358	-82.858	0.387	0.554	0.482	28.487	24.622	3.279	0.864	-0.857	1.150	-0.434	7.642	-7.654
RUN2247	NPR50 Hole 3	-3.758	-60.419	0.045	0.416	0.376	20.360	18.196	2.434	0.894	-0.886	1.107	-0.517	7.669	-7.686
RUN2248	NPR50 Hole 3	-2.765	-40.016	-0.105	0.330	0.272	14.901	12.205	1.615	0.819	-0.812	1.211	-0.692	7.571	-7.602
RUN2249	NPR50 Hole 3	-2.249	-19.331	-0.138	0.174	0.161	6.486	5.799	0.802	0.894	-0.885	1.083	-0.786	7.913	-7.951
RUN2250	NPR50 Hole 3	-0.759	-7.134	0.034	0.096	0.097	2.458	2.326	0.310	0.946	-0.937	0.987	-0.888	7.616	-7.667